1993

Studies on the optimization of deformation processed metal metal matrix composites

Timothy Walter Ellis
Iowa State University

Order Number 9413974

Studies on the optimization of deformation-processed metal metal matrix composites

Ellis, Timothy Walter, Ph.D.

Iowa State University, 1993

U·M·I
300 N. Zeeb Rd.
Ann Arbor, MI 48106

Studies on the optimization of deformation processed metal metal matrix composites

by

Timothy Walter Ellis

A Dissertation Submitted to the

Graduate Faculty in the Partial Fulfillment of the

Requirements for the Degree of

DOCTOR OF PHILOSOPHY

Department: Materials Science and Engineering
Major: Metallurgy

Approved:

Signature was redacted for privacy.

In Charge of Major Work

Signature was redacted for privacy.

For the Major Department

Signature was redacted for privacy.

For the Graduate College

Members of Committee:

Signature was redacted for privacy.

Iowa State University
Ames, Iowa

1993

TABLE OF CONTENTS

ACKNOWLEDGMENT

I have now hopefully come to the end of a very long journey. The attainment of my academic credentials, such as they are, has taken the better part of 20 years of which 11 were spent in universities. Along the way I have been truly blessed. To paraphrase Winston Churchill, never in the course of human history have so many done, so much for but one individual. My thanks and appreciation can never come near to reconciling the debt which is owed by me. My sincerest gratitude goes to Dr. John Verhoeven for his patience and tolerance during my tenure in his group. Occasionally I have wandered far afield of my course of study he has always been able to kindly put me back on track. The staff of the Materials Preparation Center has been outstanding in supplying my research work. Rick Schmidt, Larry Jones, Lester Reed, Lanny Lincoln and John Wheelock have all given me very strange and knowing looks, but, allowed me to continue on my merry way. The guidance and friendship of Dr. Rohit Trivedi, Dr. Iver Anderson, Dr. Harry Downing, Ed Gibson, and Fran Laabs has helped me through those rough spots that inevitably seem to crop up. Ms. Patti Boone has kept me on the straight and narrow making sure the various and asundered pieces of paper work necessary to such an undertaking were in place. She has saved me more than once from myself. The ongoing support of my grandmother Velta Gries and my father Dr. Thomas Ellis allowed me to keep my eyes on the prize. My daughters, Alayna and Jennifer have suffered through my years of academic pursuit with only an occasional trip to the mall. Through most of their childhood they have taken a second place to tests and papers. And to you, Paula June, it has been a particularly difficult time for you. Without your love and compassion I would be just another bewildered technologist. Thank you for showing me education is more than facts in books.

This work was done under United States Department of Energy Contract W-7405-Eng-82. The U.S. Government has assigned report number IS-T 1676 to this dissertation.

ABSTRACT

A methodology for the production of deformation processed metal metal matrix composites from hyper-eutectic copper-chromium alloys was developed. This methodology was derived from a basic study of the precipitation phenomena in these alloys encompassing evaluation of microstructural, electrical, and mechanical properties. The methodology developed produces material with a superior combination of electrical and mechanical properties compared to those presently available in commercial alloys.

New and novel alloying procedures were investigated to extend the range of production methods available for these material. These studies focused on the use of High Pressure Gas Atomization and the development of new containment technologies for the liquid alloy. This allowed the production of alloys with a much more refined starting microstructure and lower contamination than available by other methods.

The knowledge gained in the previous studies was used to develop two completely new families of deformation processed metal metal matrix composites. These composites are based on immissible alloys with yttrium and magnesium matrices and refractory metal reinforcement. This work extends the physical property range available in deformation processed metal metal matrix composites. Additionally, it also represents new ways to apply these metals in engineering applications.

GENERAL INTRODUCTION

An Explanation of the Dissertation Organization

This dissertation is a compilation of 5 papers. These cover a bank of work which is focused on the production and optimization of deformation processed metal metal matrix composites.

Background

Deformation processed copper-refractory metal alloys have been under extensive development for quite some time [1]. These alloys exhibit the combination of high mechanical strength with excellent electrical conductivity. The particular microstructure which defines a deformation processed metal-metal matrix composite, DMMCs, is unique in terms of structure and processing. DMMCs have a continuous metallic matrix phase which is reinforced by a high aspect ratio non-continuous metallic reinforcing phase. The fibrous morphology of the reinforcing phase is produced in-situ by the co-deformation of the matrix and reinforcing phases. This production is a distinction that separates these materials from the wide range of non-metallic reinforced metal matrix materials, as an example SiC fibers in Aluminum.

Early work by Bevk found that the mechanical strengths of deformation processed alloys of copper-niobium, which when codeformed produced an in-situ composite, greatly exceeded the strength that would be predicted by a rule of mixtures calculation [2]. The electrical conductivity of these materials was also found to be excellent, greater than 60 % of the International Annealed Copper Standard (% IACS). The combination of mechanical strength and electrical conductivity are better than commercial available copper alloys, e.g. Cu-Be, Cu-Zr, Cu-Al_2O_3.

Experimental observation found that the ultimate tensile strength of a DMMC increased the higher the total mechanical strain. Mechanical strain in these systems is defined as $\eta = Ln(A_i/A_f)$, where A_i is the initial and A_f is the final cross sectional area [1]. A great deal of effort has been expended on modeling the strengthening mechanism in these materials [3, 4, 5, 6, 7, 8, 9, 10]. There is still disagreement about the exact mechanism of strengthening in these materials. One approach is to investigate how the spacing of the fibers changes as a function of the true strain (η) and how this relates to the mechanical strength observed. Inter-fiber matrix thickness as a function of eta was fit to an exponential curve of the following form:

1) $$t_m = a \exp(-b^n)$$

where a and b are constants, tm is the thickness of the matrix material between fibers and n is the deformation strain. The measured tensile strength is related as follows [3]:

2) $$\sigma = c\, t_m^{-n}$$

Again c is a constant, σ is the ultimate tensile strength and n is the strength coefficient. The strength coefficient was found in early studies, using spacing data from SEM and optical microscopy, to be approximately 0.5 which lead to the assumption that these materials followed a Hall-Petch type relationship. Unfortunately, this result did not agree with electrical resistivity measurement made on the same material. Electrical resistivity measurements predicted a much narrower fiber spacing than that found by microscopy [11]. The discrepancy was solved by using dynamical scanning dark field imaging during TEM analysis. Recalculation of the strengthening coefficient, using this new data, found a value of 0.38 at high eta values. This value is much lower than that predicted for the Hall-Petch mechanism. A new model for the strengthening has been put forth by Spitzig and Verhoeven to better fit the experimental data [8]. This model is based on the work of Sevillano on the strengthening of steels by cementite [12]. This analysis uses the concept of a critical stress necessary to propagate a dislocation. This stress is modeled in the following equation:

3) $$\sigma_c = \sigma_o + 1/2\Pi t\,(MAGb)\,Ln\,(t/b)$$

σ_c is the critical stress necessary to break a dislocation through a lamellar barrier, t is the barrier thickness, M is the Taylor factor, b is the Burgers vector for the dislocation, G is the shear modulus, A= 1.2 for a mixed dislocation and σ_o is the friction stress. For a composite a value σ_c must be calculated for each phase and weighted for the volume fraction of that phase present. This is shown for a two component system as:

4) $$\sigma_{comp} = X_1(\sigma_{c1}) + X_2(\sigma_{c2})$$

This type of strengthening will predominate until the spacing between filaments becomes so small as to prevent the generation of dislocations by a Frank-Read mechanism. This phenomena, known as Koehler hardening, has been found in nano scale materials [13, 14].

Although the spacing predicted for Koehler hardening appears to be larger than that found in these materials, the concept does provide for a logical limit to the mechanical strength of these materials.

The electrical properties of these alloys are also determined by the spacing of the fibers within the matrix phase. Niobium has a very low solubility in copper at room temperature. Unlike other copper alloys which rely on the presence of precipitate dispersions or solid solution elements for strengthening, the copper in the matrix of these materials is essentially pure. Therefore, the matrix phase has the electrical conductivity of pure copper. However, as the composite is deformation processed, the refinement of the spacing of the reinforcing fibers, which leads to an increase in strengthening, also reduces the electrical conductivity. As the spacing of the filaments approaches the mean free path of an electron in the copper matrix, the electrons increasingly scatter off the interfaces between the copper and the reinforcing phase. Of course the same effect is seen in conventional alloys where precipitate particles and/or atoms in solid solution act as scattering sites which decrease electrical conductivity.

Both the strength and the electrical conductivity are a function of the spacing between particles or fibers within the matrix. There is a natural competition between these two physical properties. A heuristic argument for this competition can be displayed by the following functions:

5) $\sigma = f(\lambda)$

$\sigma =$ Tensile Strength of the Material

$\lambda =$ The Spacing of Particles in the Matrix

$f =$ A Mathematical Function Relating Particle Spacing to Tensile Strength.

6) $\Omega = f'(\lambda)$

$\Omega =$ The Electrical Resistivity of the Alloy

$f' =$ A Mathematical Function Relating Particle Spacing to Electrical Resistivity.

If the tensile strength increases more rapidly, with a reduction in spacing, than the resistivity, a material with both high strength and good electrical conductivity can be produced. In precipitation hardened materials an optimum particle size exists which gives the highest mechanical properties. This optimum size is a balance of many factors including the ability

of dislocations to loop or cut these precipitates. Electrical resistance is caused by scattering of the electron off of discontinuities within the matrix. A Bragg condition can be created with these discontinuities leading to an increase in the resistance of the material. Each of these effects is unique to a particular alloy system.

The focus of work in this study took a three fold approach heavily based on the earlier work performed on copper-niobium. To improve the physical properties of these materials will require careful management of the competition between processing which leads to enhanced mechanical properties and processing which gives good electrical properties. First, extend the range of physical properties available. Second, improve the methodology for production of these materials. Finally, extend the concept of deformation processed metal matrix composites into other alloy systems. Each one of these tasks will be outlined individually in the following three sub-sections.

Precipitation Hardening in DMMCs

The desire to improve and extend the range of properties available in DMMC's has motivated a study on the possibility of carrying out precipitation hardening of the matrix phase. The copper-chromium alloy system was chosen for this study as Cr exhibits a large solid-solid solubility in copper of 0.89 At. % (0.7 Vol. %) at 1076°C [15]. The copper-chromium phase diagram is shown in Figure 1. The extended solubility of chromium in copper suggests the possibility of precipitation hardening a hyper-eutectic copper alloy material prior, during, or after deformation processing. The wealth of processing experience gained in the study of copper-niobium deformation processed alloys provided a strong foundation on which to build as age hardening is not present in the Cu-Nb system. The precipitation of chromium from a hypo-eutectic copper alloy has been extensively studied by other authors presented in the review. Studies by several groups of the thermomechanical treatment behavior for hypo-eutectic copper-chromium alloys have determined that thermomechanical treatment can improve both the electrical and physical properties of these materials [16, 17, 18]. A literature survey has revealed very little work on hyper-eutectic copper chromium alloys. The most extensive study on hyper-eutectic copper-chromium is by Drits et al. [19]. The only reported data is the electrical resistivity and the Brinell hardness of the material. The authors did not discuss or present any micrographs of the microstructure. The combination of precipitation hardening in conjunction with the production of a DMMC appears not to have undergone either an extensive experimental or theoretical treatment.

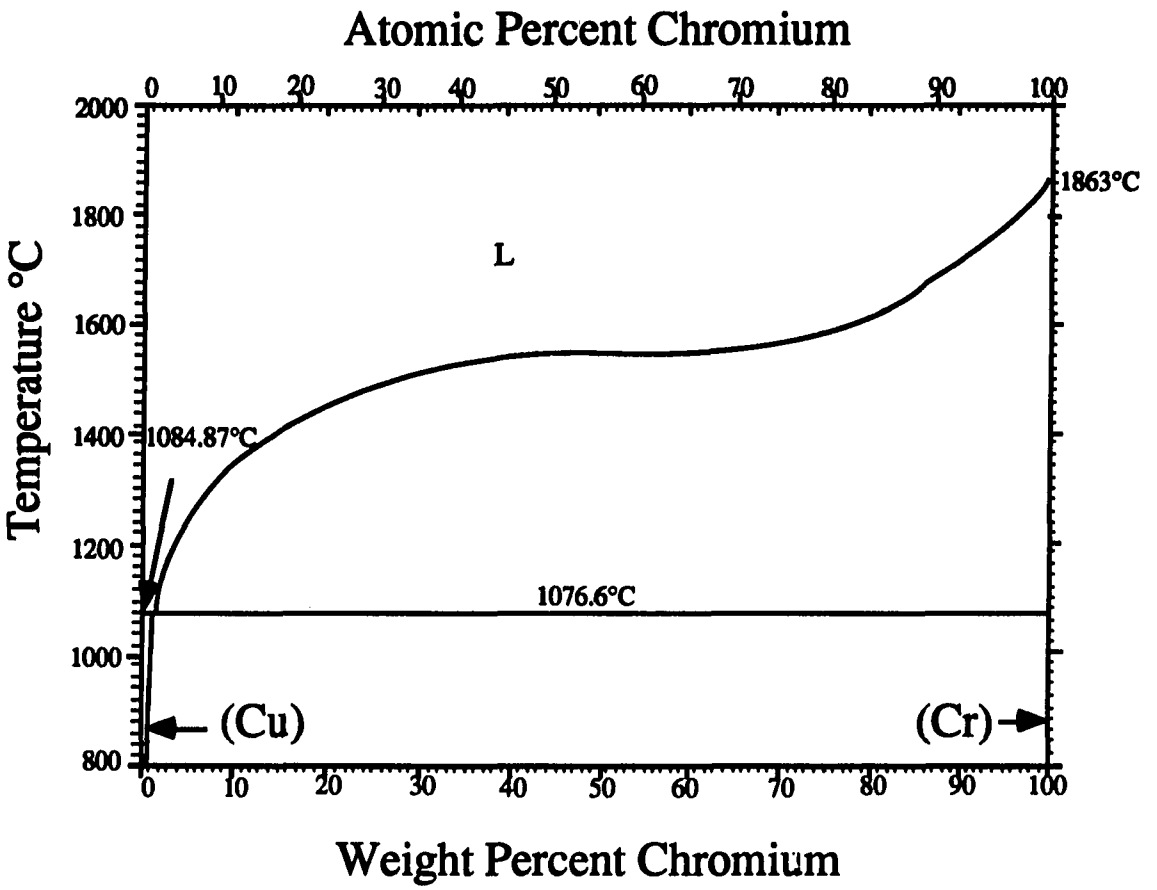

Figure 1. Copper-Chromium Equilibrium Phase Diagram

The primary task of this section was to develop an understanding of the precipitation phenomena and whether this may provide a road to improvement in the properties available in these materials. This study will also provide a model for other deformation processed alloy systems where one may want to take advantage of precipitation hardening. The kinetics of precipitation reaction was characterized by isothermal electrical resistivity measurements while microstructural evaluation was accomplished by TEM. The physical properties, mechanical strength, and electrical resistivity were correlated with microstructural developments brought about by thermomechanical treatment. This information was then used to optimize both the physical and electrical properties of the alloy.

Improvement in Material Production

Basic to understanding the following discussion is the premise that refinement of the microstructure to obtain an inter-particulate or inter-fiber spacing in the sub-micron range is the key to development of high mechanical strength in DMMCs. This limits the total amount of deformation necessary to obtain any particular strength level [4, 5, 6]. Homogeneity of the microstructure is also important as large unalloyed globules or large variations in dendrite size across a precursor billet can lead to non-uniform deformation and over working of limited areas leading to fracture or breakage of the billet during deformation processing. Additionally, chemical contamination of precursor material should be kept to a minimum. Many refractory metals, which have desirable properties as reinforcement, are very susceptible to embrittlement by carbon, oxygen, and nitrogen.

Solidification processing by consumable arc casting or crucible based rapid solidification techniques can produce very refined starting microstructures. Both processes have some inherent limitations. It may be necessary, for example in consumable arc casting, to do a secondary remelt in large ingots to improve homogeneity. Crucible melting practice always calls into question what amount of contamination is brought about by the presence of the crucible. Since crucible melting is a widely accepted industrial practice, some time was expended during this investigation on possible containment systems for the copper-refractory metal alloys. This screening study proved to be very successful in producing new methodologies for crucible melting.

Powder metallurgical techniques can be used with great success to produce precursor billets. Billets can be formed from prealloyed powders produced by High Pressure Gas Atomization (HPGA), mechanical alloying, or mixed elemental powders [6, 7]. The use of HPGA and mechanically alloyed precursor powders allows refinement of the microstructure prior to formation of billets to be deformation processed. Elemental powder processing is most amenable to the production of alloys which are impossible to melt process, due to the physical chemistry of the constituent elements, or if binary elemental alloys would be unavailable through solidification metallurgy, due to intermetallic compound formation. HPGA was used in this experimental work (Cu-18.0 Vol. % Nb) to investigate the use of rapid solidification to reduce the microstuctural scale prior to deformation processing. Magnesium-refractory metal based systems have been deformation processed, as a part of this study from the mixed powder state.

Extension into other Alloy Systems

The first consideration in the investigation of deformation processed metal-metal matrix composites is the development of the desired microstructure. The primary material to be deformation processed may be produced by powder metallurgy or solidification processing. Microstructures formed during deformation processing of a two phase immiscible alloy (as an example the copper-niobium phase diagram presented in Figure 4) is one of a continuous matrix phase and a high aspect ratio fibrous reinforcing phase. Prototypical microstructures formed upon deformation processing by a) rolling and b) drawing of a copper-20 Vol. % alloy are shown in Figure 2. The precursor material was

Figure 2. Microstructure of Deformation Processed a) Sheet and b) Wire Material

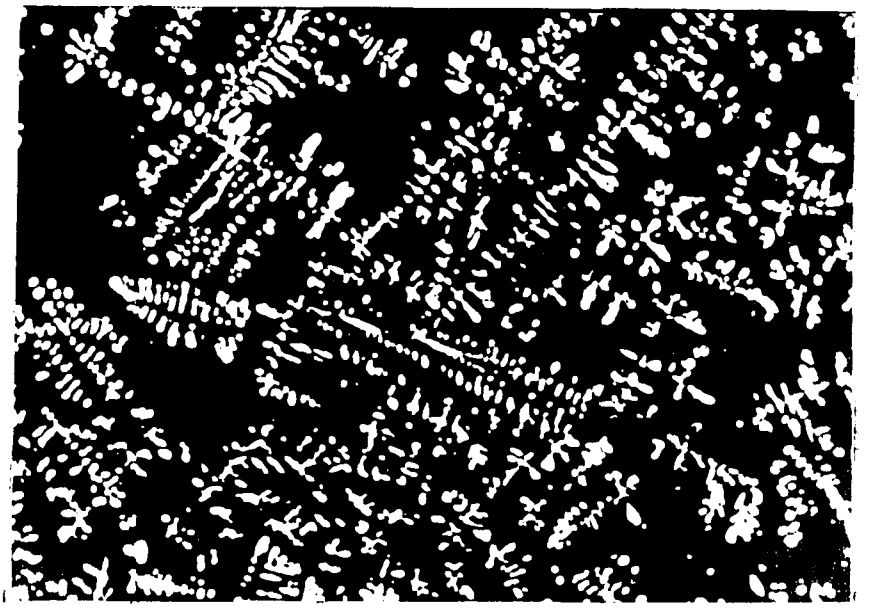

Figure 3. Microstructure of Consumably Arc-Cast Copper- 20 vol% Niobium

produced by consumable arc melting for which the original starting microstructure is shown in Figure 3. The as produced microstructure consists of primary niobium dendrites within a continuous copper matrix. Niobium nucleates and grows from the melt as dendrites followed by the solidification of the copper matrix phase as would be expected upon examination of the copper-niobium phase diagram. Niobium fibers form from these primary dendrites during deformation and have been shown to do so in a plane strain condition [2, 7]. During deformation both the reinforcing phase and matrix phase become highly textured. The <110> texture development in the niobium limits the number of available slip systems to two, which produces a ribbon shape cross section of the niobium, a BCC metal. Other copper-X alloys investigated have shown identical behavior, X= (Cr, Fe, Mo, Ta, V). The kinked morphology of the fibers produced by wire drawing are brought about by the axisymmetric nature of this deformation process. Axisymmetric deformation only produces plane strain conditions in the radial direction and hence the filaments develop kinked sections in order to

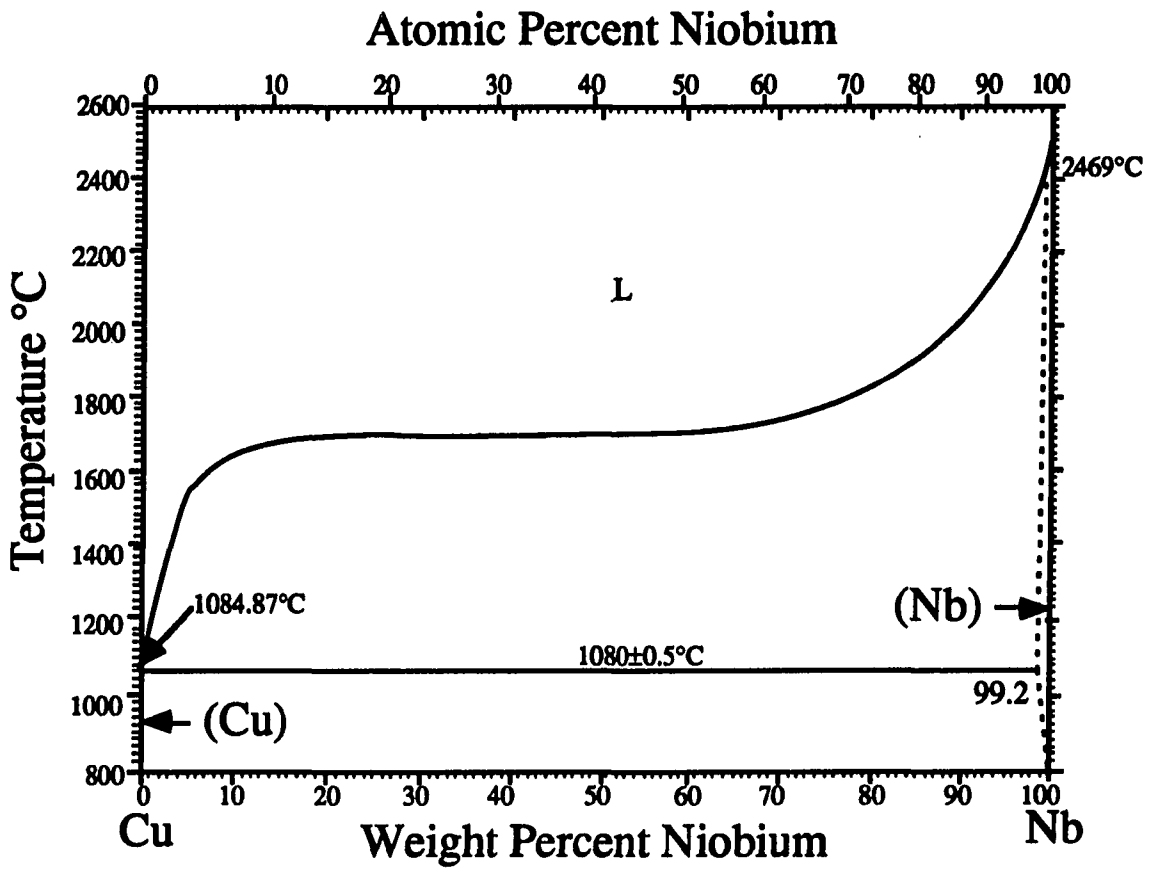

Figure 4 Equilibrium Phase Diagram for the Copper-Niobium System

better accommodate the axisymmetric flow. This is unlike rolled material which approximates plane strain conditions and forms planar arrays. Fiber morphology of wire drawn material does not, however, appear to be limited to composites with FCC-BCC crystallography, as is the case in the copper-niobium example. Research was done on deformation processed composites with other crystallographies. This was done to investigate whether the morphology of the fibers, within deformation processed material, is a function of the deformation mode or component phase crystallography. Deformation processing to form composites with other crystallographies has shown similar results to the FCC-BCC case. The following systems have been deformation processed: HCP-HCP (yttrium-titanium), and HCP-BCC (magnesium-refractory metal), and FCC-HCP (copper-rhenium). All show the same low mutual solubility in the solid state which has been found most amenable to the formation of DMMCs.

PAPER 1. PRECIPITATION HARDENING IN HYPER-EUTECTIC COPPER-CHROMIUM DEFORMATION PROCESSED METAL-METAL MATRIX COMPOSITES

By Timothy W. Ellis, Ames Laboratory, Iowa State Univ., Ames IA

INTRODUCTION

This paper investigates the use of precipitation hardening as a mechanism for improving the mechanical properties of deformation processed metal metal matrix composites (DMMCs). The possibility of precipitation hardening the matrix phase of these composites prior to, during or after deformation processing has not been previously investigated. The high strengths developed in DMMCs is due to the production of a very fine spacing between the matrix and the reinforcing phase. Precipitation hardening of the matrix phase while producing a DMMC, may allow the spacing between these phases to be refined faster than in a non-precipitation hardened case, thereby improving strength in addition to any gain produced by strengthening the matrix phase. The alloy system chosen for this investigation is copper-chromium. A review of Cu-Cr alloys is presented to familiarize the reader with the metallurgy of this material. An investigation into the basic kinetics of the precipitation reaction and how it is affected by prior deformation in a hyper-eutectic alloy follows. This is a background investigation into understanding what similarities and differences exist between the hypo and hyper eutectic cases. The final section deals with an experimental study which is an attempt to optimize the properties of a DMMC of Cu-Cr by the use of thermomechanical processing. The combination of thermal treatment and deformation processing was used to produce alloys with superior properties to those produced by simple one or two step schemes.

REVIEW OF COPPER-CHROMIUM

Introduction

Copper-Chromium alloys have been exploited as structural materials for quite some time. The family of copper alloys utilizing chromium, which came into existence in the 1880's, are designated 18XXX and find extensive use in the electrical industry as electrodes and high strength current carrying members [1]. These alloys were first investigated by Hunter et al. [2], while Corson received a patent on copper-chromium materials for electrical conductors in 1929 [3]. Early studies of Guillet followed by those of Hindrich investigated the microstructure and the phase equilibria of the system [4, 5]. The mechanical properties of these materials are dependent upon the extended solid solubility of chromium at elevated temperature, 0.89 At. % @ 1076.6°C, followed by a reduction in solid solubility as temperature is reduced, essentially 0.0 At. % @ 25°C. The currently accepted phase diagram for copper-chromium is shown in Figure 1 [6].

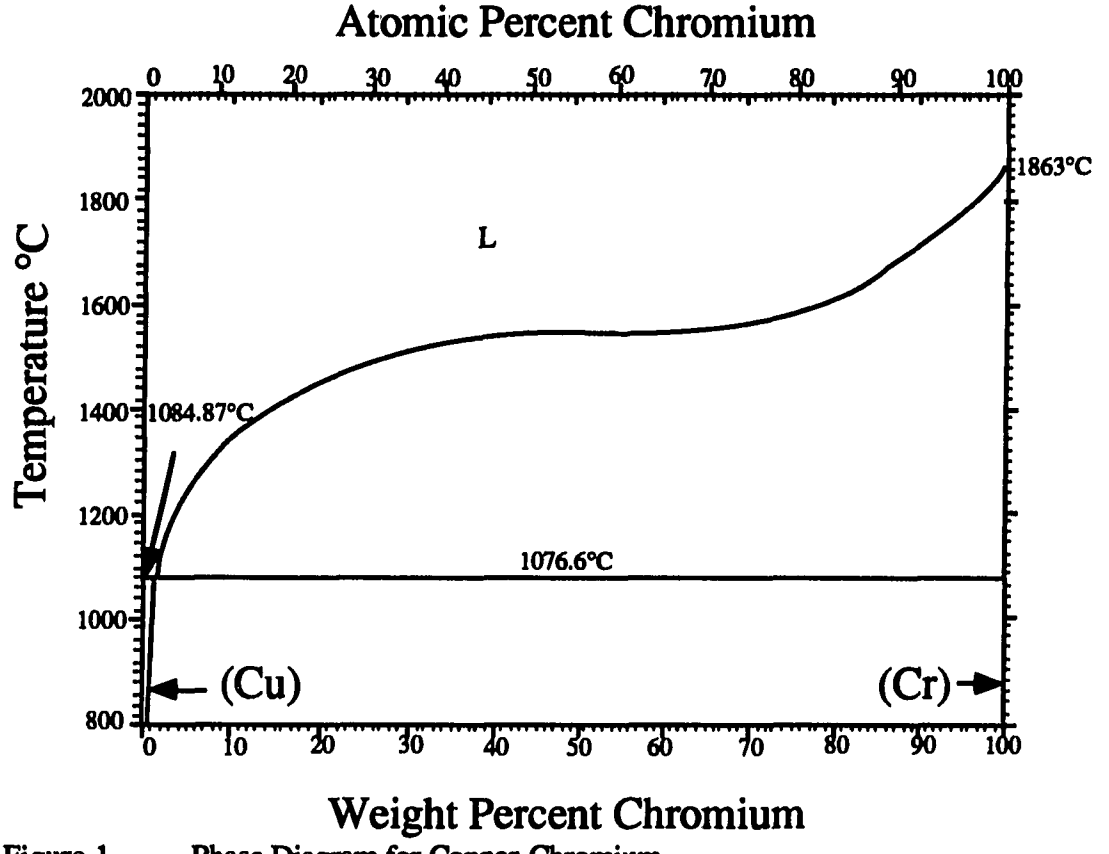

Figure 1. Phase Diagram for Copper-Chromium

The excellent electrical conductivity of these materials is based upon the very low solubility of chromium in copper at ambient temperatures. These alloys are classic precipitation hardenable materials and the attainment of optimum physical properties is dependent on the ability to remove chromium from solid solution with copper. The precipitation reaction has been extensively studied by Koda et al.[7], Bunge et al.[8], Koster et al.[9], Doi et al. [10], Williams [11], Nagata et al. [12], Suzuki et al. [13], Rezek et al. [14], Rys et al. [15], Priester et al. [16] and Rashkov et al. [17] . The objective of this review is to develop a clear and concise picture of the work already done on these materials and provide a background for the study of deformation processed hypereutectic Cu-Cr alloys.

Precipitation Hardening of Copper-Chromium Alloys

There have been a large number of investigations on the phase equilibria of copper-chromium [3, 10, 18, 19, 20]. The solubility of chromium within a copper matrix has been determined by five investigations as shown in Table 1.

The currently accepted solid solution limit for chromium in copper is 0.89 At. % at 1076.6°C as given by the experimental data of Doi [10] and published in the ASM Binary Alloy Phase Diagrams [6]. The solubility of chromium in copper can be calculated by the following expression, Equation 1.

1) $X(\text{Cr. in Cu}) = 24480 \exp.(-114880/RT)$

R is in Joules/Mole K

The diffusivity of chromium in a copper solid solution has been determined by tracer diffusion studies and by studies of the coarsening of precipitates [14, 21, 22, 23]. Values for the preexponential, D_O, and activation energy are given in Table 2.

The commonly used value of the diffusion coefficient of chromium in copper is that of Barreau [22] as the other authors noted a oxide coating on their samples. An oxide coating may tie up chromium on the surface thereby slowing the diffusion of chromium within the sample. The Arrhenius form of the diffusion equation can be represented as:

2) $D = 0.80 \exp. (-29{,}040/RT)$

R = Joules/Mole K

Table 1. Experimental Values for the Maximum Solubility of Chromium in a Copper Solid Solution

Author	Eutectic Temperature (C)	Composition Atomic % Chromium	
Corson	1076	1.52	[3]
Alexander		1.03	[18]
Hibbard	1070	0.74-0.92	[19]
Doi	1076.6	0.89	[10]
Zakarov	1073	0.77	[20]

Table 2. Frequency Factor and Activation Energy for the Diffusion of Chromium in a Copper Solid Solution

Temperature Range (C)	D_o cm^2 sec	Activation Energy Joules/Mole	Ref.
796-1035	1.56	26,767	[21, 22]
800-1070	0.50	27,020	[23]
700-960	0.80	29,040	[22]
500-700		24,050	[14]

The solubility and diffusivity of chromium within a copper matrix are plotted versus temperature in Figure 2 using Equations 1 and 2 The diffusivity of Cr within a Cu matrix drops off more rapidly than the solubility. Since the diffusivity of Cr within the Cu matrix is approximately 10^{-9} cm^2/sec at 275°C, the removal of chromium by precipitation below this temperature would require extremely long times. However, the solubility of Cr in Cu reaches 0.001 At. % at 550°C. Therefore, the precipitation of Cr should be done below this temperature to minimize the effect of solid solution Cr on the electrical conductivity of these materials. By this analysis the precipitation of Cr from Cu should be done in the range 270°C to 550°C.

Previous studies of precipitation hardening in copper-chromium alloys fall into two investigative regimes: either constant aging times with a variation in temperature or constant aging temperatures with a variation in time. It may be concluded that both phenomena are important and that in a perfect environment both approaches are necessary, for any specific

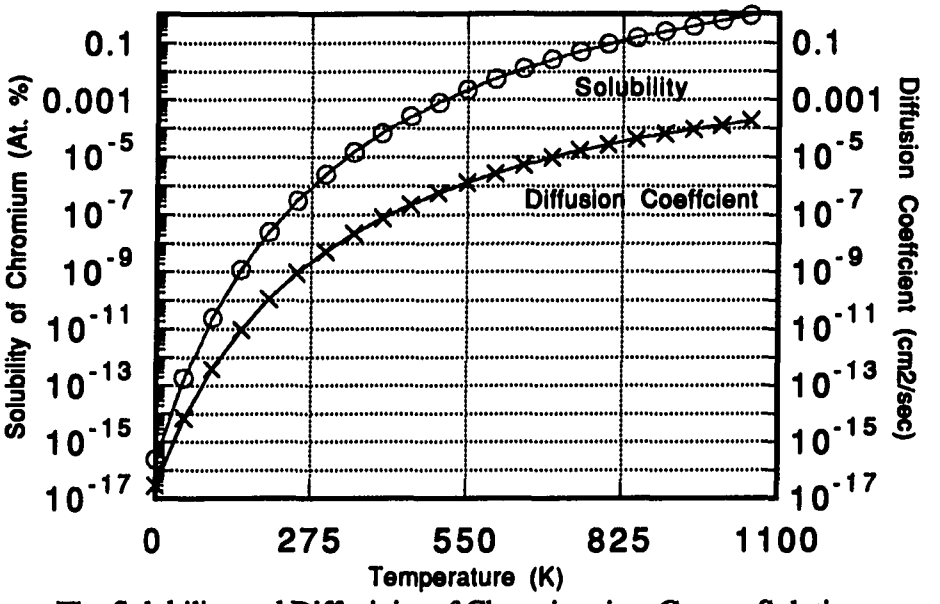

Figure 2. The Solubility and Diffusivity of Chromium in a Copper Solution as a Function of Temperature

alloy composition, if one is to develop a complete picture. This is particularly true if one is to compare the maximum physical properties available at different aging temperatures. Unfortunately, the diffusion coefficient of chromium within a copper solid solution drops by approximately two orders of magnitude between 550°C and 275°C, see Figure 2. This indicates that a comparison of materials aged at 550°C and 275°C with an eye on evaluation of the alloy at comparable microstructural states, i.e. an identical amount of chromium removed from solid solution by aging, will require vastly different aging times. Classically the fraction reaction (f(r)) completed within a matrix is modeled by the Johnson-Mehl equation [24]. By inspection one can determine that for the same value of f(r) obtained at two different temperatures two very different aging times may be necessary. Nagata has used the value of the growth exponent to determine the shape of the Cr precipitates [12]. Experimentally they have determined the value of the growth exponent to be approximately 2, see Table 3, which correspond to disc shaped precipitates. Although the value can be predicted from analytical modeling, experimental determination of the exact value is ambiguous at best. Additionally, since the value of n predicted by analytical models is very close for many different perceived growth mechanisms, the value of the growth exponent is not unique enough to be of use.

An inspection of the available data has been made in various experimental dimensions. First is an evaluation of the effect of the percentage of chromium on the maximum available mechanical properties, in this case represented by the hardness of the material, of a precipitation hardened material. Figure 3 is a plot of the hardness obtained upon aging of solutionized and quenched copper-chromium alloys with a composition between 0.05 At. % and 1.16 At. % in the temperature range 20°C to 550°C [9, 14, 18, 25]. These materials were solution treated in the temperature range 950°C to 1030°C. This data is all for an aging period of 2 hours.

Table 3. Values of the Growth Exponent as predicted from Modeling

MODEL	n	Ref
Growth, Bulk Diffusion Controlled, in One Dimension Fixed Number of Particles	3/2	45
Growth, Bulk Diffusion Controlled, in Two Dimensions Fixed Number of Particles	2	45
Growth, Bulk Diffusion Controlled, in Three Dimensions Fixed Number of Particles	5/2	45
Growth, Interface Controlled, Fixed Number of Particles	3	47
Growth on Dislocations	2/3	46
Nucleation at a Constant Rate and Diffusion Controlled Growth	5/2	45
Growth of a Fixed Number of Eutectoid Cells	3	48
Nucleation at a Constant Rate and Growth of a Eutectoid	4	48

Increasing the chromium concentration directly increases the increment of hardening available upon aging. There is an apparent contradiction in the data as the alloys with compositions above 0.6 At. % chromium have poorer properties than those between 0.3 At. % and 0.6 At. %. This contradiction can be explained as follows: the data of Nagata and Nishikawa, alloy compositions of 0.05, 0.10, 0.30, 0.49, and 0.91 at. % Chromium were solutionized at 950°C [12], whereas the 0.6 At. % alloy was solutionized by Koster and Knorr at 1030°C [9], and the data of Priester [16], 0.80 At. %, and Suzuki [13], 1.16 At. % were solutionized at 1000°C. By referring to Figure 2 we find that in order to obtain maximum

saturation prior to age hardening the highest possible solutionizing temperature must be used as the chromium concentration reaches its limit. Therefore, the reduction in properties noted in the alloys of 0.49, 0.80, 0.91, and 1.16 At. % chromium is most likely due to an insufficient solutionizing temperature which, thereby, limits the amount of chromium in solution prior to aging. Additionally, a subtle effect is the possibility that undissolved chromium particles within the matrix may prevent the formation of the maximum number of precipitates possible as they may act as nuclei on which the chromium within solution may precipitate. This phenomena would be expected to be most prevalent at compositions above the accepted solid solution limit of 0.89 At. %. In Figure 4 the electrical resistivity data, for the same materials as displayed in Figure 3, shows that the higher the chromium concentration in the as-quenched condition the higher the electrical resistivity. It is important to consider the solutionizing temperature to evaluate the % Cr in solid solution here. For example, the 0.60 At. % material, solutionized at 1030°C, has a higher initial resistivity than the 0.91 At. % material, solutionized at 950°C. Again these materials were only aged for 2 hours, therefore, the precipitation reaction may not have gone to completion.

Inspection of the electrical resistivity data indicates that the precipitation reaction is not complete after 2 hours of aging unless the isothermal aging temperature is above 450°C. Therefore, a longer time may be necessary in order for the precipitation reaction to go to completion. It is interesting to note that the electrical resistivity of the alloys, when aged above 450°C, is approximately equal indicating completion of the precipitation reaction regardless of composition. Precipitation phenomena in the Cu-Cr system is intimately associated with the following: obtainment of the highest possible chromium concentration within the copper matrix prior to aging, the reduction in the solid solubility of chromium in copper, and the ability to transport chromium atoms within the copper solid solution during aging. Suzuki and Kanno [13] have done a great deal of work on the copper-chromium system including extensive investigation of the Time-Temperature-Transformation diagrams (T-T-T) for both hardness and electrical resistivity.

These materials were directly aged, i.e., no quenching before aging, in contrast to the previous authors who all measured their material after quenching. The result of the resistivity study is shown in Figure 4. Electrical resistivity is found to drop in a manner similar to that in Figure 5, however, their aging study was carried to much higher temperature than those of the other cited authors. A bay seems to exist in the resistivity data at 700°C. This would imply a double nose to the Time-Temperature-Transformation Diagram (T-T-T). A later study by the same authors indicated that aging after quenching lead to a double nose for the T-T-T diagram.

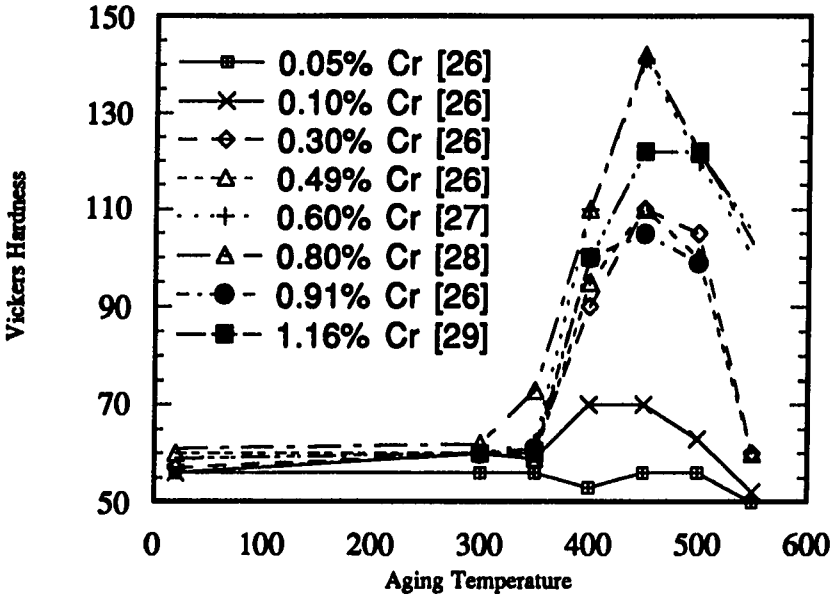

Figure 3. Hardness Obtained upon the Aging of a Solutionized and Quenched Copper-Chromium Aged Isothermally for 2 Hours

Behavioral differences between the directly aged and the quenched aged materials were attributed to the difference in nucleation and growth mechanisms.

Investigations of the morphology, spacing and boundary orientations of chromium precipitates in the copper matrix should give insight into the mechanistics of precipitation hardening in these alloys. There is common agreement that a rod type morphology is present in the over aged condition and the chromium precipitates have either a Kurdjemov-Sachs or a Nishiyama-Wasserman relationship to the matrix [17, 19, 25, 30, 31, 32, 33]. At short isothermal aging times the morphology of the precipitates is ambiguous. There is disagreement on rod versus spherical shapes and BCC versus HCP crystal structure for the precipitate particles. Several possible reaction pathways were proposed by Williams [11]. He stated that in the early stages of precipitation chromium precipitates are congruent with the copper matrix and possess an FCC crystal structure [33, 34]. This has not been observed in Transmission Electron Microscopy, TEM, done by other investigators without some doubt as to the imaging conditions. Table 4 is a compilation of size and spacing data for several precipitation hardened copper-chromium alloys obtained by a number of authors.

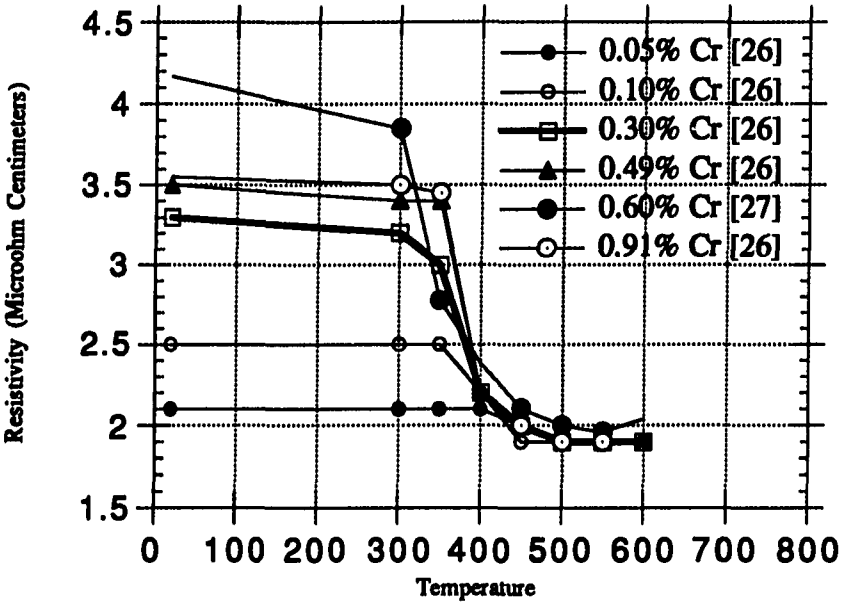

Figure 4. Electrical Resistivity of Solutionized and Quenched Copper-Chromium Alloy Isothermally Aged for 2 Hours

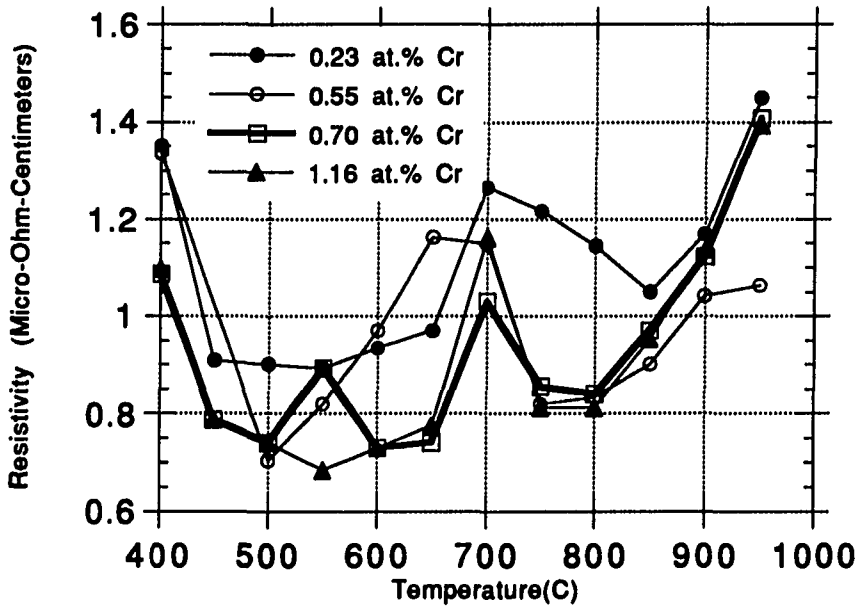

Figure 5. Electrical Resistivity as a Function of Temperature for Several Directly Quenched Copper-Chromium Alloys Solutionized at 950°C

Taking the data for the spacing of the 0.35 At. % and the 0.60 At.% alloys and plotting on a common scale (Figure 6) we can observe that the spacing develops in the same manner in both alloys. The very large increase in the spacing upon aging at 700°C is most assuredly due to enhanced diffusion at elevated temperatures. One can look at Figure 2 as a reference. It is also of interest to note that the finest precipitate spacings are available at the lowest aging temperatures, however, the diffusion necessary for precipitate growth is also limited.

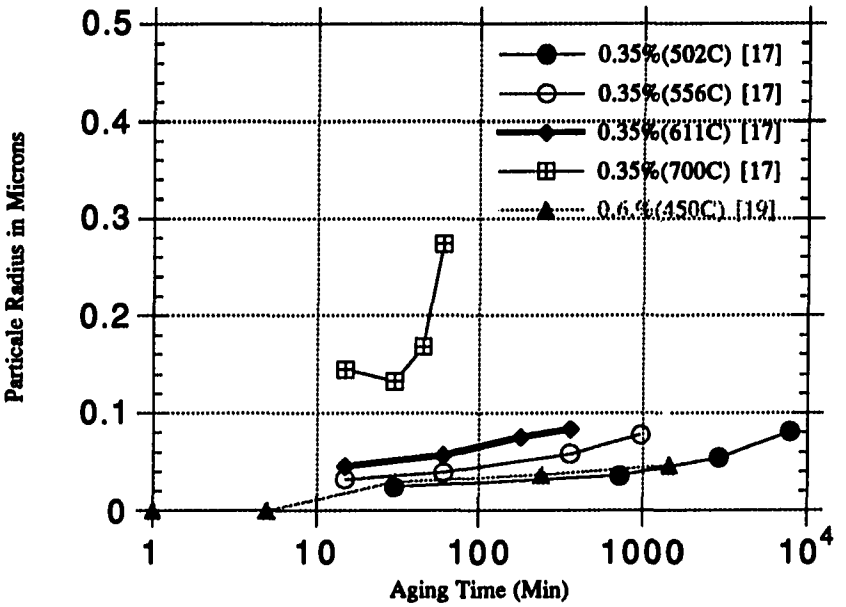

Figure 6. Precipitate Spacing obtained by Isothermally Aging Copper-Chromium Alloys

Several studies have been done evaluating the effect of mechanical working prior to age-hardening [16, 17]. The effect of plastic deformation on the aging process in three alloy compositions, 0.6, 0.35 and 0.12 At. %, has been studied by Rashkov and Martinova [17]. The precipitate spacing were also measured and compared to those of a conventional solutionized/quenched/aged material of the same compositions. The data is presented in Table 5.

Table 4. Precipitate Size Obtained by Aging

Atomic % Chromium	Aging Temp	Aging Time in Sec.	Particle Radius μm	Particle Length μm	Particle Spacing μm	
0.35	502	30	0.0251		0.0247	[17]
"	"	720	0.0383		0.0360	
"	"	2880	0.0501		0.0541	
"	"	7800	0.0635		0.0813	
"	556	15	0.0235		0.0324	
"	"	60	0.0300		0.0395	
"	"	360	0.0468		0.0585	
"	"	967	0.0657		0.0781	
"	611	15	0.0407		0.0459	
"	"	60	0.0489		0.0572	
"	"	180	0.0625		0.0755	
"	"	360	0.0732		0.0834	
"	700	15	0.0949		0.145	
"	"	30	0.0106		0.133	
"	"	45	0.117		0.168	
"	"	60	0.124		0.274	
0.6%	450	5	0	0	0	[19]
"	"	30	0.040	0.050	0.0292	
"	"	240	0.060	0.120	0.0368	
"	"	1440	0.0100	0.180	0.0464	
0.94%	500	60	0.090			[25]
"	"	120	0.110			
"	"	420	0.135			
"	600	60	0.110			
"	"	120	0.160			
"	"	240	0.210			

These materials were quenched from 1000°C followed by cold deformations of 10, 50 and 70%, hence the nomenclature quench/cold deform/ age (Q/X/A, where X= % deformation). The variation of mean precipitate spacing and mean volume are shown as a function of aging time at 450°C on Figures 7 and 8. Their results show two distinct effects of mechanical work. First, the deformation processing of a solid solution copper-chromium alloy starts the formation of chromium precipitates prior to aging. Additionally, the second effect finds that deformation processing reduces the mean size of the precipitates and the mean spacing from that obtained by quenching and aging without prior deformation.

Table 5. Precipitate for a Cu-0.6 at. % Cr Alloy Spacing Measuredby TEM after Deformation and Isothermal Aging

Alloy Condition	Aging Temp C	Time (Min)	Particle Radii μm	Particle Length μm	Particle Spacing μm
As Quenched	450	5	0	0	0
	"	30	0.040	0.050	0.0292
"	"	240	0.060	0.120	0.0368
"	"	1440	0.100	0.180	0.0464
As Quenched		0	0.040	0.050	0.0405
10%/Deformation		5	0.040	0.050	0.0283
"	"	240	0.060	0.090	0.0368
"	"	1440	0.075	0.100	0.0425
As Quenched		0	0.035	0.050	0.0368
50%/Deformation"		5	0.035	0.050	0.0272
"	"	1440	0.085	0.100	0.0405
As Quenched		0	0.030	0.040	0.0368
70%/Deformation		5	0.030	0.050	0.0272
"	"	30	0.040	0.050	0.0272
"	"	100	0.050	0.075	0.0296
"	"	240	0.075	0.100	0.0357
"	"	1440	0.100	0.125	0.389

The data of Martinova and Rashkov [17] show an interesting effect, Table 6. If one takes the ratio of the radii/length we find a difference in the aspect ratio of the particles depending on whether or not it was cold worked, but all cold worked samples have about the same ratio. Since cold deformation causes the formation of precipitates prior to isothermal aging of the material, the second effect noted by Raskov and Martinova is not surprising. Their results note an anomalous increase in the electrical resistivity, also observed by Nagata et al. [12] and Priester [16], of the material at short aging times, and this increase reduces directly with the amount of prior cold work. The presence of chromium precipitates within the copper matrix brought about by cold work provides preexisting nuclei upon which the chromium remaining in solution may precipitate. This probably prevents the formation of an excessive number of very small nuclei which lead to an anomalous increase in the electrical resistivity [33]. Anomalous increases in resistivity have been found in the Aluminum-Copper, Aluminum-Silver, Aluminum-Zinc and the Copper-Beryllium systems. A review of this work and the efforts made on modeling such behavior are presented in the book by Rossiter [33].

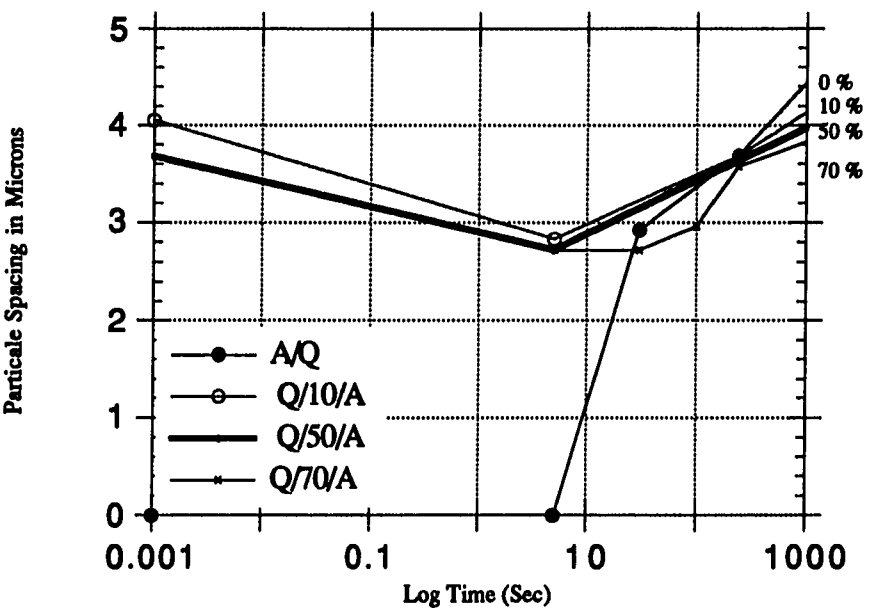

Figure 7. Spacing of Precipitates in a Copper-0.6 at. % Chromium Alloy Aged after Quenching and Deformation Processing

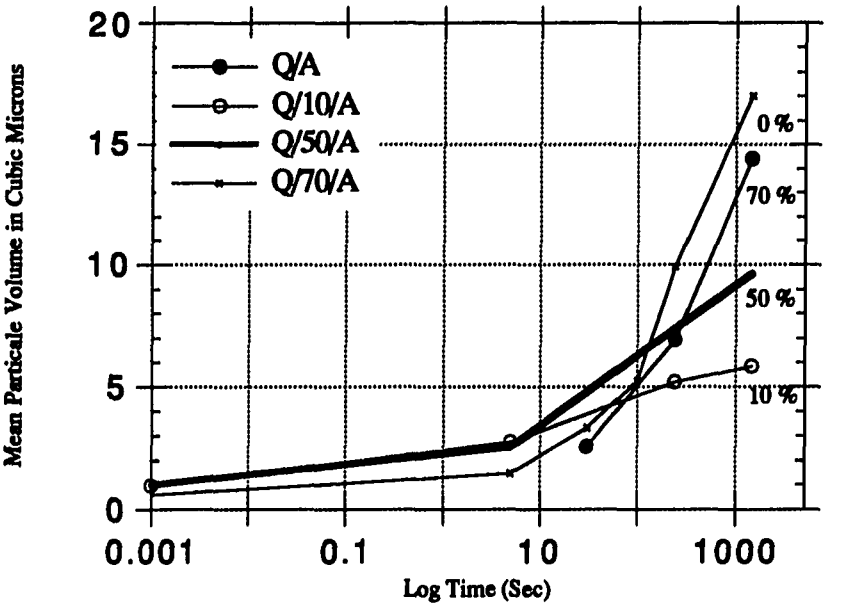

Figure 8. Mean Particle Volume of Chromium Precipitates After Aging from a Quenched and Deformation Processed Condition

Table 6. Comparison of Aspect Ratios for Precipitate Particles

Alloy Condition	Aging Time>	Radii/Length 0	5	30	100	240	1440	Mean
As-Quenched		0	.8		.55	.556		.618
10% Reduction		.8	.8		.67	.75		.755
50% Reduction		.7	.7			.85		.75
70% Reduction		.75	.6	.8	.66	.75	.8	.73
						Overall		.72

The anomalous increase in electrical resistivity, previously noted for quenched/ isothermally aged in the absence of cold deformation specimens may, however, be indicative of a separate nature of the early precipitates when compared to those in the overaged condition. Examination of the work by Nagata and Nishikawa shows that the maximum mechanical

properties of the aged alloy are obtained after the drop in resistivity expected by the precipitation of chromium from the saturated solid solution [12], as shown in Figure 9. The particle size which corresponds to the maximum hardening is approximately 0.30 microns. Therefore, the exact nature of the nuclei is, in the practical sense, a trivial point because maximum strength occurs at minimum resistivity. It is also found, on inspection of the data of Koster and Knorr, that the isothermal aging temperature does have an effect on the maximum obtainable hardness, but the strongest effect is related to the time necessary to obtain maximum hardness [9]. This is shown in Figure 10. The reduction in hardness noted above 500C^{o} is brought about by the increase in the solubility of chromium within the copper lattice, see Figure 11, thereby reducing the total amount of chromium available to form precipitates. In a similar manner the maximum hardnesses obtained by some authors appear to have been limited by the use of solutionizing temperatures lower than 1000^{o}C [12]. The effect of time can also be related using Figure 2, as aging at lower temperature requires long periods of time to transport chromium by diffusion through the copper lattice. Mechanical deformation prior to aging should enhance the transport of chromium within the copper solution due to the presence of dislocations and dislocation cells.

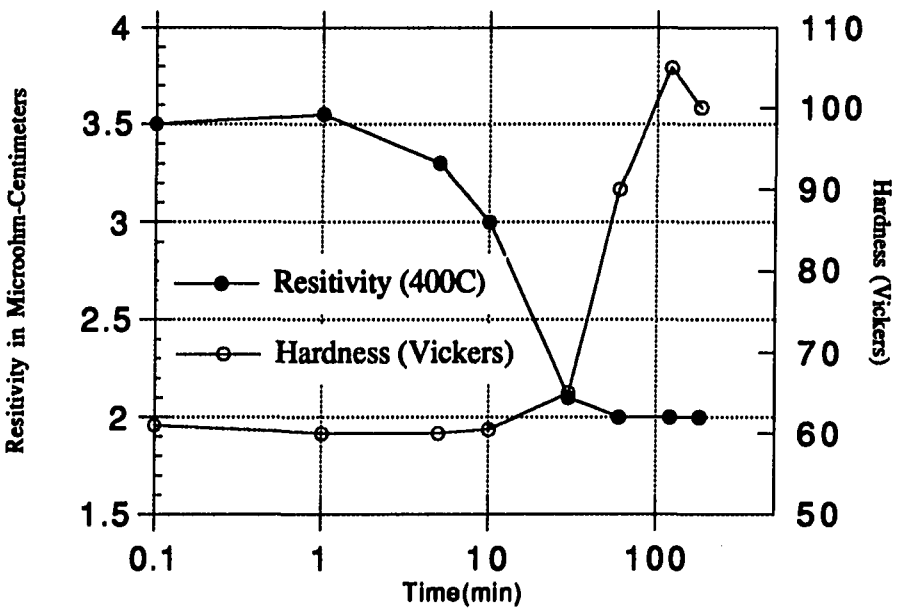

Figure 9. Resistivity and Hardness versus Time for a Copper-0.91 At. % Chromium Alloy Aged at 400^{o}C

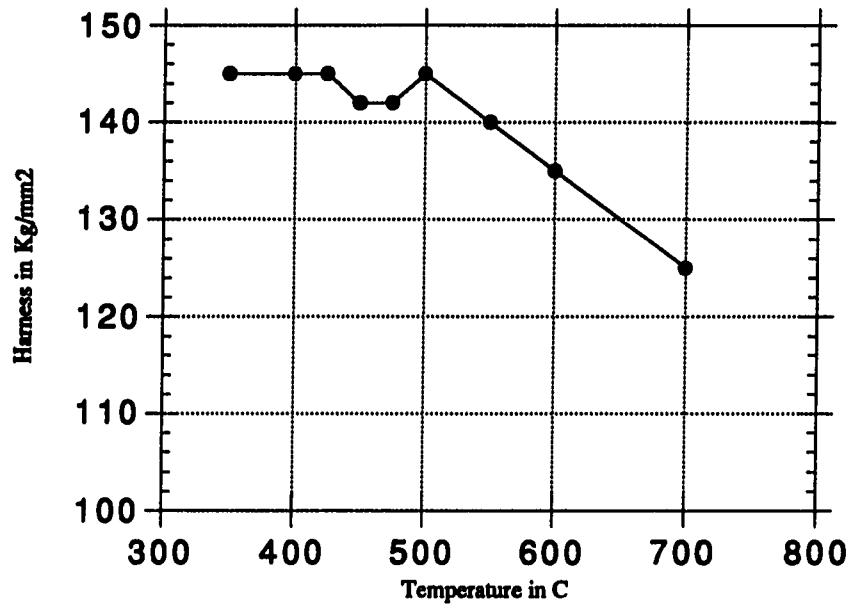

Figure 10. Maximum Hardness Obtained by a Copper-0.6 At. % Chromium Alloy Aged between 700 °C and 350 °C

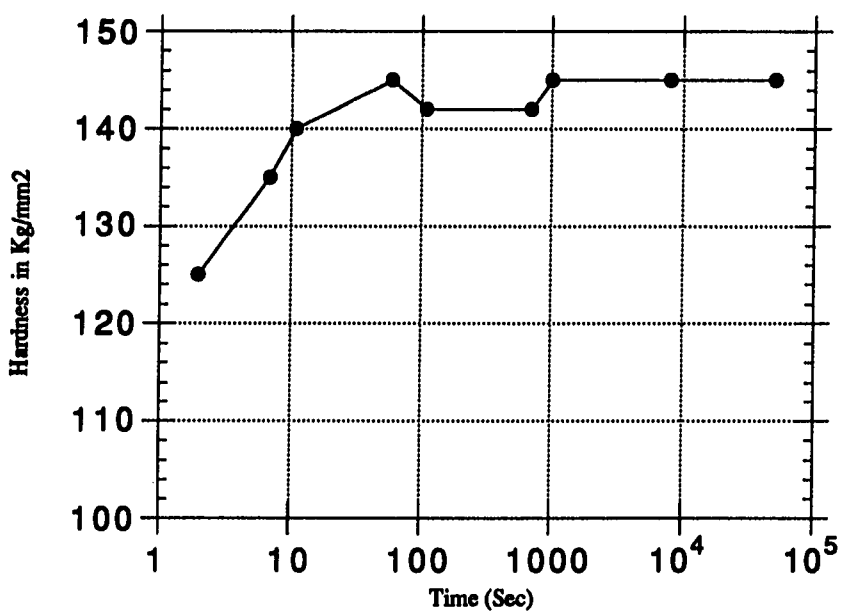

Figure 11. Maximum Hardness Obtained upon Aging at 400°C

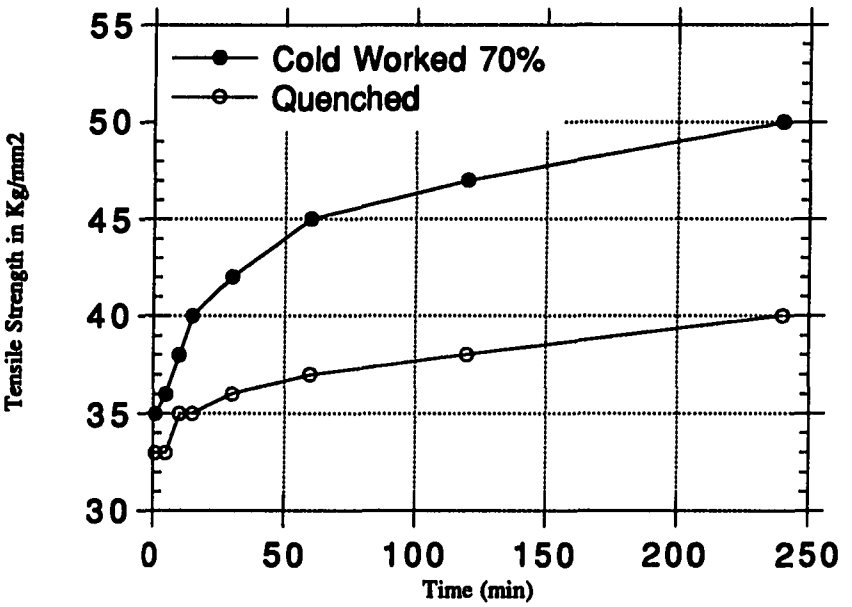

Figure 12. Tensile Strength of a Copper-0.35 At. % Chromium Aged at 450°C in the As-Quenched Condition and after Cold Deformation of 70%

These provide energetically favorable locations for nucleation/precipitation and pathways for chromium migration. This seems to be born out again using the data of Rashkov and Martinova displayed in Figure 7 [17]. As can be seen in the previous graph not only is the tensile strength increased by cold working prior to aging, a phenomena eluded to earlier in Figure 7 and 8 where both the mean particle size and spacing were reduced by cold work, but additionally the time necessary to obtain a large increment of the final strength has been reduced.

As shown in Figure 9 the electrical resistivity of the material is reduced upon isothermal aging from a supersaturated state. This observation is brought about by the reduction of chromium within the copper matrix thereby reducing the resistivity contribution due to impurity scattering [34]. The residual resistivity of chromium has been calculated to be approximately 6 μm/cm per atomic % chromium [34, 35]. Due to the extensive use of copper-chromium alloys in electrical equipment the optimum properties of these materials normally involves the attainment of both high mechanical strength and high electrical conductivity. Figure 8 presents

the electrical conductivity obtained upon isothermally aging a copper-0.6 At. % chromium alloy to a terminal value [9]. The aging of a copper-chromium alloy below 475°C does not appear to reduce the terminal electrical conductivity appreciably. However, aging the material above this point does start to degrade electrical conductivity. This is to be expected as the solubility of chromium increases with temperature it increases the impurity scattering component of the resistivity. Inspection of Figure 10 also shows that the maximum hardness obtained in these alloys also does not increase greatly upon lowering the isothermal aging temperature below 475°C. This is of practical importance as the selection of aging temperature and time can be done to best suit industrial production requirements rather than alloy behavior. Additionally, this would seem to indicate that there may be a minimum size requirement for the precipitates to provide hardening. That is to say, the precipitates must grow to a certain minimum size before they can enhance the mechanical properties of the copper matrix. This is contrary to the experience in other precipitation hardenable copper alloys, i.e., Copper-Beryllium, where the attainment of the finest structure possible gives the maximum mechanical properties [1]. However, the very fine G-P zone microstructure that gives Copper-Beryllium alloy their superior strength also leads to very poor electrical properties when compared to other copper based materials due to the anomalous increase in resistivity discussed above [35].

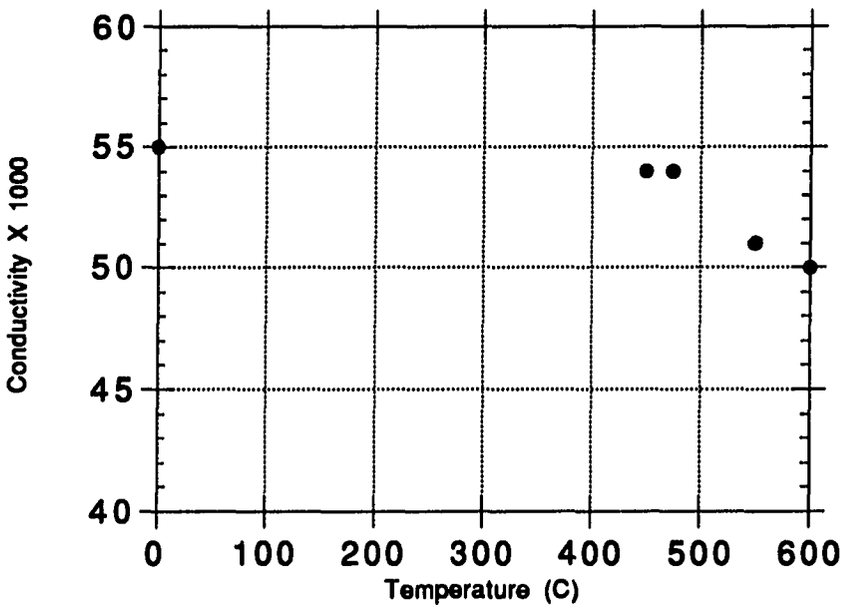

Figure 13. Maximum Electrical Conductivity of a Copper-0.6 At. % Chromium Alloy Obtained by Isothermal Aging

An empirical model of the electrical and mechanical properties obtain by aging a solid solution copper-chromium alloy, 0.44 At. % and 0.94 At. %, has been published [17]. The descriptive equation is of the following form presented for the 0.94 At. % alloy.

3) $$Hv= 319.0- 48.0T- 17.2t-3.15Tt+2.1T^2+5.96t^2$$

4) $$R= -34.78+24.5T+4.7t+4.4Tt-0.5T^2t-0.5Tt^2 -2.16T^2-1.6t^2+0.04T^2t^2$$

Hv= Vickers Hardness
R= Resistivity
T= Temperature
t=Time

These equations were derived using the author's own data [17] and data presented by prior workers in the area. Although this brute force computation shows both hardness and electrical conductivity are maximized by judicious selection of aging time and temperature, little is gained in understanding the phenomena taking place.

All the previous work reviewed was done on hypo-eutectic alloys. A paucity of data exists for alloys in the hyper-eutectic region, i.e. > 1.2 At. % chromium. An extensive search of the literature found but one prior study by Drits et al. [36]. In this work a series of copper-chromium alloys were prepared in the range of 0.25 to 40.0 Wt. % chromium. These alloys were produced by non-consumable arc melt on a water-cooled copper hearth followed by thermal and mechanical processing. Hardness and resistivity values for each alloy composition and thermomechanical process were then compared to the values for the as-cast material. Three thermomechanical treatments were undertaken with these alloys: 1) solutionizing and quenching, 950°C for 1 hour, 2) solutionizing and quenching followed by aging at 500°C for 2 hours, and 3) hot deformation to an $\eta = 0.5$ at 850°C. Hardness versus composition for all alloy compositions and treatments is shown in Figure 14. It is apparent in Figure 9 that solutionizing and quenching degrades the hardness of these materials. Although aging does recover some of the hardness lost it does not obtain the as-cast value. Since the alloys were produced by arc melting on a cooled copper hearth one could assume that the combination of rapid cooling of the melt and microsegregated region of maximum solubility has lead to super-saturation of chromium beyond that available in solutionizing and quenching. As was shown in the case of hypo-eutectic alloys by other authors, the combination of mechanical deformation and thermal treatment provides the best mechanical properties. [13, 17, 19, 25]. The resistivity

data presented by Drits et al.. [19], has some interesting and confusing trends. First in hot deformed and aged material the resistivty increases regularly with the chromium content from 75.0% IACS at 0.27 Wt. % Cr to 45.0% IACS at 25.0 Wt. % Cr. Interestingly for the as-cast and solutionized material the resistivity increases from 75.0% IACS at 0.27 Wt. % Cr to 45.0 % IACS at 5.0 Wt. % Cr were it remains constant for all subsequent additions of chromium.

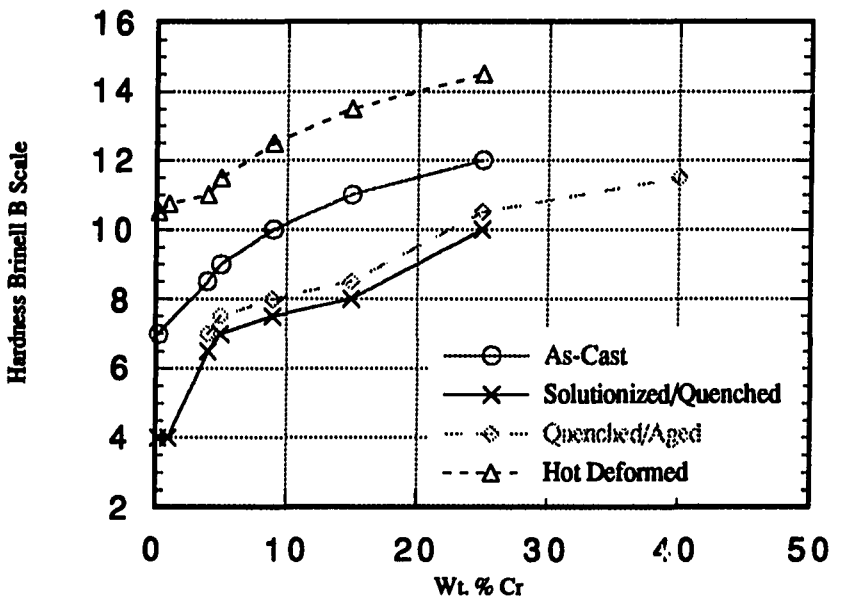

Figure 14. Hardness versus Composition for Copper-Chromium Alloys after Various Thermomechanical Treatments

This is troublesome as the volume % copper is being reduced from 95.0 % to 40.0 %. This is surprising as a regular increase in resistivity would be expected as the chromium content is increased. Due to the graphical presentation of the resistivity data abstraction of quantitative data is difficult at best, but the trends presented are clear and not addressed by the authors. Unfortunately, only resistivity and hardness data are presented. No information is given on the microstructures of the material nor is other mechanical test data given.

Due to the large amount of data present in the literature for the hypo-eutectic alloys, certainly due to their industrial importance, and the almost total lack of information on hyper-eutectic alloys the time appears to have come to put more effort into correlating the two cases in this alloy system.

A BASIC STUDY IN PRECIPITATION HARDENING IN COPPER-CHROMIUM DEFORMATION PROCESSED METAL METAL MATRIX COMPOSITES

Introduction

The major advantage of the deformation processed metal metal matrix composite, DMMC, approach to high strength copper based materials is the ability to maintain a large percentage of the exceptional electrical conductivity of pure copper. Since refractory metals, e.g. Cr, Co, V, Nb, Fe, Ta, used as the reinforcing phase have a low solubility within the copper matrix, the excellent electrical conductivity of the matrix material is preserved. Early work by Bevk found that the mechanical strengths of deformation processed alloys of copper-niobium, which produced an in-situ composite, greatly exceeded the strength that would be predicted by a rule of mixtures calculation [37]. DMMCs are unlike other high strength copper alloys which owe their enhanced mechanical properties to the presence of a fine precipitate dispersion, as for example copper-beryllium alloys. Near its melting point copper has a significant solubility for cobalt, iron and/or chromium; 8.0 At. % Co, 4.2 At. % Fe and 0.89 At. % Cr [1]. At room temperature the solubility of these metals in copper goes essentially to zero. Additionally, since there are no intermetallic compounds in these systems, they are good candidates for the production of DMMCs. In these copper alloy families, it may be possible to enhance the mechanical properties of the copper matrix by the combination of fiber strengthening and precipitation hardening. Several commercial copper alloys use cobalt, iron and chromium as precipitation hardening agents. Chromium was chosen for this study because a great deal of work on hypo-eutectic alloys has been reported in the literature, and exploratory work on cobalt and iron alloys showed that removal of these elements from solid solution was much more difficult. The extended solid solubility of chromium, 0.89 At. % @ 1076.6 ^{o}C [6], has lead to the development of 18XXX series of precipitation hardened copper alloys. However, the composition of these commercial alloy is less than the eutectic at 1.2 At. %. Only one study, by Drits et al. [36], that investigated the properties of hyper-eutectic Cu-Cr alloys was found during the literature review. During their investigation direct evaluation of precipitation hardening to improve the mechanical performance of hyper-eutectic alloys was not made.

A basic understanding of precipitation phenomena in hyper-eutectic Cu-Cr alloys and its effect on physical properties was required to develop Cu-Cr materials with more than 1.2 At. % Cr. Several fundamental questions were to be addressed in this study. First, can precipitation hardening be used to improve the mechanical properties of these alloys?

Second, what would the presence of both precipitates and fibers do to the electrical conductivity of these materials? Third, could materials with better combinations of electrical conductivity and mechanical strength be developed? To answer these questions a study of the effect of simple mechanical and thermal treatments on the electrical and mechanical properties was undertaken. Simple resistivity testing and tensile testing was done. However, additional time was devoted to mapping the kinetics of the precipitation phenomena in time/temperature space. Mapping of the precipitation phenomena in time and temperature could be used to optimize properties. The results obtained in this study can stand alone as a reference for the production of Cu-Cr alloys with excellent electrical and mechanical properties but also as a foundation from which more complicated regimes of thermomechanical processing may be designed.

Materials Production

Three Cu-Cr alloy compositions (0.7, 7.0 and 15.0 Vol. %) were produced by bottom pour chill casting from a Yttria washed graphite crucible as 25 mm ingots. After casting the ingots were solutionized for 24 hours at 1025°C and quenched into ice water. The material was cold deformed by swaging to a diameter of 15 mm after which cold drawing was used. Table 7 shows the thermal and mechanical treatment for each alloy investigated in this basic study with its nomenclature. All materials were deformed to 3 mm ($\eta = 4.2$) at this point the given nomenclature describes subsequent processing.

Table 7. Thermomechanical Treatment Schedules for the Copper-Chromium Alloys

Alloy	Composition	Steps in Processing
007Q	0.7 Vol. % Cr	S/Q A
007	" "	no further processing
007cc	" "	cc A
070Q	7.0 Vol. % Cr	S/Q A
070	" "	no further processing
070cc	" "	cc A
150Q	15.0 Vol. % Cr	S/Q A
150		no further processing
150cc		cc A

cc= Cold Deformed from 3 mm to 1.7 mm, Total η =8.2
S/Q = Solutionize 24 Hr 1025°C Quenched into Ice Water
A = Isothermally Age Material Measuring Resistivity

The three compositions of 0.7, 7.0 and 15 Vol. % Cr are coded in this nomenclature as 007, 070, and 150 respectively. The 0.7 Vol. % Cr alloy was chosen because this is the solid solution limit of Cr in Cu. This material allowed the evaluation of how the methods of producing a DMMC would affect the matrix material without the presence of fibers.

The two compositions have been commonly used in other DMMC studies. These compositions reflect the trade-offs between maximum strengthening and low deformation strain (η to strength ratio) which are enhanced by high Cr content. Good electrical properties and low production cost demand low Cr content. Three mechanical work configurations were used in this study solutionized/quenched, $\eta = 4.2$, and $\eta = 8.2$. The term η is defined as the natural log of the ratio of initial diameter to final diameter ($\eta = \text{Ln}\ (A_i/A_f)$. Solutionizing and quenching followed by aging is the classic route to precipitation hardened materials. Deformation to an $\eta = 8.2$ puts the material produced into the realm of a DMMC. Material deformed to $\eta = 4.2$ spans the gap between these two extremes.

Electrical Resistivity Measurements

Electrical resistivity measurements were conducted, using the standard 4-probe technique, to follow the removal of chromium from solid solution during the aging processes [38]. Generally, the bulk resistivity can be approximated by a simple summation of all the possible resistivity contributions as in Equation 5 [33].

5) $\rho_t = \rho_o + \rho_d + \rho_{ss} + \rho_{int}$

ρ_t = Total Measured Resistivity
ρ_o = Pure Element Resistivity at 0^oK plus thermal motion
ρ_d = Defects
ρ_{ss} = Solid Solution Atoms
ρ_{int}= Interfaces and Boundaries

In this study the aging phenomena was measured by changes in the electrical resistivity. It was desired to perform these measurements in real time at the selected isothermal aging temperature. This is unlike other studies where the material was isothermally aged then quenched to room temperature prior to the measurement of physical properties [39, 15]. This procedure leaves to question whether quenching truly halts the microstructural changes taking place. In order to get an accurate picture of the isothermal

aging process, the sample must be heated to the desired temperature as quickly as possible. Additionally, since the aging phenomena was to be measured by electrical resistivity, electrical isolation is imperative. To this end a fluidized bed furnace was constructed with an immersible four point resistivity apparatus. In this device aluminum oxide is suspended in a helium atmosphere within a quartz tube and heated by a conventional resistance furnace. The fluidized bed maintains a heat transfer coefficient similar to that for liquid media while the alumina and helium heat transfer media also provide for electrical isolation. Calculations have shown that the samples placed within the hot zone reach 90% of the bed temperature in 2 minutes at a bed temperature of 500°C [40]. This was verified using a pure copper sample, a wire 3.0 mm in diameter, which obtained 500°C in the same time as previously calculated. The variation in electrical resistivity due to thermal fluctuations, as the sample approaches the bed temperature, is less than 0.1 μΩ-cm. The thermal variation, within the bed over time, was also measured and found to be +/- 3.0°C over an 8 hour period.

Electrical Resistivity Data Treatment

The first task undertaken was the development of the time/temperature/resistivity maps characterizing the precipitation reaction. The kinetics were measured by holding a sample isothermally and measuring the change in electrical resistance over time. To investigate the aging process measurement of the electrical resistivity and sample temperature was done at 30 sec intervals over a 6 hour period. The temperatures selected for aging were 270°C, 330°C, 380°C, 430°C, 480°C, and 520°C. Resistivity and temperature data was gathered with the aid of an Apple Macintosh II Ci personal computer using software written by Dr. Harry Downing of Drake Univ. A Keithley digital voltmeter/scanner model 1992 interfaced to the Macintosh made the resistivity and temperature measurements. Isothermal resistivity data obtained was used to create time/temperature/resistivity plots. The raw data plots are similar to that shown in Figure 15.

It was necessary to correct the raw experimental data for thermal scattering, interfaces, and the equilibrium solid solution concentration of chromium. To accomplish this the resistivity of annealed alloys was used as a standards. To obtain the value of ρ_{std} a sample of each alloy composition was solution treated at 1025°C for 24 hours. This coarsened and homogenized the microstructure of the material which was furnace cooled to

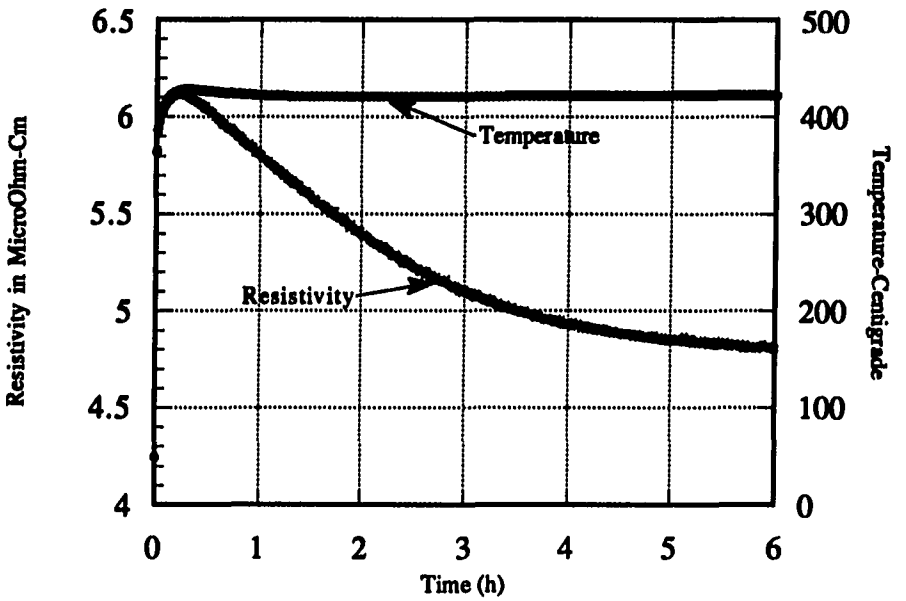

Figure 15. Temperature and Resistivity versus time for a Copper-0.70 Vol. % Chromium Alloy Aged at 430°C

room temperature over 48 hours. To measure the value of ρ_{std}, the standard for the alloy as a function of temperature, the sample was ramped from room temperature to 820°C at 1°C per minute. During the ramping processes the electrical resistivity was measured at every degree as illustrated in Fig. 16 for the 0.7 Vol. % Cr alloy.. Therefore, these data reflect the thermal resistivity response of the alloy in its aged state. The experimental data were then fitted with a third order polynomial and the results are presented in Table 15.

Equation 6 describes the measured resistivity in terms of the contribution of the standard alloy (ρ_{std}) and an increment in resistivity ($\Delta\rho$)

6) $\rho_t = \rho_{std} + \Delta\rho,$

where ρ_{std}, is the resistivity value of the aged alloy at the isothermal aging temperature. From Equation 5 ρ_{std} is given by Equation 7 and $\Delta\rho$ is given by Equation 8.

7) $\rho_{std} = \rho_o + \rho_{ss} + \rho_{int} + \rho_d$

8) $\Delta\rho = \rho_t - \rho_{std} = \Delta\rho_{ss} + \Delta\rho_{int} + \rho_{ppt}$

Where $\Delta\rho_o = 0$ as the program corrects to the isothermal aging temperature, $\Delta\rho_d = 0$ because ρ_d has been shown to be a constant above the recrystallization temperature [33]. Therefore, $\Delta\rho$ measure three microstructural changes taking place during isothermal aging: precipitation of chromium from solid solution, microstructural coarsening and the formation of chromium

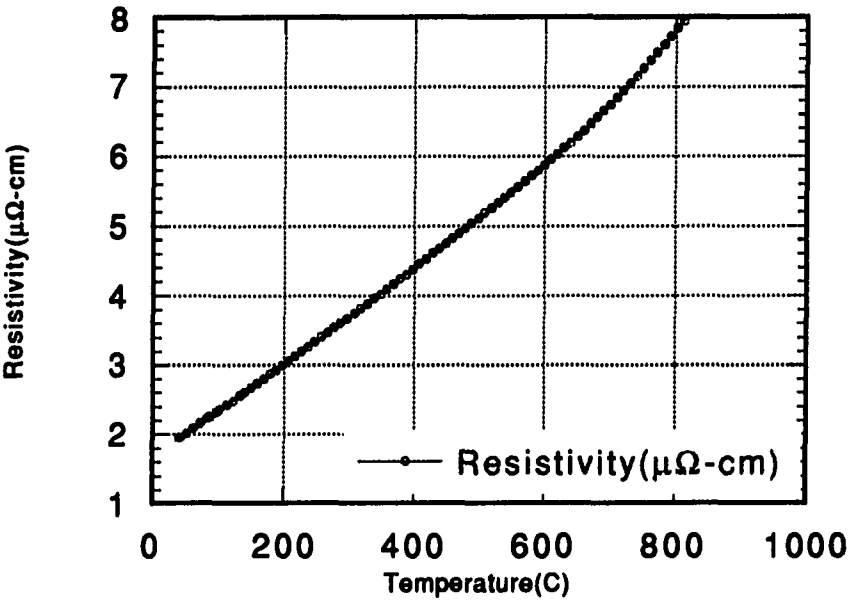

Figure 17. Resistivity of a Copper-0.70 Vol. % Chromium Alloy in the Range 20°C to 820°C

precipitates. A plot of the uncorrected data and $\Delta\rho$ is shown in Figure 18. The value of ρ_{std} may be conveniently used as a reference here, because it represents the minimum possible resistivity and, hence the optimum conductivity obtainable with an alloy of a given composition. The value of $\Delta\rho$ will decay with time and, if the precipitate and filaments coarsen adequately, it will go to zero as shown in Figure 18 Hence, the expression $1-\Delta\rho/\Delta\rho_o$ represents a measure of the fraction of the maximum electrical conductivity achieved during aging.

Table 9. Values of Constants for Standard Resistivity, ρ_{std}

Alloy Type	ρ(meas)	M0	M1	M2	R(factor)
CUCR007800	1.626	.00748	-3.2513	.4394	0.99993
CUCR070800	1.840	.00751	-1.7213	3.0647	0.99997
CUCR150800	1.850	.00830	-3.0362	4.3305	0.99996

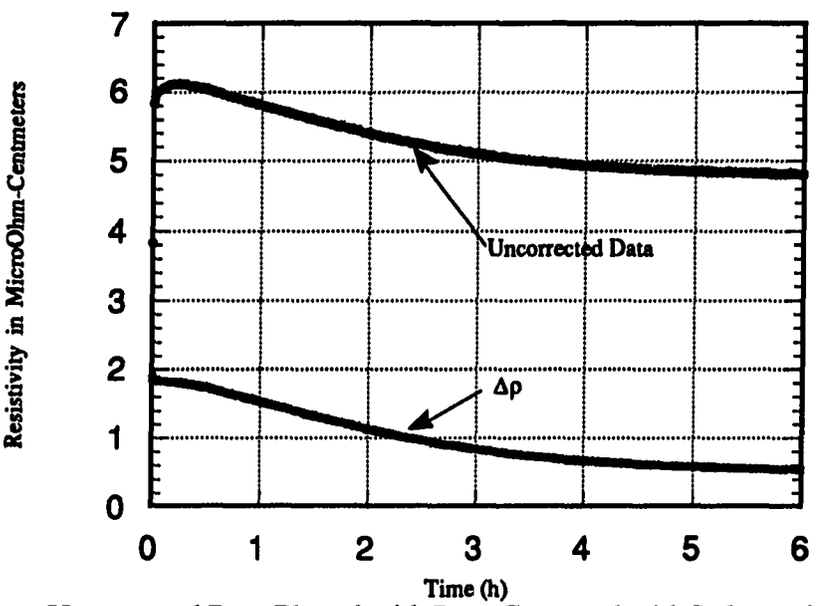

Figure 18. Uncorrected Data Plotted with Data Corrected with Polynomial and Data Corrected with Polynomial and for Volume Fraction

Experimental Data

Electrical resistivity measurements are a standard analytical technique for the evaluation of the kinetics of solid state metallurgical reactions [33]. Intimate knowledge of the kinetics of solid state reactions allows the optimization of processing to obtain the desired properties. The hope is to create a Time/Temperature/Physical Property map to aid in this endeavor. The diagrams presented here can be used to determine the time necessary to give the best electrical properties in these alloys in the temperature range 270°C to 530°C.

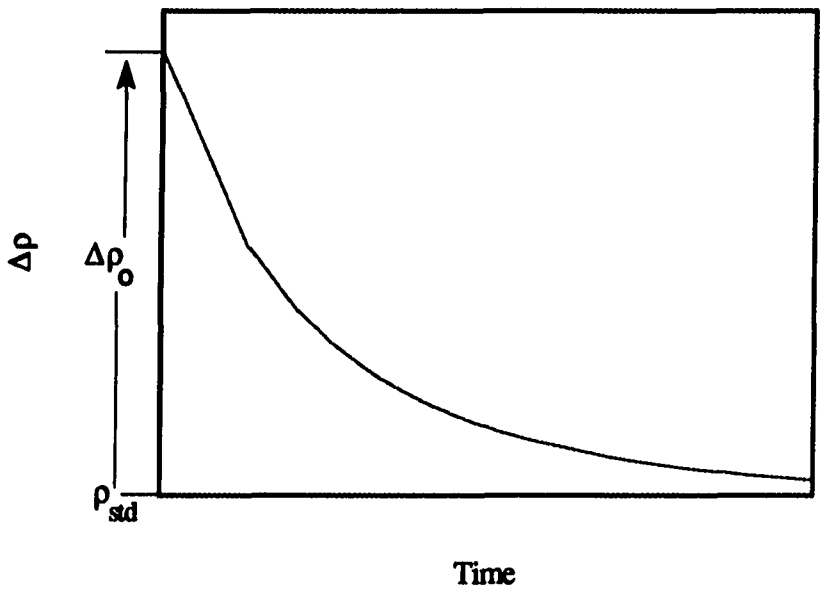

Figure 19. Decay of $\Delta\rho$ from Initial State to ρ_{std}, the Final State

Therefore, the diagrams are valuable in the design of processes to produce these materials and as a base for more complicated deformation and thermal treatment schedules. The procedure outlined in the description of the resistivity study was used with all nine alloys at all five aging temperatures (270°C, 330°C, 380°C, 430°C, 480°C, and 520°C) and used to construct an aging diagram. The value of the resistivity ratio was subtracted from one to plot the percentage approach to the maximum conductivity versus time. On these diagrams the time necessary to obtain a percentage maximum conductivity value of 0.25, 0.50, 0.75, and 1.00 is plotted along with the aging temperatures. These are shown in Figures 20 to 25 for each of the alloys investigated in this study.These diagrams are to be used in the same manner as the Isothermal Transformation (ITT) diagrams common to steel metallurgy. The materials designer selects the desired resistivity of the material and consults the diagram for the proper time and temperature necessary to reach a defined goal.

Measurements of the change in electrical resistivity during isothermal aging treatments was also done on material deformed to an $\eta = 8.2$ (samples 007cc, 070cc and 150cc). However, no response to aging was found in any of the three compositions when held for up to six hours in the temperature range 270°C to 530°C. This is a very interesting

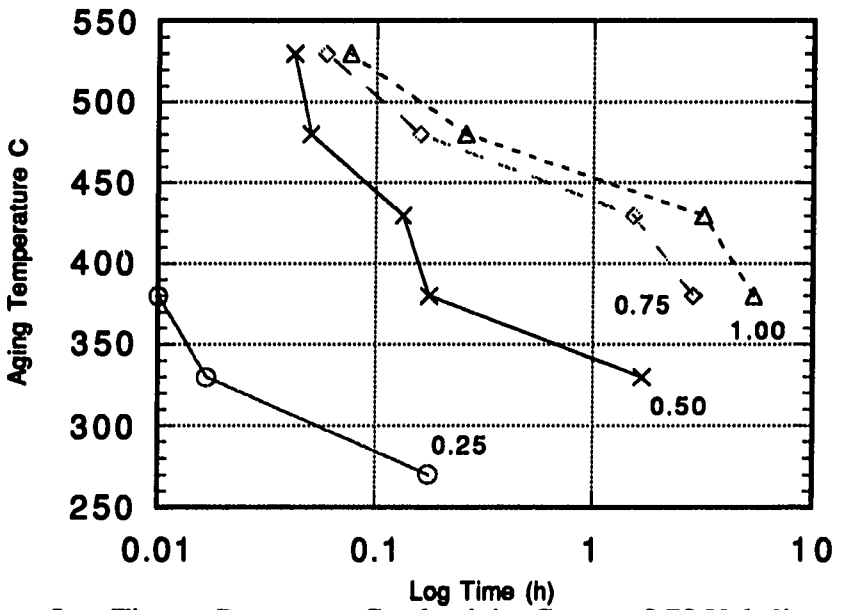

Figure 20. Log Time to Percentage Conductivity Copper- 0.70 Vol. % Chromium Alloy Solutionized and Quenched Sample, 007Q

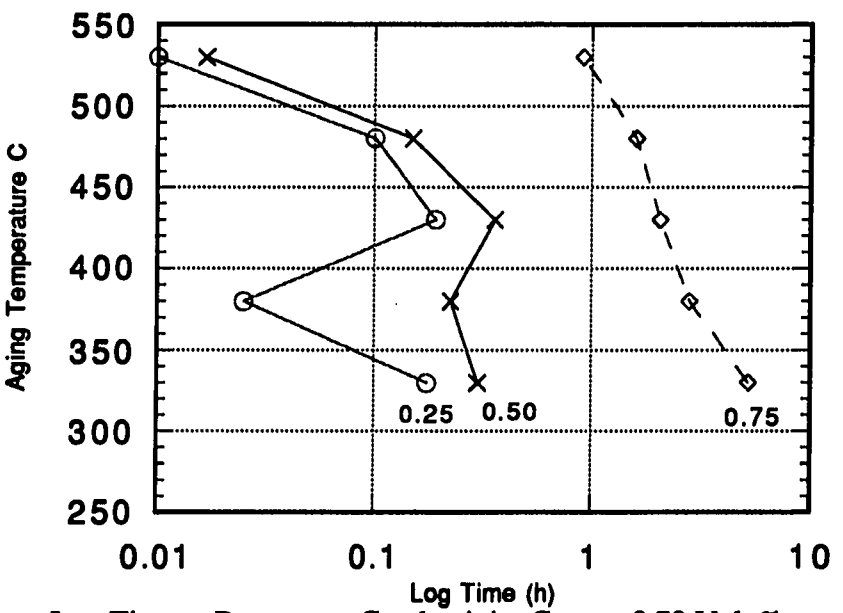

Figure 21. Log Time to Percentage Conductivity Copper-0.70 Vol. % Chromium Cold Worked Sample, 007

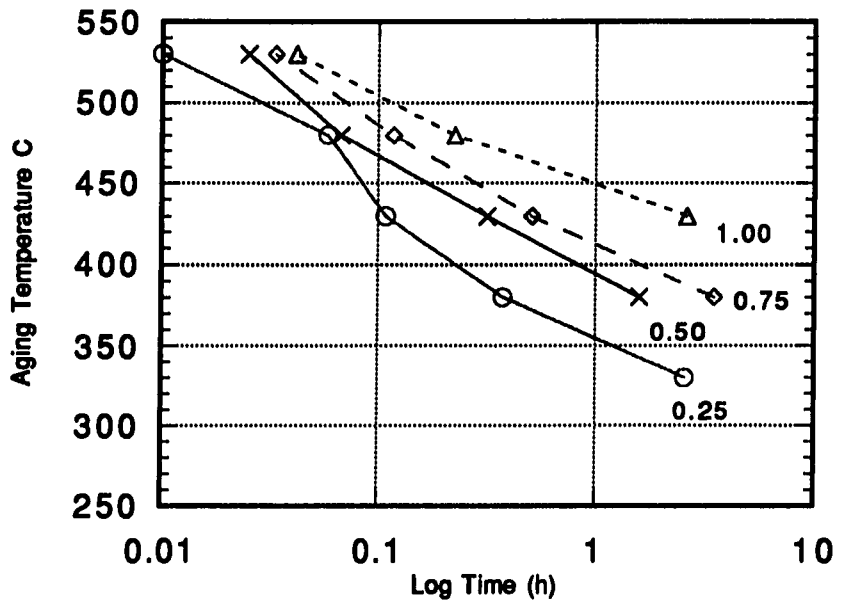

Figure 22. Log time to Percentage Conductivity Copper-7.0 Vol. % Chromium Solutionized/Quenched Sample, 070Q

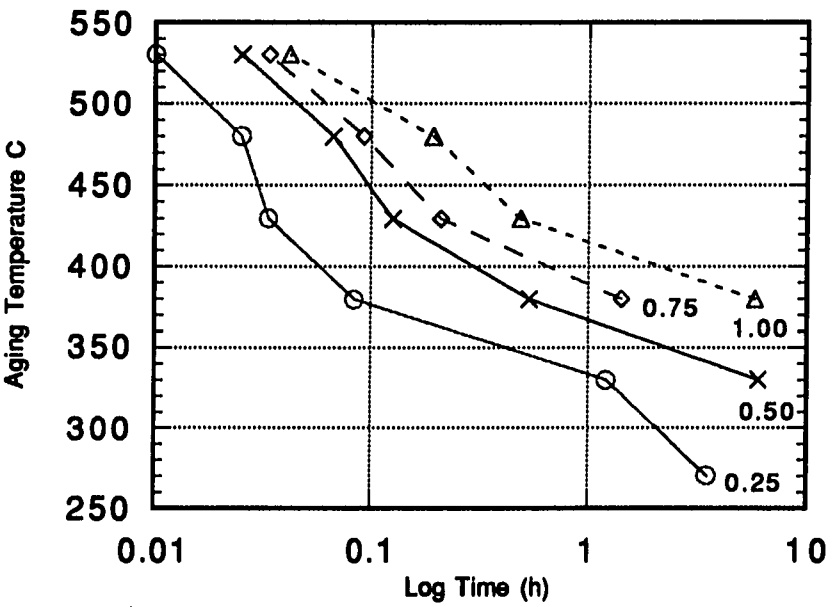

Figure 23. Log Time to Percentage Conductivity Copper-7.0 Vol. % Chromium Cold Worked Sample, 070

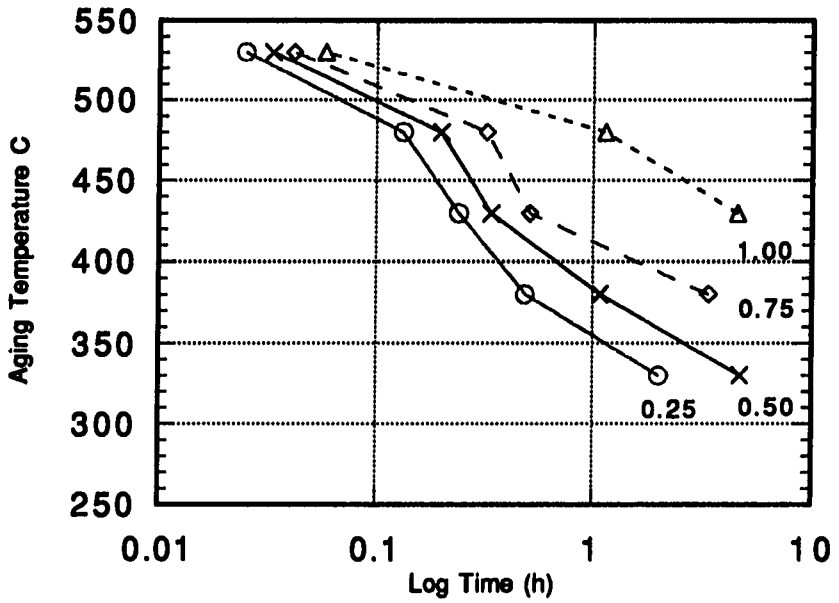

Figure 24. Log Time to Percentage Conductivity Copper-15.0 Vol. % Chromium Solutionized/Quenched. Sample, 150Q

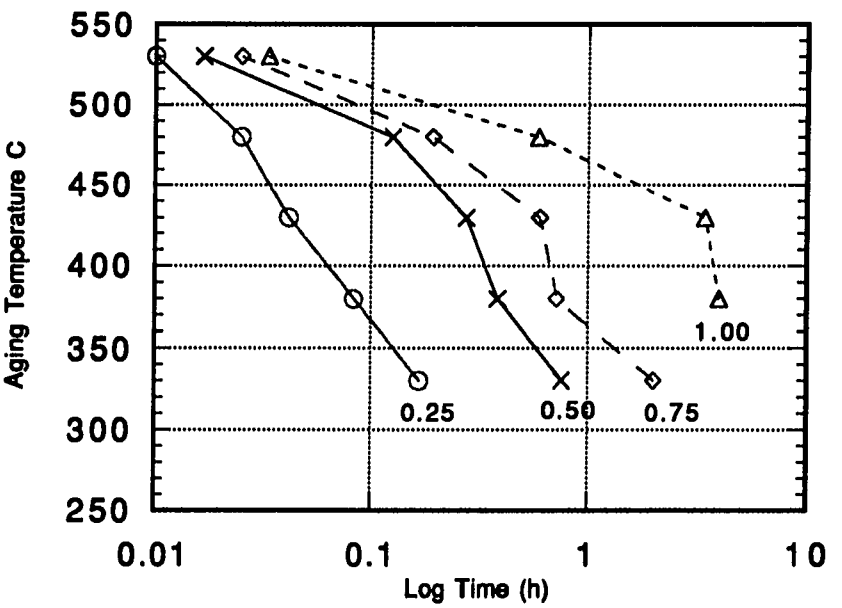

Figure 25. Log Time to Percentage Conductivity Copper-15.0 Vol. % Chromium Cold Worked Sample, 150

result as thermomechanical treatment has been shown to improve both the electrical conductivity and physical properties of hypo-eutectic Cu-Cr materials [28, 41]. These previous studies did not include the effect of deformation strains beyond $\eta = 1$. Thus it would appear that mechanical working of the present hyper-eutectic alloys to a true mechanical strain of 8.2 either leads to complete removal of chromium from solid solution or, possibly the precipitation event occurs faster than the resistivity technique can respond, a time interval of less than 30 seconds.

In Figures 26 and 27 comparison plots were created showing the time necessary to obtain a certain fraction of the maximum conductivity for both solutionized/quenched and the cold worked material. In the case of solutionized/quenched the solid solution alloy (007Q) has the fastest initiation of reaction. The initiation of 070Q causes a reaction somewhat faster than 150Q, but both are slower than 007Q. All three alloy compositions reach the same conductivity at essentially the same time. Cold worked cases 070 and 150 both initiate faster than 007. This is the reverse of the solutionized/quenched case. Cold working has, as stated, been found to greatly increase the removal of chromium from solution. This is thought to be due to the accumulation of dislocations and extra stored work which aids in the creation of nuclei and provides high diffusivity pathways for precipitate growth [42, 43]. In the 7.0 and 15.0 Vol. % alloys the kinetics of precipitation are enhanced by cold working which seems to confirm this observation. The initiation of the precipitation is slowed down by cold working in the 0.7 Vol. % alloys. Again, previous studies of the effect of cold working on the precipitation kinetics of hypo-eutectic Cu-Cr alloys indicate an improvement, but the deformation strains were low, $\eta = 1$ maximum. It is also noted that the 007 material does not reach a completed reaction in the 6 hour aging process at 430°C. In fact the 007 alloy does not reach a $\Delta\rho = O$ in the temperature range of 270°C to 520°C.

Mechanical Testing

The effect of isothermal aging on the tensile behavior of all nine alloy combinations, given in Table 9, was also studied. The materials were isothermally aged at one temperature (430°C) for 0, 0.166, 0.5, 1, 2, 3, and 6 hours. This temperature was selected as it was the lowest temperature at which all reactions went to $\Delta\rho=0$ indicating maximum conductivity. One exception was the 007 alloys which never achieved $\Delta\rho = 0$. These materials were aged using the fluidized bed to duplicate the conditions used in gathering the resistivity data. All samples were quenched into ice water to stop the aging reaction. Tensile specimens were

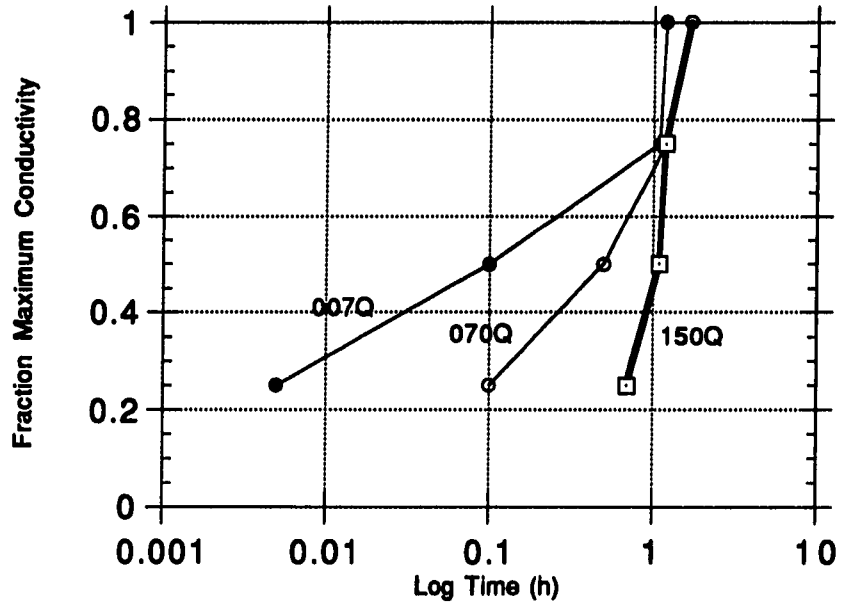

Figure 26. Fraction Maximum Conductivity versus Log Time for all Three Solutionized and Quenched Alloys aged at 430°C

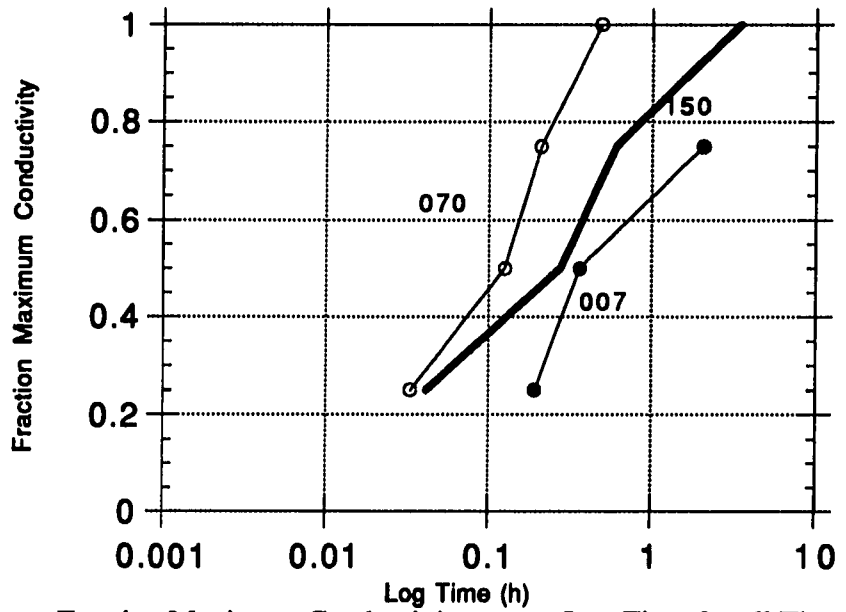

Figure 27. Fraction Maximum Conductivity versus Log Time for all Three Cold Worked Alloys aged at 430°C

prepared by abrasive polishing. Tensile testing was done using an Instron model 4505 at a strain rate of 5 mm/min. Strain measurements were accomplished using a clip on strain gauge. All tensile tests were run in duplicate and the results averaged for reporting.

In the following Figures 28 to 30, the ultimate tensile strength in Mpa versus aging time at 430°C is plotted for each alloy composition. All three deformation conditions are plotted on the same figure for each alloy. This will facilitate a direct comparision at a constant composition of the effect of cold work.

Figures 31 to 33, the ultimate tensile strength in Mpa versus aging time at 430°C is plotted for each cold worked condition. All three alloy compositions are plotted on the same figure for each deformation state. This will allow the direct comparision, for each specific amount of cold work, of the effect of composition.

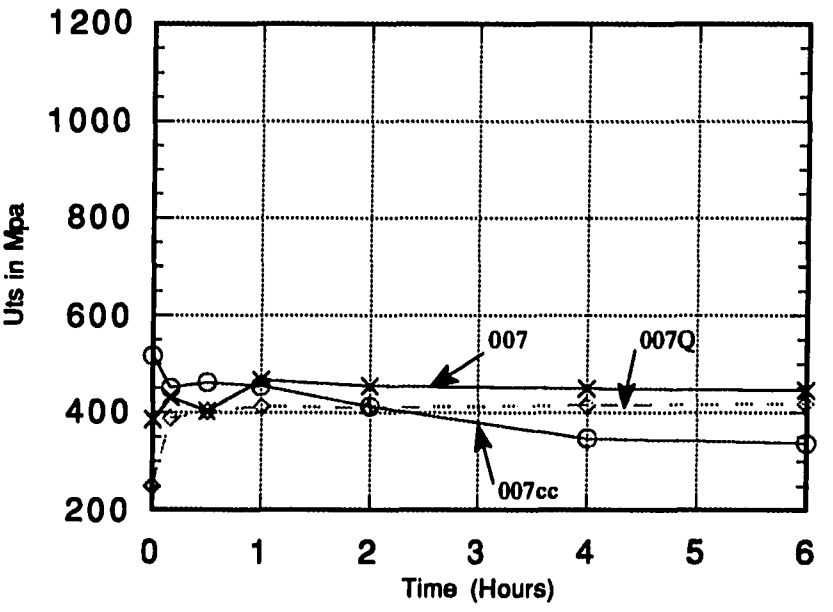

Figure 28. Cu-0.70 Vol. % Cr Ultimate Tensile Strength versus Aging Time in Hours at 430C° in Three Deformation States

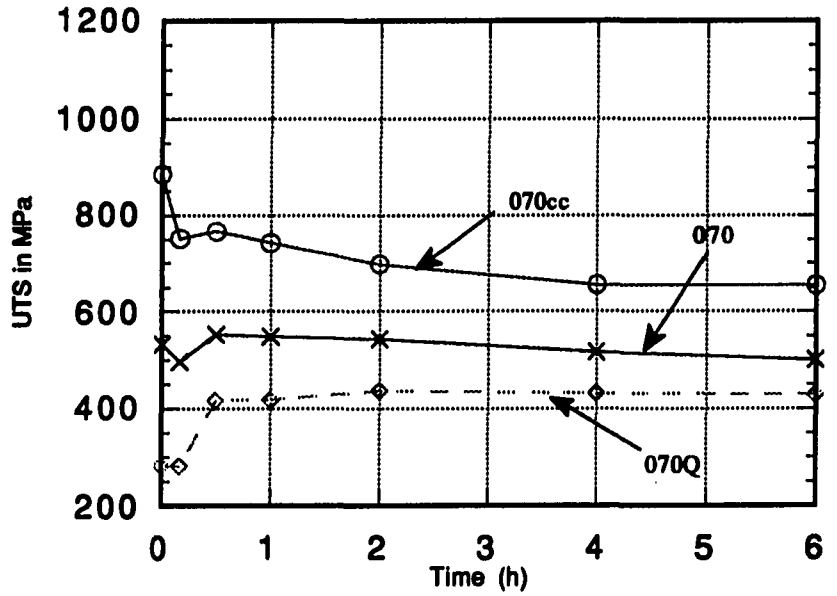

Figure 29. Cu-7.0 Vol. % Cr Ultimate Tensile Strength versus Aging Time in Hours at 430C^{o} in Three Deformation States

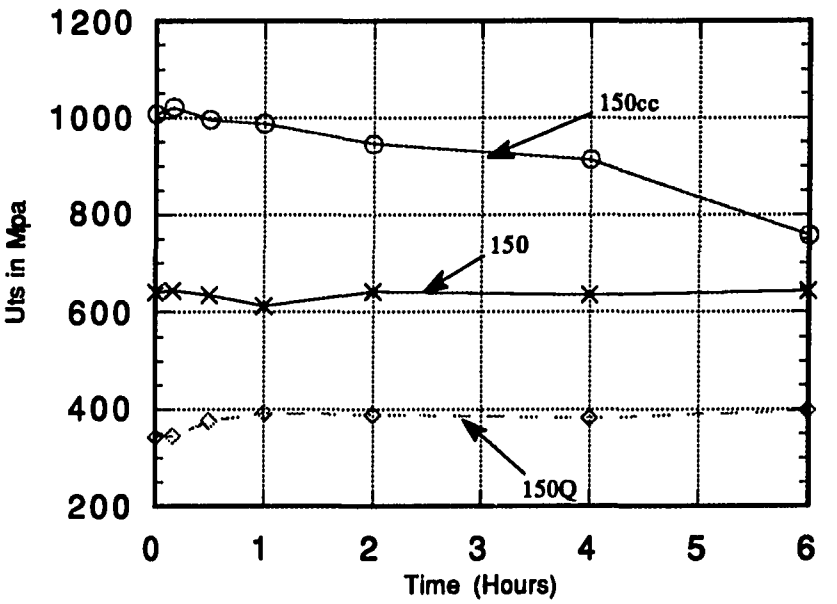

Figure 30. Cu-15.0 Vol. % Cr Ultimate Tensile Strength versus Aging Time in Hours at 430C^{o} in Three Deformation States

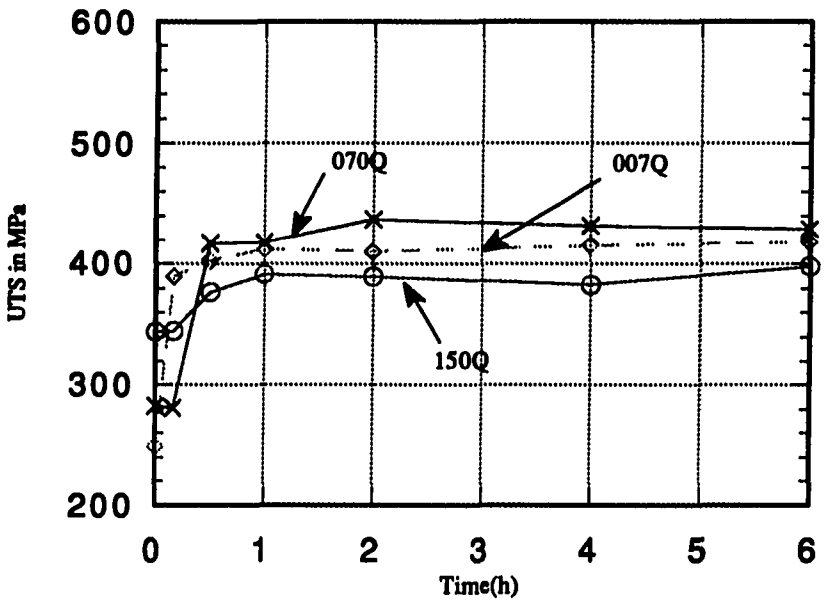

Figure 31. Ultimate Tensile Strength versus Aging Time at 430C° for Cu-Cr Alloys 0.7, 7.0 and 15.0 Vol. % aged at 430°C, after Solutionized and Quenched

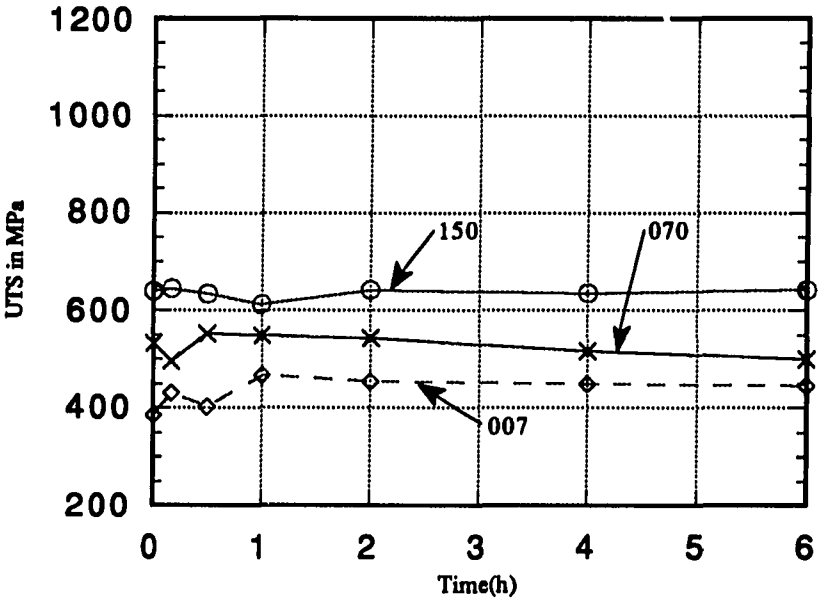

Figure 32. Ultimate Tensile Strength versus Aging Time in Hours at 430°C for Cu-Cr Alloys 0.7, 7.0, and 15.0 Vol. % in original state

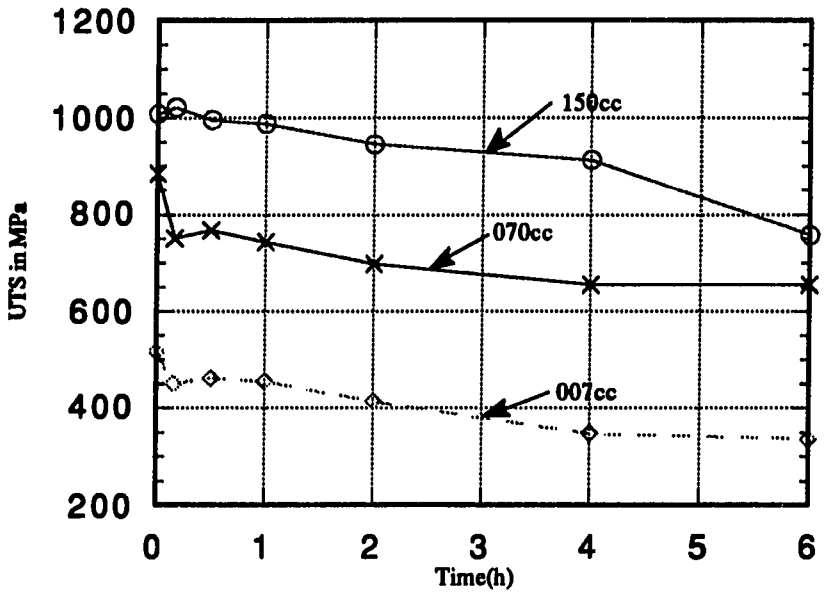

Figure 33. Ultimate Tensile Strength versus Aging Time in Hours at 430C° for 0.70, 7.0, and 15.0 Cu-Cr Vol. % Alloys after Cold Deformation of $\eta = 8.2$

Mechanical Testing Data Analysis

Several generalities can be derived by investigation of the preceding data set. First, increasing the amount of mechanical work in any of the alloys studied here also at some point increases the mechanical strength. This increase in strength may be brought about by increased dislocation density from the mechanical working. Second, increasing the chromium content, with the exception of the solutionized/quenched material, leads to an increase in the mechanical strength of the alloy. A simple rule of mixtures calculation for a two phase alloy would predict an increase in strength as the chromium content is increased. However, this simple assumption does not hold true as revealed by the solutionized/quenched samples where an increase in chromium content leads to little or a slightly negative effect on tensile strength. This result indicates that the enhanced tensile strength observed in the high chromium alloys after cold working is due to another effect not simply related to a rule of mixtures calculation. As seen in other copper-refractory metal alloys, a significant amount of dislocation blocking can be accomplished by the production of a fine two phase microstructure. Although this is dependent upon the presence of a second phase, the properties of the material have very little direct correlation to a rule of mixtures approach to predicting or evaluating mechanical properties. Third, a strong aging was only found in the

solutionized/quenched material. Aging appears to have little or no effect on the UTS of materials deformed to $\eta = 4.2$. A marked reduction in UTS is found when the material deformed to $\eta = 8.2$ is aged at 430°C. As discussed in the resistivity section, the extensive cold deformation these materials undergo could lead to precipitation of chromium from solid solution during dynamic recrystallization of the copper matrix. Refinement of the microstructure by mechanical working reduces the spacing of the primary chromium filaments. At high η values this spacing may be less than the diffusion field for the formation of precipitates. Therefore, precipitation takes place on the filaments, not as discreet particles. Without a gross change in microstructure the precipitation event does not affect mechanical strength. Additionally, increases in the amount of chromium in the solutionized/quenched state also decreases the response to aging. This is not surprising, using the previous discussion, as high primary chromium content leads to faster refinement and higher surface area for the precipitation of solid solution chromium.

Correlation of Electrical and Mechanical Property Data

Previous studies of DMMCs produced from copper-refractory metal alloys have evaluated the engineering merit of the material by plots of ultimate tensile strength (UTS) versus the percentage of the International Annealed Copper Standard (100% IACS) [44]. By this evaluation the best material would have the highest electrical conductivity and the highest strength. Figure 34 is such a plot for commercially available copper alloys used for high conductivity or high strength applications. A rough correlation can be made between strength and conductivity as indicated by the line drawn through the diagram. This is not surprising as most of the alloys owe their enhanced mechanical properties to the presence of second phase particles.

The 17XXX alloys (Cu-Be alloys) obtain high strength from the formation of monolayer plates brought about by an aging process. Since these precipitates disrupt the continuous copper lattice, they lead to maximum hardening but pay the penalty of high electron scattering leading to poor electrical conductivity. This effect is also seen in copper-chromium alloys in the solutionized/quenched condition (18200Q). When chromium is in solution it leads to poor electrical conductivity with little of enhanced mechanical properties. On the other end of the spectrum is, of course, pure copper with high electrical conductivity but poor mechanical performance. Various other combinations have been tried to improve performance in these conventional alloys, but a compromise must always be struck between electrical and mechanical properties.

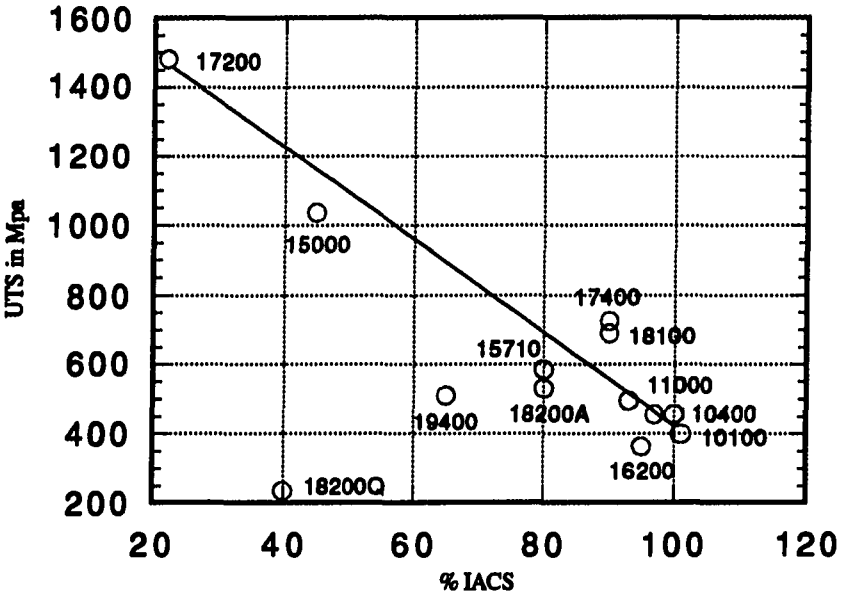

Figure 34. Ultimate Tensile Strength versus % IACS for Commercial Copper Alloys

To present the data of this section a different nomenclature from that given earlier is used. Again, the starting material is 3 mm wire prepared from the ingot by a solutionizing and quenching treatment followed by cold reduction from 25 mm to 3 mm, $\eta = 4.3$. Additional processing steps are coded as shown in Table 10:

Table 10. Nomenclature for Thermomechanically Processed Copper-7.0 Vol. % Chromium

Sample Code	Steps in Processing
007	No Additional Processing, Original Material
007A	Isothermal Age 6 hours 430°C
007cc	Deformed to total $\eta = 8.2$
007ccA	Deformed to total $\eta = 8.2$ Followed by Aging 430°C for 6 hours
007Q	Solutionized and Quenched
007QA	Solutionized and Quenched Followed by Aging 430°C for 6 hours

Figures 35 to 37 are identical plots for the three alloy compositions and each of the three mechanical states produced for this study. In the tensile strength data the UTS was determined at seven aging times over a six hour period. Here the data obtained at t = 0 and at t = 6 hours at 430°C only was plotted.

Aging of the alloys for 6 hours improves the electrical conductivity in all cases. When the materials are solutionized/quenched there is an improvement in mechanical properties after aging. Cold deformation to an $\eta = 4.2$, gives a small reduction in UTS after aging. Cold deformation of the materials to $\eta = 8.2$, which are then aged for 6 hours at 430°C, leads to a degradation of mechanical strength although electrical properties are improved. Only the materials cold deformed to an $\eta = 8.2$, either in the cold worked or aged condition, fall within the range of properties available in present commercial alloys. The material deformed to $\eta = 8.2$ shows a marked decrease in strength unlike the other two cases. This result supports the conclusion of the resistivity study where no response to aging in the range 270°C to 520°C was found. Therefore, mechanical deformation to $\eta = 8.2$ prevents the use of precipitation hardening as a mechanism to improve the mechanical strength of these materials. Additionally, electrical conductivity is also not markedly improved. As such little, if any, benefit is directly gained by aging these materials in the $\eta = 8.2$ range.

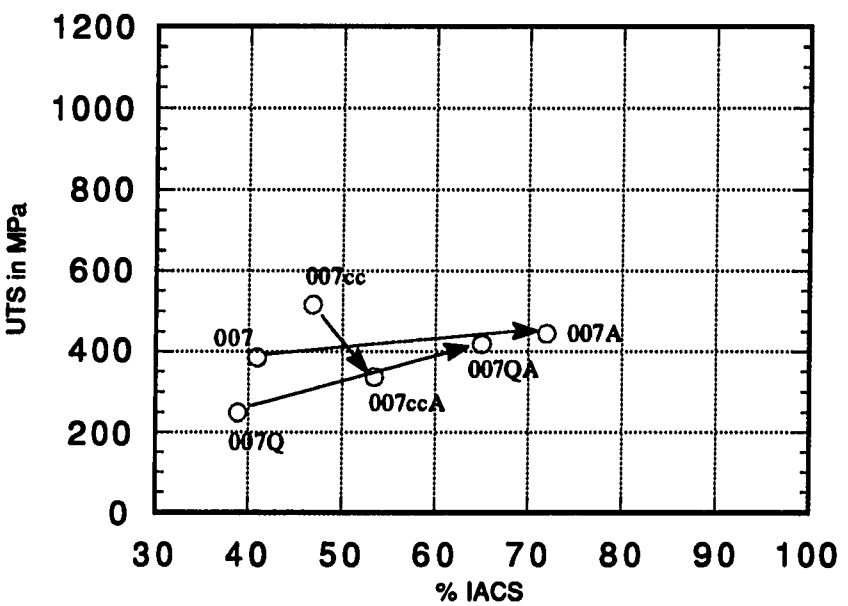

Figure 35. Ultimate Tensile Strength versus % IACS for Cu-0.7 Vol. % Cr in each Mechanical State Before and After aging at 430°C for 6 Hours

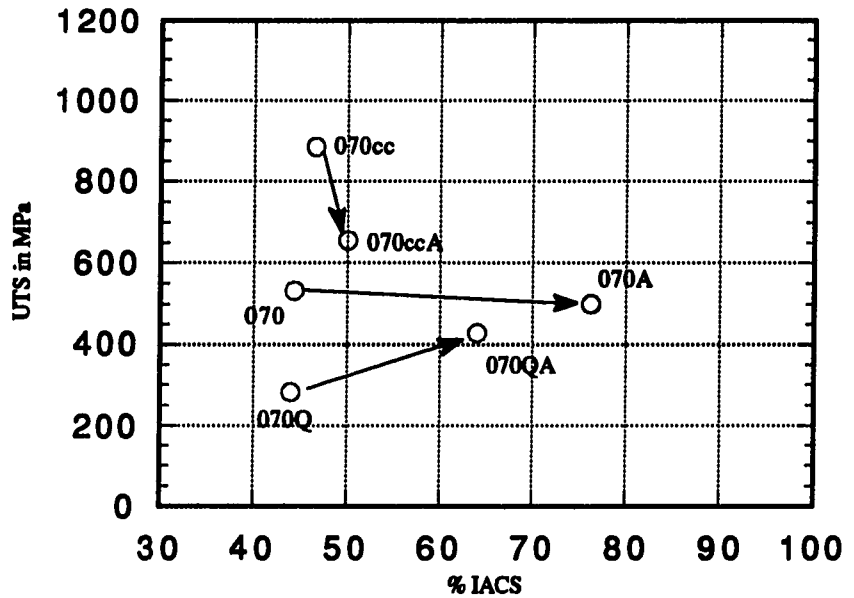

Figure 36. Ultimate Tensile Strength versus % IACS for Cu-7.0 Vol. % Cr in each Mechanical State Before and After aging at 430°C for 6 Hours

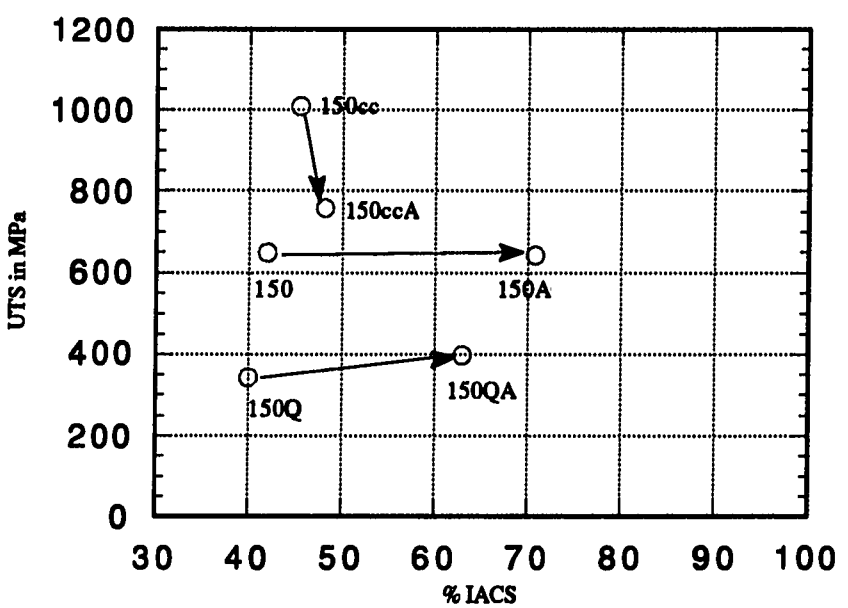

Figure 37. Ultimate Tensile Strength versus % IACS for Cu-15.0 Vol. % Cr in each Mechanical State Before and After aging at 430°C for 6 Hours

Plots of IACS vs UTS allow presentation of the experimental data in a manner in which an informed discussion of materials properties is possible. However, this method does not definitively indicate which particular material has the highest overall combination of properties. To aid in quantifying which materials have the best combination of properties, a new definition of performance was developed. This is a Figure of Merit (FM) analysis. Defining a figure of merit to compare these materials to the IACS standard material allows us to compare all the compositions and thermomechanical treatments on an equal playing field. The experimentally measured tensile strength and electrical conductivity are multiplied together. This equally weights the merit of both types of physical performance, electrical and mechanical. This value is then divided by the electrical conductivity, defined as 100 % of the International Annealed Copper Standard (IACS), and the tensile strength of that standard, 220 MPa. This normalizes the data to a standard material. The value of the FM indicates the performance of a chosen material as a multiple of the IACS standard material. Calculation of the FM is shown in Equation 7.

7) $$\frac{\text{UTS(sample)*\%IACS(sample)}}{\text{UTS(IACS) * 100 (\% IACS)}} = \text{Figure of Merit (FM)}$$

In Figure 37 this analysis has been carried out on commercially available materials for Figure 34. The highest FM is approximately 3. These correspond to 17200 (a Cu-Be alloy) and 18100 (a Cu-Cr alloy). These alloys present the best overall performance.

Using the FM analysis to select the optimum alloy can be missleading. A comparision of two copper alloys, with widely varying physical properties but a similar FM, illustrates this point. The alloy 17200 has a very poor (32 % IACS) conductivity but excellent mechanical strength (1500Mpa). In contrast the electrical conductivity of 18100 is very good (85 % IACS) while its mechanical performance is, however, much poorer at 700 MPa. Therefore, if the engineering application requires a UTS of 1000Mpa and a conductivity of 50 % IACS neither alloy will be suitible even though the FM for this application can be matched by either alloy. Most commercial alloys seem to have a FM of approximately 1.5 to 2.0 The same data treatment has also been carried out on the DMMCs produced in this study using the data from Figures 35 to 37. Figures 39 to 41 show the FM versus deformation strain, η, for all three alloy compositions, three mechanical treatments, and with and without aging at 430^{o}C for 6 hours. Inspection of these plots shows the best

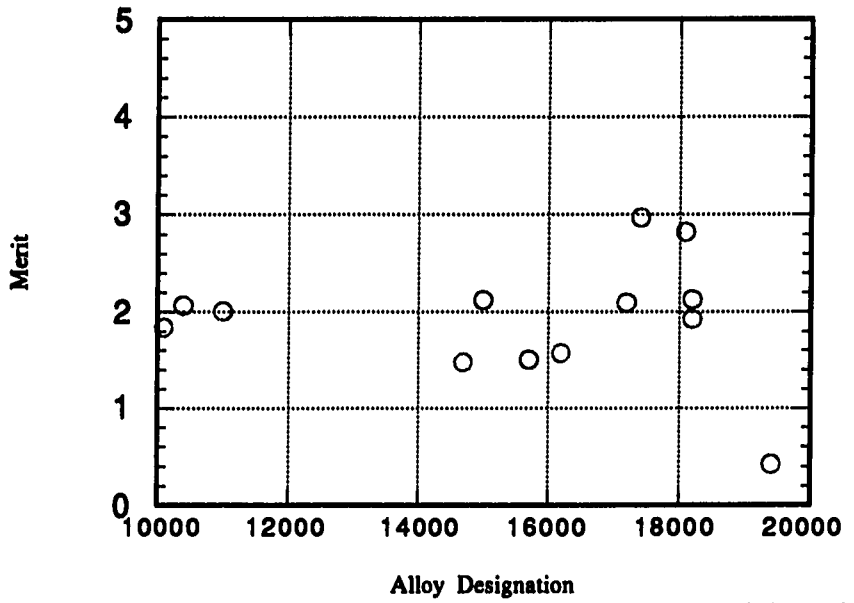

Figure 38. Figure of Merit versus Alloy Designation for Commercial Precipitation Hardend Copper Alloys by INCA Designation

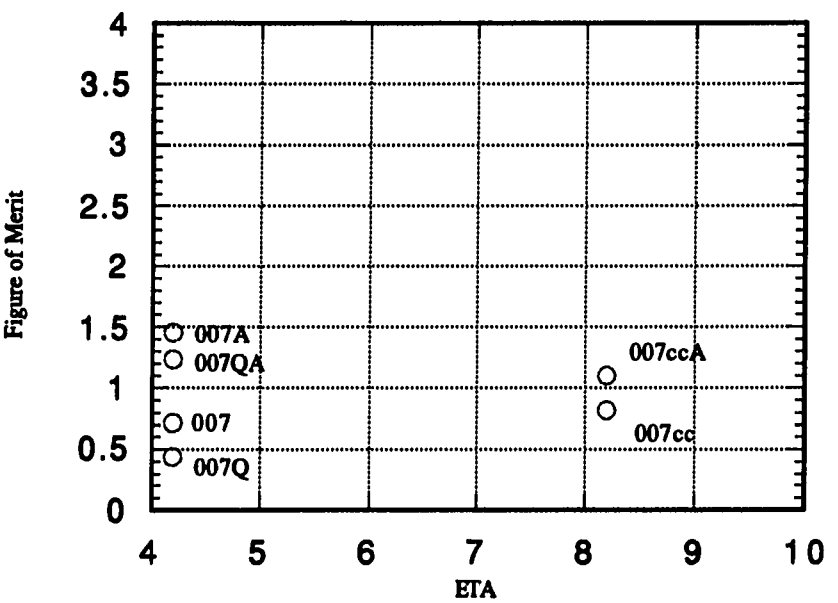

Figure 39. Figure of Merit versus Eta for Cu-0.7 Vol. % Cr in each Mechanical State Before and After Aging at 430°C for 6 Hours

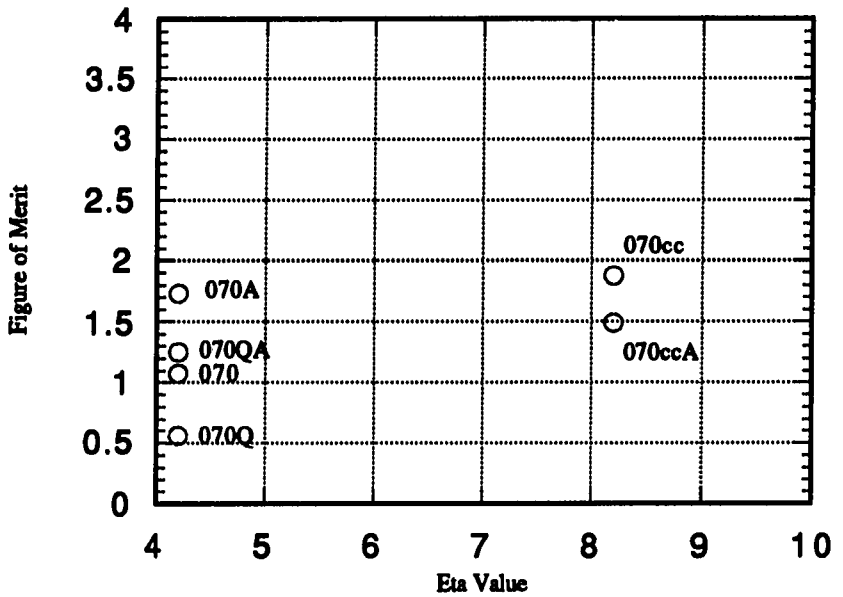

Figure 40. Figure of Merit versus Eta for Cu-7.0 Vol. % Cr in each Mechanical State Before and After Aging at 430°C for 6 Hours

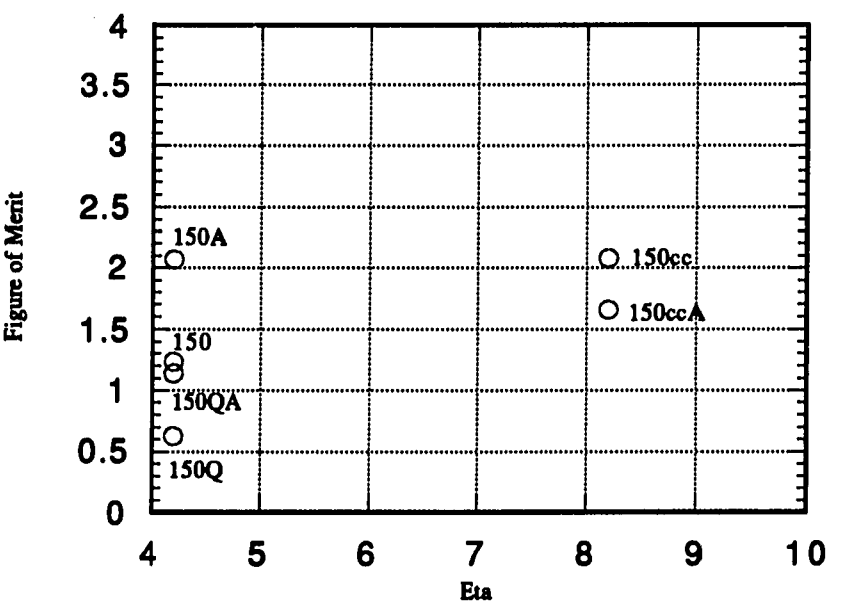

Figure 41. Figure of Merit versus Eta for Cu-15.0 Vol. % Cr in each Mechanical State Before and After aging at 430°C for 6 Hours

materials produced in this study have an FM = 2 It is interesting to note that an FM of 2 can be accomplished in two ways: either cold working to an $\eta = 8.2$ or cold working to $\eta = 4.2$ followed by aging for 6 hours at 430°C. Both the 7.0 and 15.0% alloys give an FM = 2 in these conditions. Therefore, a given FM can be obtained by several different mechanical and thermal treatments and by several alloy compositions.

Conclusion

It is very apparent in this study that the best material properties are obtained by combining thermal and mechanical treatment. Electrical and mechanical properties are both improved by combination processing. The total performance of the alloys produced in this study, determined by their FM, is poorer than expected. Although not worse than many commercial alloys, the total property package does not compete favorably with the copper-beryllium alloys or with modified precipitation hardened copper-chromium alloys. The original three questions posed in the introduction, have been answered. Isothermal aging leading to the precipitation of chromium can be used to improve the electrical properties of these alloys. Mechanical properties are also improved by aging the solutionized and quenched material. While the material deformed to $\eta = 4.2$ shows a small reduction in mechanical strength after aging, isothermal aging after cold deformation to $\eta = 8.2$ greatly reduces the UTS of these materials. The electrical and mechanical properties of the alloys produced in this study are not as promising as hoped for. This work does, however, provide a solid base from which to investigate more elaborate schemes of thermomechanical processing. In the next section of this dissertation, more complex modes of thermomechanical processing are explored for the 7.0 Vol. % alloy. This was done to produce materials with a FM equal to or greater than 3.

THERMOMECHANICAL PROCESSING OF A CU-7.0 Vol. % CR DMMC

Introduction

As outlined in the previous section simple thermomechanical processing does improve the properties of both hypo and hyper- eutectic Cu-Cr alloys. All the processing schemes used in in the basic study consisted of solutionized/quenched followed by combinations of mechanical working and aging. With the highest Figure of Merit (FM) being about 2 these materials did not show properties which are exceptional to others which are already commercially available. Using the information gathered in experimental work presented in the basic study, more complex regimes of thermomechanical processing have been designed which may produce materials with higher FMs. Work in this area has been done by Gary Haupt and Paul Berge under the direction of Dr. John Verhoeven. This work was funded by the Center for Advanced Technology and Development (CATD) at Iowa State University. Their efforts centered on optimizing the processing of these materials. However, their study did not have the benefit of the kinetics maps produced in Section 3 of this work, nor did it use TEM to evaluate microstructural causes for the observed changes in strength and conductivity. Using the results of their work as a global view of the problem, this study has focused on how the properties are developed in these materials.

Experimental Results

One alloy composition, 7.0 Vol. % Cr, one solutionizing condition (1025^{o}C) and one aging temperature (430^{o}C) were chosen from the myriad of possible conditions to be representative of this type of processing. Essentially the procedures followed were combinations of the previously outlined work where material was solutionized, deformed and aged. Extensive reference was made to the time/temperature/conductivity kinetics map and to the tensile strength versus aging time (at 430^{o}C) plots. Therefore, the basic work was helpful to designing more complicated processing schedules. The following nomenclature was used for sample identification in this work. All theses materials started from the same 25.4 mm Cu-Cr ingot which was solutionized for 24 hours at 1025^{o}C, quenched, and drawn to 3 mm (η = 4.2). This is termed the original materials and the following nomenclature describes various subsequent processing. The alloy composition in all cases is 7.0 Vol. % Cr. Composition was omitted from the sample nomenclature in the interest of clarity when identifying points on the following figures.

Sample Nomenclature:

Q = Solutionizing, 1025°C for 12 hours, and Quenching into Ice Water

A = Aged 430°C for 6 hours and Quenched into Ice Water

c = Deformed from $\eta = 4.2$ to $\eta = 7.1$

cc = Deformed from $\eta = 4.2$ to $\eta = 8.2$

ccc = Deformed from $\eta = 7.1$ to $\eta = 9.1$

Example: QcAccc

After solutionizing/quenching at 25.4 mm and cold deformation to 3 mm this material was:

1) resolutionized/quenched (Q)
2) Cold Deformed $\eta = 4.2$ to $\eta = 7.1$ (c)
3) Aged at 430°C for 6 hours (A)
4) Cold Deformed $\eta = 7.1$ to $\eta = 9.1$ (ccc)

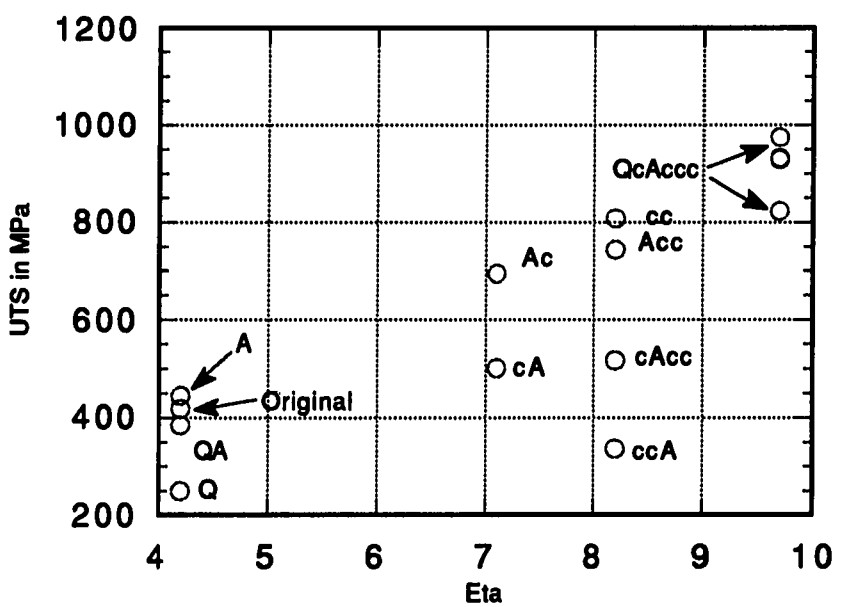

Figure 42. Ultimate Tensile Strength vs. Deformation Strain for Thermomechanically Processed Cu-7.0 vol. % Cr.

As done previously, the UTS in MPa and the % IACS are plotted versus Eta for each thermomechanical treatment schedule, Figures 42 and 43. Deformation was limited to η = 8.2, i.e. cc, for material only cold deformed as further drawing was impossible due to fracture. After aging at 430°C deformation was limited to an additional η = 2.0 as again material failure prevented further drawing.

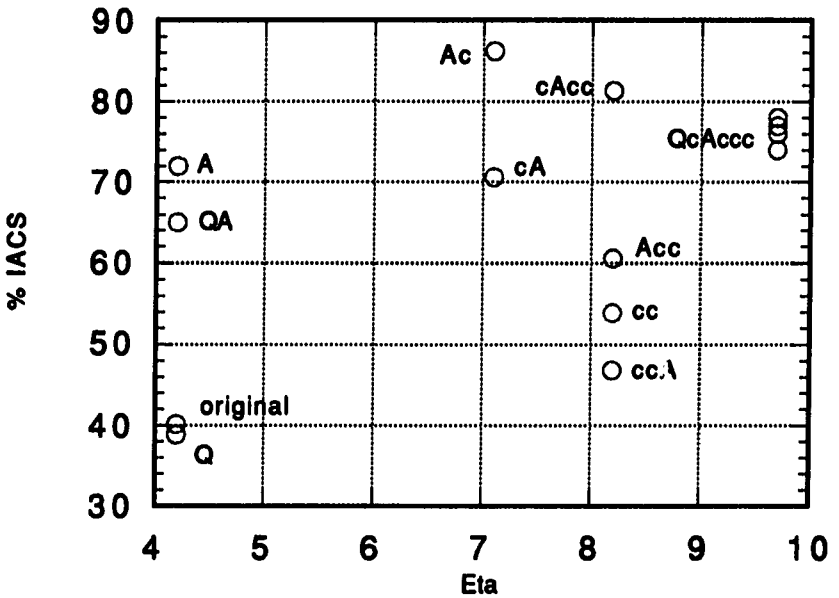

Figure 43. % IACS vs. Deformation Strain for Thermomechanically Processed Cu- 7.0 Vol. % Cr

Data Analysis

Unlike the previous study the best electrical and mechanical properties do not come in the same material. The highest mechanical properties are produced by the QcAccc treatment while the best electrical properties are found in the Ac followed by cAcc material. It is also noted that drawing after aging, A to Ac, cA to cAcc improves both electrical and mechanical performance. After an η = 7.1 the electrical properties of the material start to degrade

although the mechanical properties continue to improve. This effect is shown in Figure 44 to 46 following three different thermomechanical schedules. In the first schedule, Figure 42, the material is deformed and aged as the final treatment, aged for 6 hours at 430°C. In Figures 45 and 46 the schedule shows deformation to $\eta = 4.2$ and $\eta = 7.1$ followed by cold deformation. All three schedules show a rapid decrease in electrical properties and a rapid increase in mechanical properties after $\eta = 7.1$. These materials appear to act as conventional precipitation hardened alloys below $\eta = 7.1$. At higher η their behavior is more similar to that of a DMMC. Unfortunately, regardless of mechanical or thermal treatment, mechanical failure during drawing limited the total η available. Most DMMCs do not start to develop truly anomalous properties until $\eta = 8.0$. Aging these materials a second or third time may improve ductility allowing high η values but, as pointed out in other studies this also leads to breakdown and coarsening of the fibrous DMMC microstructure due to Raleigh instability [45, 46].

The Figure of Merit (FM) analysis was carried out to determine which thermomechanical treatment leads to the best combination of properties. The result of the FM analysis is shown in Figure 47. The materials which have a combination of thermal and mechanical processing have the highest FMs. Again the effect of aging is decreased as cold work is increased. Also cold working after aging improves the FM of these materials. Complex thermomechanical processing has led to the production of material with a better FM than what is commercially available. The thermomechanical treatment QcAccc produces a material with a FM = 3.25. This is better than the best commercialalloys (Cu-Be) FM = 3 and near to the value for the best research alloy Cu-20 vol. % Nb FM = 3.5. At the same deformation strain (η) Cu-Cr has slightly less FM than Cu-Nb. It is important to realize that the chromium alloy is much less expensive than the niobium version. First, the cost of chromium is less than that of niobium. Secondly, the amount of refractory metal required for alloying is lower by almost a factor of three.

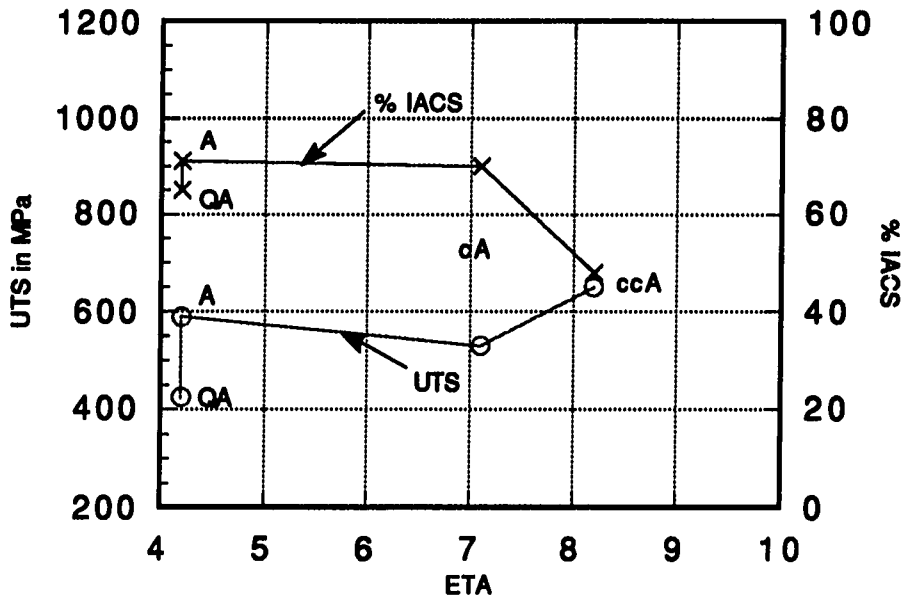

Figure 44. UTS and %IACS versus Eta for Cu-7.0 Vol. % Cr. Deformation Processed followed by Aging for 6 hours at 430°C

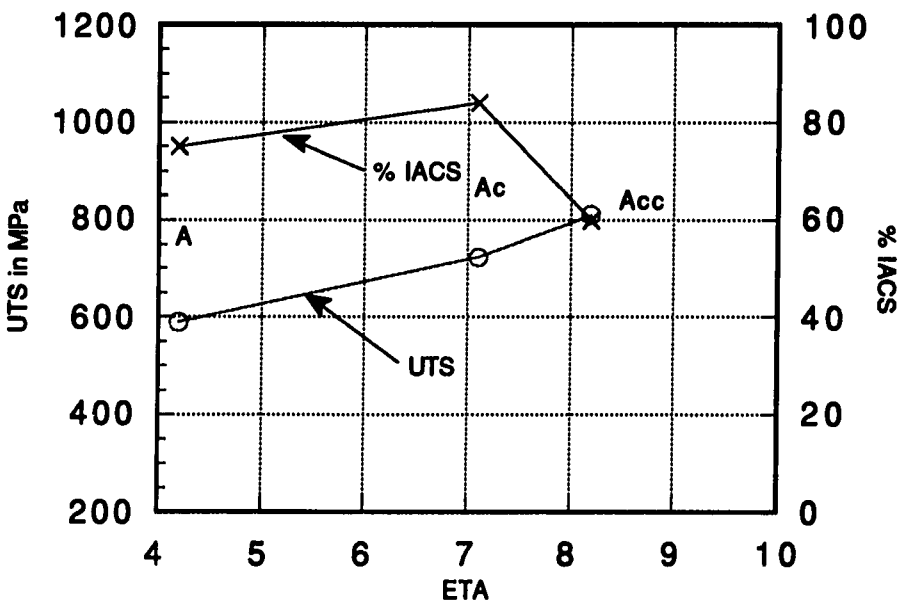

Figure 45. UTS and %IACS versus Eta for Cu-7.0 Vol. % Cr Deformation Processed $\eta = 4.2$ Aged for 6 hours at 430°C then Deformed Again

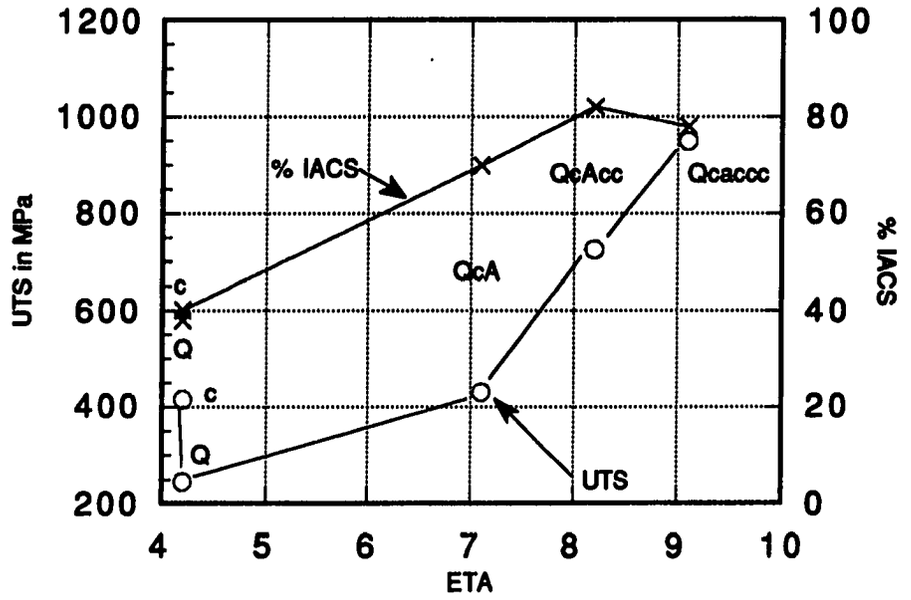

Figure 46. UTS and %IACS versus Eta for Cu-7.0 Vol. % Cr Deformation Processed $\eta = 7.1$ Aged for 6 hours at 430°C then Deformation Processed Again

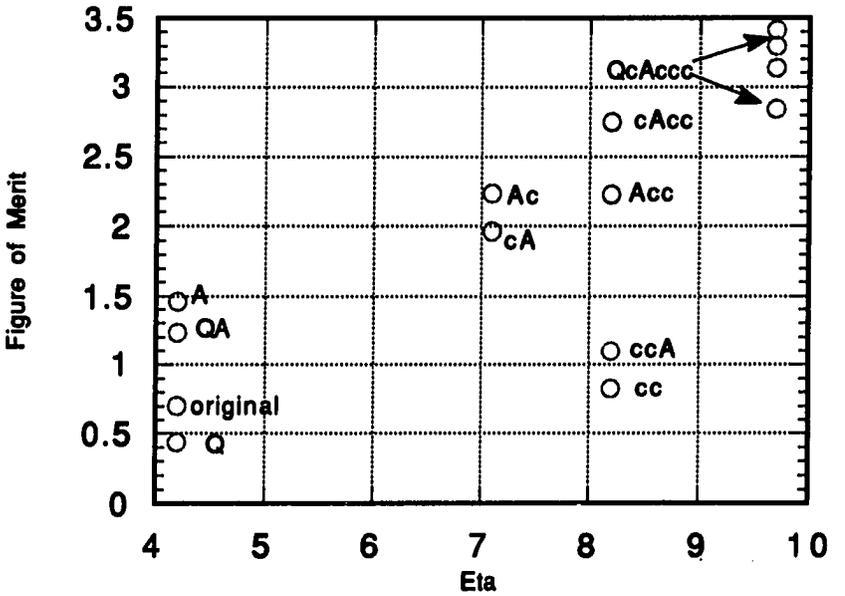

Figure 47. Figure of Merit versus Eta for DMMCs produced by Thermomechanical Processing

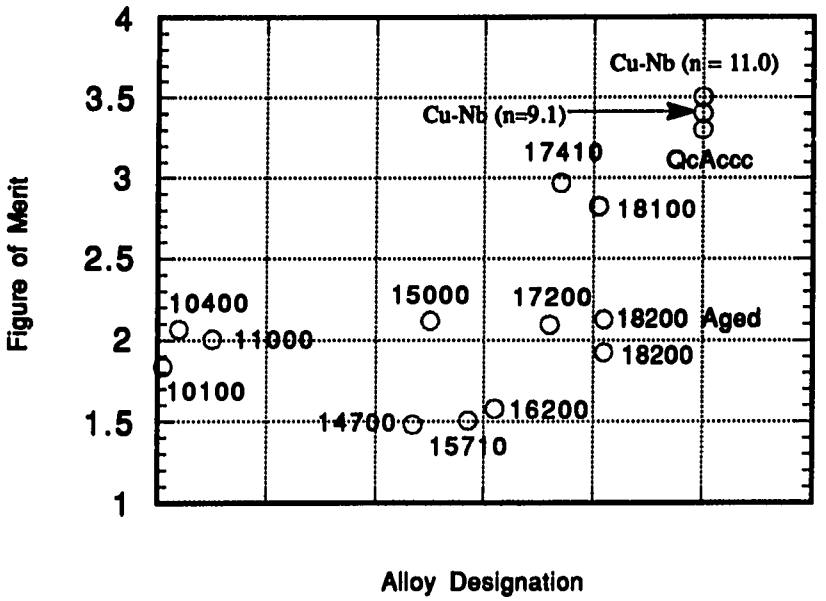

Figure 48. Figure of Merit for Several Commercial Alloys and Copper 20 Vol. % Niobium Compared with the Best Copper-7.0 Vol. % Chromium Alloy in this Study

In the following discussion the effect of each processing step on the physical properties of the material with the highest FM is traced. In Figure 49 the UTS in MPa is plotted versus deformation strain for a Cu-7.0 Vol. % Cr alloy. This is the thermomechanical treatment found to produce the highest electrical conductivity as seen in Figure 49. Drawing from a solutionized/quenched state (S/Q) gives the material excellent ductility. Straight cold drawing does not produce very high strength prior to fracture during drawing. Fracture during the drawing process limits drawing strain to $\eta = 7.0$ fracture. Aging the material at 430°C for 6 hours, at an $\eta = 7.1$ after previous S/Q treatment at $\eta = 4.1$ has two effects. First, the tensile strength of the material is decreased. Data was not obtained at $\eta > 9.1$ due to failure of the material during the drawing operation. The final aging treatment followed by cold drawing has produced the material with the highest tensile strength 930 MPa and acceptable electrical conductivity of 80.0 % IACS. Of greater importance is the evaluation of the effect of each processing step to more clearly understand how the mechanical properties develop in these alloys.

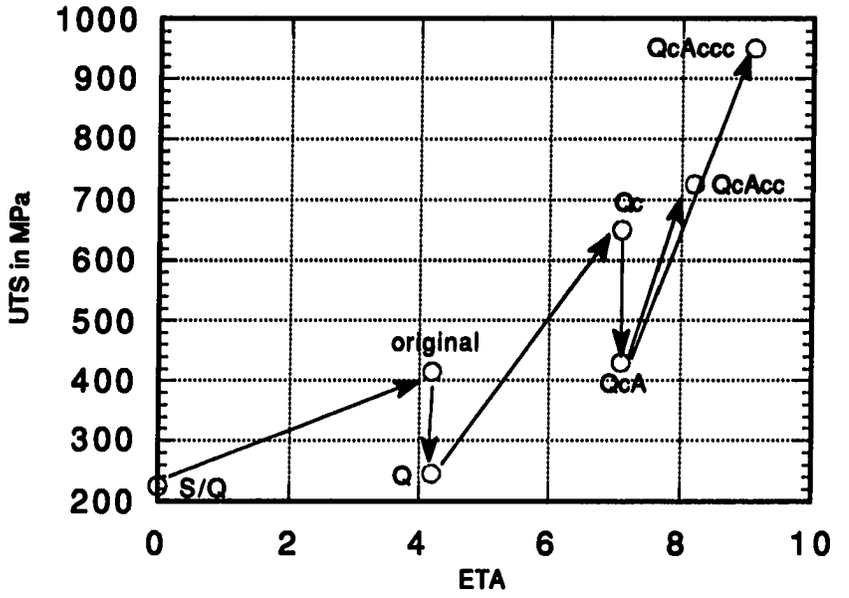

Figure 49. UTS versus η during the Production of the Material with the Highest Figure of Merit

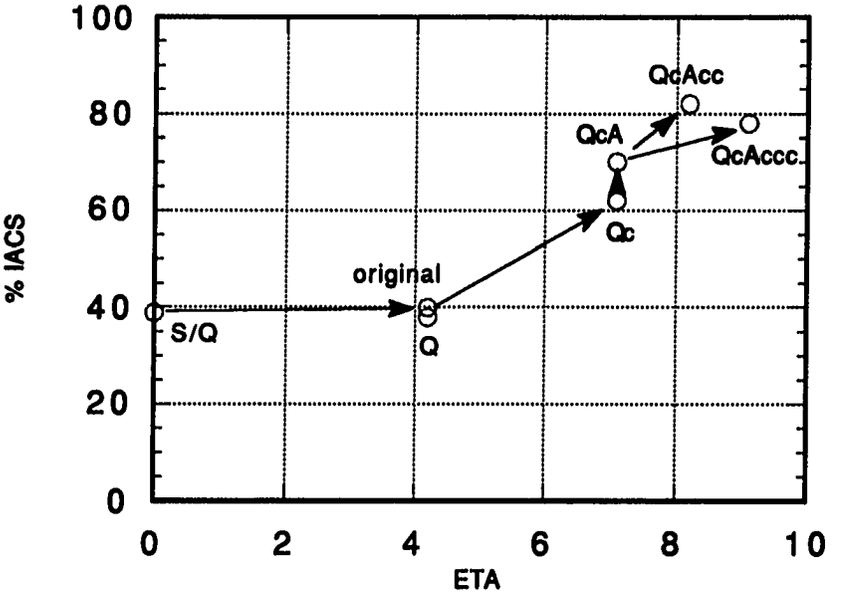

Figure 50. % IACS versus η during the Production of the Material with the Highest Figure of Merit

Microstuctural Development

Noticeably absent in this discussion is evaluation of the microstructure of these materials and a comparison of electrical and mechanical property development. This study brings together the interrelationship between electrical, mechanical, and microstructural developments. This part of the investigation has proven that thermomechanical processing leads to material with the highest mechanical strength in a manner very similar to that found for improvements in electrical resistivity. Optimally processed these materials have excellent mechanical properties which compare favorably to those for presently available commercial alloys. The alloy Cu- 7.0 Vol. % Cr processed, by the QcAccc scheme has been found to have the best combination of properties. The microstructural development of this alloy has been followed by TEM analysis. Each sample was dimpled using 10 μm diamond paste followed by ion milling. All micrographs were taken on a Phillips model CM 30 transmission electron microscope. The exact processing for each sample is outlined in Table 11.

Table 11. Processing Path for Each TEM Sample

Sample	Processing Path	Code
1	Solutionized/Quenched 1025°C 24 h., Cold Deformed to $\eta = 4.2$	original
2	Sample 1 + Re-Solutionized/Quenched 1025°C, 12 h.	Q
3	Sample 2 + Cold Deformation to $\eta = 7.1$.	Qc
4	Sample 3 + Aging at 430°C, 6 h.	QcA
5	Sample 4 + Cold Deformation $\eta = 9.1$.	QcAccc

Figure 51. Microphotograph Original Material

Figure 52. Sample Q Microphotograph; Material Re-S/Q after Drawing to $\eta = 4.2$

Figure 53. Sample Qc Microphotograph; Material Drawn to $\eta = 7.1$ after S/Q at $\eta = 4.2$

Figure 54. Sample QcA Microphotograph; Material Aged for 6 h. at $\eta = 7.1$

Figure 55. Sample QcAccc Microphotograph; Material Drawn to $\eta = 9.1$ after Aging at $\eta = 7.1$

In the original material (Figure 51) the ribbon shaped morphology of the chromium reinforcing phase has started to develop. Table 12 gives the mean copper grain size, chromium spacing, and chromium particle thickness for all processing steps. Two distinct morphologies and sizes of the chromium phase are present. Chromium is present as undeformed spheroidal blobs while the rest has formed a classical ribbon morphology. Resolutionizing/Quenching changes the morphology of the chromium from fibrous to spherical, Sample Q (Figure 52). The mean spacing of these spheroids is 2.70 μm and they have acquired a mean diameter of 4.17 μm. These values are two orders of magnitude greater than that observed for precipitate particles in these alloys [28, 45,39]. Coarsening of

the fibrous microstructure has been investigated by Courtney et. al. [45, 46]. The coarsening is driven by reducing the surface energy associated with the filamentary morphology of the reinforcing phase. Analysis of the surface energy shows that the fibers are unstable and will coarsen leaving the reinforcing phase in the observed spherical morphology. Figure 53, Sample Qc, shows the microstructure after drawing again from the Solutionized/Quenched state. Two chromium morphologies are present. While a high volume fraction of the chromium has reassumed the ribbon morphology of a DMMC some undeformed chromium spheres still exist. The mean value for ribbon spacing is 0.48 μm and 0.22 μm for the thickness. Sample QcA is Sample Qc plus an isothermal aging treatment @ 430°C for 6 hours. The aging process has significantly coarsened the chromium fibers. Further mechanical deformation to $\eta = 9.1$ leads to further refinement of the microstructure. The mean spacing of the fibers has been reduced to 0.18 μm and the filaments have a mean thickness of 0.03 μm. Sample 5 shows the microstructure in its final deformation state. This microstructure has only the filaments produced by deformation processing and noticeably absent are any precipitates caused by aging.

Table 12. Microstructural Spacings in Each Step Used to Produce Cu-7.0 Vol. % Cr DMMC with the Best Properties.

Condition	Copper Grain Size in μm	Chromium Spacing in μm	Chromium Thickness in μm
Original	0.34	1.30	0.33
Q	4.17	2.70	1.53
Qc	0.22	0.48	0.09
QcA	0.17	1.1	0.14
QcAccc	0.14	0.18	0.03

The question which can now be addressed is how each processing step affects the development of the observed physical properties of these alloys. Mechanical working of the alloy from the S/Q state is shown to improve the electrical properties of the material, Figure 49. Precipitation of chromium on pre-existing filaments reduces the amount of chromium in solid solution with copper. As the amount of chromium in solution is reduced the electrical conductivity is improved by a reduction in impurity scattering. It is also noted that aging of the material at 430°C for 6 hours. at $\eta = 7.1$ also improves the conductivity of the material. However, this improvement is not as great as would be predicted from the reduction of chromium in solid solution. Further drawing reduces the spacing between filaments which in turn should lead to higher resistivity. This is not what is observed as deformation to $\eta = 9.1$ also gives an improvement in electrical conductivity. Fargette et. al. [34] conclude that mechanical working can help chromium to precipitate out of solution in these alloys. Diffusion of the chromium to pre-existing chromium particles may be aided by the movement of recrystallization fronts through the matrix.

The mechanical properties follow a more conventional path. Mechanical working leads to fiber refinement and strain hardening of the matrix with subsequent increases in UTS. Heat treating of the alloy coarsens the reinforcing fibers and reduces this stored strain energy; and thereby mechanical performance. However, heat treating enhance the ability of the material to regain mechanical performance. First by refining the size of the chromium in the matrix. This reduces the chromium spacing and improves the recovery of mechanical properties as a lower total eta is necessary to regain a small fiber spacing. Second, heat treating allows the material to regain lost ductility such that high deformation strains may be attained. The higher the deformation strain the more refined the spacing of the chromium fibers and again the higher the mechanical strength.

The formation of precipitates in hyper-eutectic Cu-Cr alloys is limited by the large volume fraction of chromium. Pre-existing primary filaments are energetically favorable locations for the precipitation of chromium. Another comparison can be developed from analysis of Cu-Nb alloys (which are DMMCs) and Cu-Be alloys (which are classic precipitation hardened materials). The Cu-Nb alloys have better or comparable strength to the Cu-Be alloys but much better electrical properties. Cu-Nb DMMCs develop their properties by a fine dispersion of niobium fibers. While in Cu-Be alloys a dispersion of very fine precipitates, GP zones, account for their strength. Even though mechanical properties are similar the electrical properties are not. The matrix of the Cu-Nb alloy is free of niobium in solid solution or as fine precipitate particles, whereas, the Cu-Be matrix is full of fine

coherent particles which can be thought of as part of the copper matrix. The scattering of electrons by the niobium fibers in the Cu-Nb alloys is less than that found by placing a fine dispersion of particles in copper. The resistivity contribution due to surface scattering, as in the case of Cu-Nb, is lower than the combination of particle and solid solution scattering found in Cu-Be alloys. In the case of Cu-Cr we have both possibilities since chromium has some solubility in the copper matrix. To develop the best combination of mechanical and electrical properties we must produce a material analogous to Cu-Nb and not Cu-Be. This study has shown with proper thermomechanical processing this goal can be accomplished.

Conclusion

This study has shown that thermomechanical processing can produce a material with superior properties than those available in either other copper-chromium alloys or in presently available commercial copper alloys. The FM of 3.25 is comparable to that for Cu-20 Vol. % Nb research alloys which are the present benchmark for high performance in copper based systems. Thermomechanical processing has been shown to aid in both the removal of chromium from solid solution (which improves electrical properties) and in the refinement of the deformation processed microstructure (which improves strength). Without a doubt thermomechanical processing is required in hyper-eutectic copper-chromium alloys to obtain maximum properties. The formation of precipitate particles analogous to those produced in hypo-eutectic alloys does not appear to play a direct role in these materials. The best properties are developed in these alloys when they become DMMCs only, i.e. no precipitates.

REFERENCES

1. W.F. Smith, Structure and Properties of Engineering Alloys, McGraw-Hill, New York, New York (1981).

2. M.A. Hunter and F.M. Sebast, J. Amer. Inst. Met., 11, 115 (1917/1918).

3. M.G. Corson, Rev. Met., 27, 83 (1930).

4. L. Guillet, Rev. Met., 3, 176 (1906).

5. G. Hindrichs, Z Anorg. Allg. Chem., 59, 420 (1908).

6. Copper-Chromium Phase Diagram, D.J. Chakrabarti and D. E. Laughlin, Phase Diagrams, T.B. Massalski, ed., ASM International, Materials Park, Ohio (1984).

7. N. Koda and E. Isono, J. Jpn. Inst. Met., 16, 213 (1952).

8. G. Bunge, R. Honak and W. Nielsch, Z. Metalk., 44, 71 (1953).

9. W. Koster and W. Knorr, Z. Metallk., 45, 350 (1954).

10. T. Doi, J. Jpn. Inst. Met., 21 (5) 337 (1957).

11. R.O. Williams, Trans. ASM, 52, 530 (1960.

12. K. Nagata and S. Nishikawa, Report of the Insitute of Industrial Science, University of Tokyo, 24 (4) Serial No. 153, 115 (1975).

13. H. Suzuki and H. Kanno, J. Jpn. Inst. Met., 37(1) 13 (1973).

14. J. Rezek, Can. Met. Quart., Vol. 8, 179 (1969).

15. J. Rys and Z. Rdzawski, Metals Technology, 32, Jan 1990.

16. P. Priester, B. Fargette, D. Whitwham, O. Diner and J. Herenguel, Mem. Sci. Rev. Met., 67, No. 10, 677 (1971).

17. N. Rashkov and Z. Martinova, Proc. Int. Heat Tr. Conf. 16th (1976).

18. W.O. Alexander, J. Inst. Met., 64, 93 (1939).

19. W.R. Hibbard, Trans. AIME,175, 283 (1948).

20. M.V. Zakarov and O.E. Osintev, Inv. Vyssh. Ucheb. Zaved., Tsvetn. Met., 5, 152 (1967).

21. W.L. Seitz, Diffusion of Chromium 51 into Copper, M.S. Thesis, Univ. of Ariz., Tempe, Arizona (1963).

22. G. Barreau, G. Brunel and G. Cizeron, C. R. Acad. Sci., 618 (1971).

23. M.C. Saxena, Trans. Indian Inst. of Met., 24, 56 (1971).

24. W.A Johnson and R.F. Mehl, Trans. A.I.M.E., 135, 416 (1939).

25. G.C. Weatherly, P. Humble and D. Borland, Acta Metall. Vol. 27, 1815 (1979).

26. J.G. Sevillano, Strength of Metals and Alloys, Proc. ICSMA 5 P. Haasen, V. Gerold and G. Kowtorz, Eds., Pergamon Press, Oxford 819 (1980).

27. P.D. Funkenbush, T.H. Courtney and D.G. Kuibsh, Scripta Metall. 18, 1099 (1984).

28. H. Dyiec, Z, Rdzawski and M. Richert, Mater. Sci. Eng., A, A108, 97 (1989).

29. J.S. Koehler, Phys. Rev., Vol. 2, 547 (1970).

30. Y. Komen and J. Rezek, Met. Trans A, Vol. 6A , 549 (1975).

31. M.G. Hall, H.I. Aaronson and K.R. Kinsma, Surface Science, Vol. 31, 257 (1972).

32. N.J. Long, C.H. Lloyd and M.H. Loretto, Inst. Metall., Ser. London (1979).

33. The Electrical Resistivity of Metals and Alloys, P.L. Rossiter, Cambridge University Press, 258 (1991).

34. S.N. Khanna and A. Jain, J. Phys. F., Metal Phys., Vol. 4, 1982 (1974).

35. A. Lodder, P.M. Boerrigter and P.J. Braspenning, Phys. Stat. (b), 114, 405 (1982).

36. M.E. Drits, N.R. Bochvar, E.V. Lysova and N.P. Leonova, Soviet Journal of Non-ferrous Metallurgy, Vol. 2, 312 (Eng trans.), (1976).

37. J. Bevk, J.P. Harrbison and J.L. Bell, J. Appl. Phys., Vol. 49, 1143 (1978).

38. Applications Overview, Keithley Instruments, Cleveland, Ohio (1990).

39. N. Rashkov and Z. Martinova, Z Metallkd, 79 (11), 752, (1988).

40. G.H. Geiger and D.R. Poirier, Transport Phenomena in Metall., Addison-Wesley, Reading, Massachusetts (1980).

41. Z. Rdzawski, H. Dydiec and M. Richert, Z Metallkd., 79 (11), 746.(1988).

42. F.S. Ham, J. Appl. Phys., Vol. 30, No. 6, 915 (1959).

43. A.H. Cottrell and B.A. Bibly, Proc. Phys. Soc. A62, 49 (1949).

44. J.D. Verhoeven, W.A. Spitzig, F.A. Schmidt, P.D. Krotz and E.D. Gibson: J. Mat. Sci., 1989, Vol. 24, 1015 (1989).

45. J.C. Kampe, T.H. Courtney and Y. Leng, Acta Metall., Vol. 37, No. 7, 1735 (1989).

46. T.H. Courtney and J.C. Kampe, Acta Metall., Vol. 37, No. 7, 1747 (1989).

PAPER 2. EVALUATION OF PLASMA SPRAYED CRUCIBLE COATINGS FOR MELT PROCESSING COPPER-REFRACTORY METAL ALLOYS

Timothy W. Ellis, Daniel J. Sordelet, and Francis C. Laabs,
Ames Laboratory, Iowa State University, Ames, IA 50010

ABSTRACT

A study was made to access the suitability of several plasma arc sprayed coatings applied to graphite for application as containment crucibles for melt processing copper-refractory metal alloys. Coatings of Ta, TaC, TaB_2 and ZrO_2•8w/o Y_2O_3 were evaluated and compared to uncoated graphite. The ZrO_2•8w/o Y_2O_3 coating was sprayed over a tungsten bond coat. Prealloyed samples of Cu-15v/o Cr and Cu-15v/o Nb were placed within the crucibles and heated inductively to 1800°C and 2100°C, respectively. Compatibility of the coating-alloy system was evaluated by optical and scanning electron microscopy, EDS, XRD and combustion chromatography.

INTRODUCTION

Deformation processed copper-refractory metals are being studied because of their combined properties of high mechanical strength and excellent electrical conductivity (1). Precursor alloys are typically produced by consumable arc melting techniques and conventional crucible melting. The latter process, however, is subject to melt contamination due to the high melt temperatures required for melt homogenization and the strong compound forming tendencies of the Group V-VI transition metals. In addition to the need for alloy purity, it is desirable to form these alloys by rapid solidification in order to develop fine-scale microstructures prior to deformation processing (2). The Ames Laboratory High Pressure Gas Atomization (HPGA) facility was employed to produce the alloy in a rapidly solidified powder form. However, the large superheat temperatures required for proper flow during melt processing lead to alloy contamination, crucible degradation and ultimate inability to atomize the alloy due to flow obstruction and mechanical failure of the crucible.

The current study was initiated to evaluate plasma arc sprayed coatings for use in melt processing applications. Refractory coatings which would provide chemical stability at required temperatures are often characterized as thermally shock resistance. Therefore, it was decided to apply the plasma spray coating onto a graphite base. Graphite was chosen due to its high temperature stability, thermal shock resistance and compatibility with induction heating. This hybrid design was aimed to provide the combination of chemical stability of selected plasma sprayed materials and the mechanical durability of graphite.

EXPERIMENTAL MATERIALS

Copper-refractory metal alloys. The Cu-15v/o Nb and Cu-15v/o Cr alloys used in this study were prepared at the Ames Laboratory Materials Preparation Center by consumable arc melting and bottom pour chill casting, respectively. These prealloyed materials were chosen to enhance melt homogeneity during melt processing evaluation.

Graphite crucibles. High purity graphite crucibles were purchased from POCO Graphite, Inc. Total ash content for this material is reported to be <5ppm by weight.

Plasma arc sprayed powders. The coating systems evaluated were ZrO_2•8w/o Y_2O_3, Ta, TaC and TaB_2. A thin W base coat was applied to the graphite crucible before the ZrO_2•8w/o Y_2O_3 layer. SEM micrographs of the powders used are displayed in Figure 1.

EXPERIMENTAL PROCEDURE

Plasma arc spraying. The coating materials described above were applied to the graphite crucible by Plasma Coating Corporation, Gardena, CA. Prior to coating, the crucibles were blasted with 50 μm Al_2O_3. The Ta-based coatings were all applied directly to the graphite crucibles, while the ZrO_2·8w/o Y_2O_3 coating was sprayed over a tungsten bond layer. Spraying was performed in air using a Plasmadyne SG1B gun utilizing a front feed powder injection port. Argon and helium were used as carrier and secondary gases, respectively.

Melt processing. The prealloyed copper alloys were placed within the plasma sprayed crucibles. Uncoated graphite crucibles were also tested with both alloys. The crucibles were then set inside a 6 inch diameter graphite containment dish. This dish was used to provide a catch basin in the event of a mechanical crucible failure and to act as a large coupling mass for the induction field in order to help develop a more uniform thermal profile within the induction furnace during experimental melt processing. The alloys were heated to approximately 400°C above their projected liquidus temperatures. This large superheat was selected to emulate the melt processing conditions during HPGA. The crucible alloy systems were inductively heated under 0.5 atmospheres of argon to approximately 1800°C for the Cu-15v/o Cr alloy and 2100°C for the Cu-15v/o Nb alloy. The temperatures were monitored by optical pyrometry. Both systems were held at temperature for 15 minutes and allowed to cool by removing the induction field.

Analytical techniques. Following the HPGA melt processing emulation tests, the alloy containing crucibles were sectioned axially to reveal the crucible-coating-alloy interfaces. The sample sections were mounted in epoxy, ground and polished to a 0.25 μm diamond finish. Grinding was performed with Omni-brade perforated diamond discs from TBW Industries. Optical microscopy was used to observe the as-polished samples. Subsequentiy, the samples were carbon coated and analyzed by scanning electron microscopy (SEM) and energy dispersive spectroscopy (EDS). X-ray diffraction (XRD) using Mo-Ka radiation was employed where appropriate to characterize regions of massive phase segregation. Combustion chromatographic analysis was used to measure approximate carbon levels in several Cu-15v/o Nb samples.

RESULTS AND DISCUSSION

Physical containment of molten alloys. Figure 2 shows the crucibles after removal from the induction furnace. It is readily apparent that the Ta-based coatings were substantially wet by the molten copper alloys, particularly the Cu-15v/oCr alloy samples. These coatings are obviously not suitable for full containment of the two alloy systems when melt processed at their respective temperatures. In addition, the Ta-based coatings chemically reacted with alloys, as discussed later.

The Cu-15v/o Cr sample did not wet the uncoated graphite crucible, while the Cu-15v/o Nb exhibited a small degree of wetting. Both copper alloys were successfully contained by the ZrO_2•8w/o Y_2O_3 coating. The ceramic coating and tungsten bond coat did not appear to delaminate from each other, but the entire tungsten, ZrO_2•8w/o Y_2O_3 and alloy completely separated from the graphite crucible upon cooling.

Chemical Compatibility of Molten Alloys and Coating Materials

Uncoated graphite crucibles. As shown in Figure 2, the Cu-15v/o Cr alloy was physically contained by the uncoated graphite crucible. However, contamination of the molten alloy by the graphite was observed in the form of chrome carbide formation and subsequent phase separation. Figure 3a shows the nearly continuous carbide layer which formed at the melt/crucible interface. A large region of this continuous phase was analyzed by XRD and was determined to be $Cr_{23}C_6$, Cr_7C_3, Cr and Cu. The spheroidal shape of the carbide phase particulate suggests a possible liquid immiscibility at the melt processing temperature. Reference to the Cr-C phase diagrams (3) indicates that certain chrome carbides have a liquidus temperature below the experimental 1800°C temperature. The cited Cr-C phase diagram shows a eutectic reaction between pure Cr and $Cr_{23}C_6$ around 1576°C. Furthermore, the Cr_7C_3 compound is liquid above 1766 °C. The phase diagram also predicts a very low carbon solubility in copper at the processing temperatures. The addition of excess carbon to chromium during melting should promote liquid immiscibity.

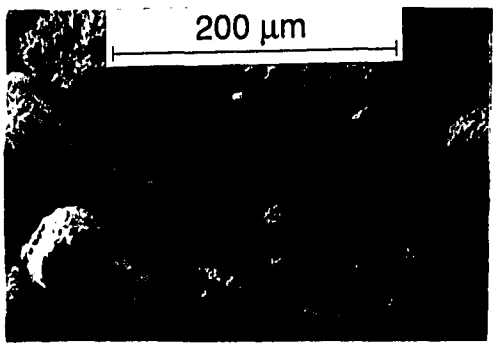

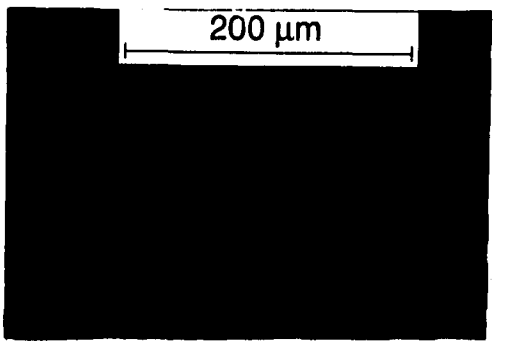

ZrO_2•8w/oY_2O_3

Ta

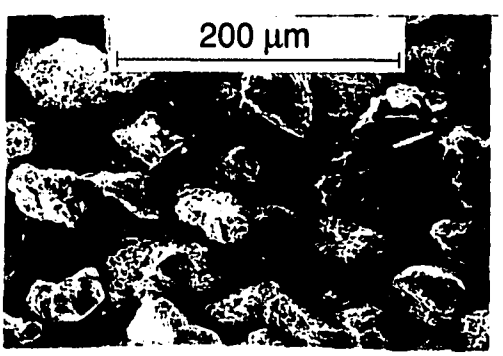

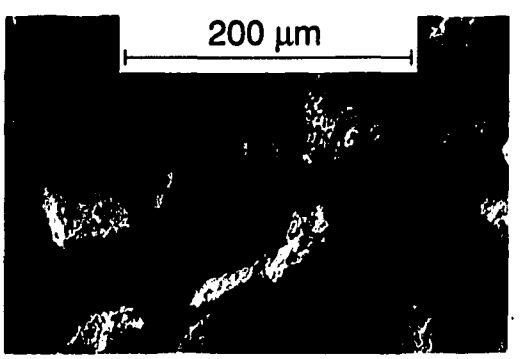

TaC

TaB_2

Figure 1. SEM micrographs of starting powders

The Cu-15v/o Nb alloy did not exhibit similar behavior. A continuous layer was formed at the melt/crucible interface; however, Nb-rich dendrites were present throughout the bulk of the copper matrix specimen. No chrome containing precipitates separate from the continuous layer discussed above were found throughout the copper bulk. Figure 3b reveals the continuous interface layer formed in the Cu-15v/o Nb alloy. The appearance of this layer is indicative of a diffusion controlled passivation reaction. Its morphology is different than that in the chrome system; however, phase equilibria data (4) indicate that niobium carbides, if formed, have melting temperatures in excess of the 2100°C experimental temperature. The melt/crucible reaction layer was not identified. Chemical analysis detected over 0.10% by weight carbon in a 0.5g sample taken from the bulk of the alloy. Although the transport mechanism and reaction products of carbon into the Cu-15v/o Nb alloy was not determined, the presence of carbon in the alloy dictates the unsuitability of uncoated graphite for melt processing this system at 2100°C.

ZrO_2•8w/o Y_2O_3/W coated crucibles. The ceramic coated crucibles did not exhibit any detectable reaction with either copper alloy at the melt processing temperatures used. Figure 4 displays the tungsten/ceramic/melt interfaces. The black region adjacent to the tungsten is the epoxy sample mount and not the graphite crucible. Sample A is Cu-15.0 Vol. % Cr and sample B Cu-15.0 Vol. % Nb. Visually, the interfaces appear clean and well-defined. The appearance of debonding between the tungsten and ZrO_2•8w/o Y_2O_3 in Figure 4b is actually an artifact of overaggressive grinding. Subsequent improved metallography techniques on companion samples showed that the tungsten and ceramic layers were not separated. EDS spot analysis did not detect any migration of coating elements into the melt nor any transport of copper or alloying elements into the coating. Table I outlines the elements detected by EDS at various locations in the ZrO_2•8w/o Y_2O_3 samples. Data obtained from the Ta and TaC coated samples are also given and will be discussed briefly below. The spots labeled A-D in Table I correspond to areas marked on the figures referenced in the table. Spots A and B in Figure 4 show no detectable reaction occurred between the ceramic coating and tungsten bond layer. The tungsten was applied primarily as a diffusion barrier to carbon migration into the ZrO_2•8w/o Y_2O_3 coating and molten alloy. However, since the samples were carbon coated for SEM and EDS analysis, observation of carbon at any location was quite suspect and was ignored in this study.

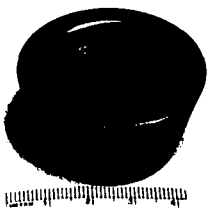

Uncoated: Cu-15v/o Cr

Uncoated Cu-15v/o Nb

ZrO_2•8w/oY_2O_3: Cu-15v/o Cr

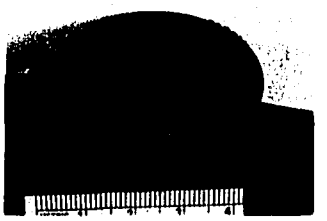

ZrO_2•8w/oY_2O_3: Cu-15v/o Nb

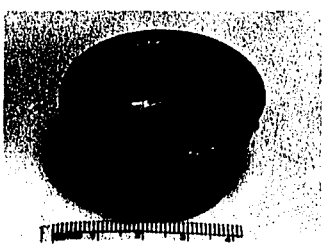

Ta: Cu-15v/o Cr

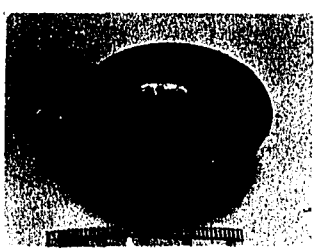

Ta: Cu-15v/o Nb

TaC: Cu-15v/o Cr

TaC: Cu-15v/o Nb

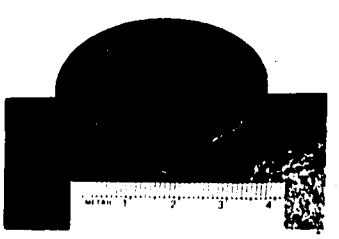

TaB_2: Cu-15v/o Cr

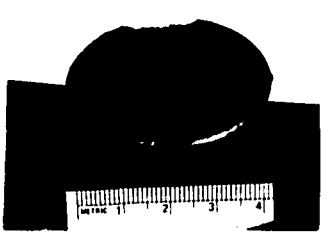

TaB_2: Cu-15v/o Nb

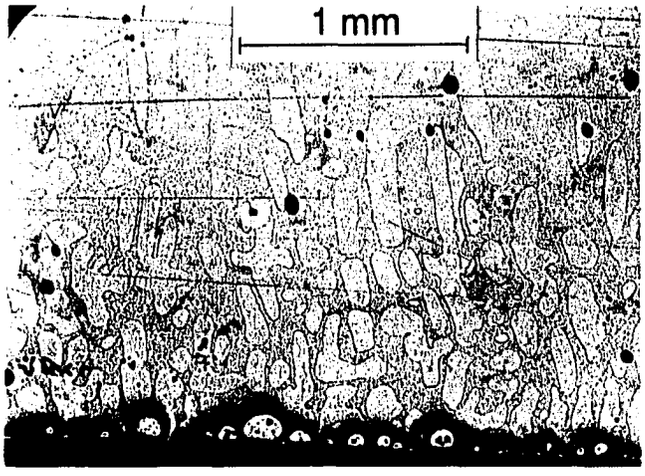

3a. Uncoated graphite: Cu-15v/o Cr

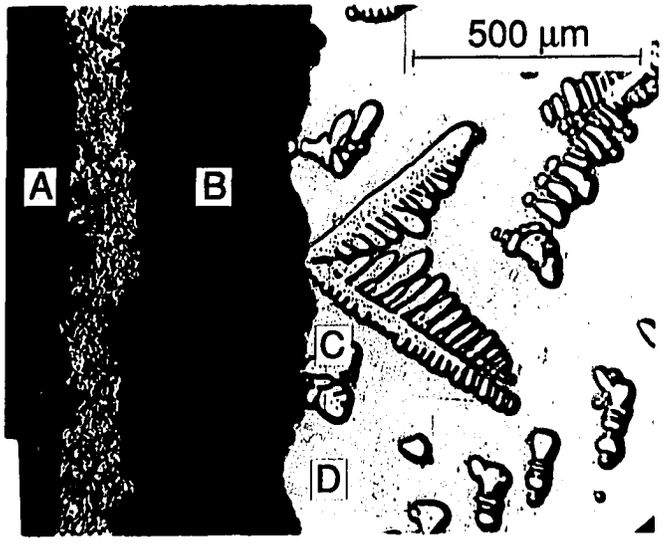

4a. W/ZrO_2•8w/oY_2O_3: Cu-15v/o Cr

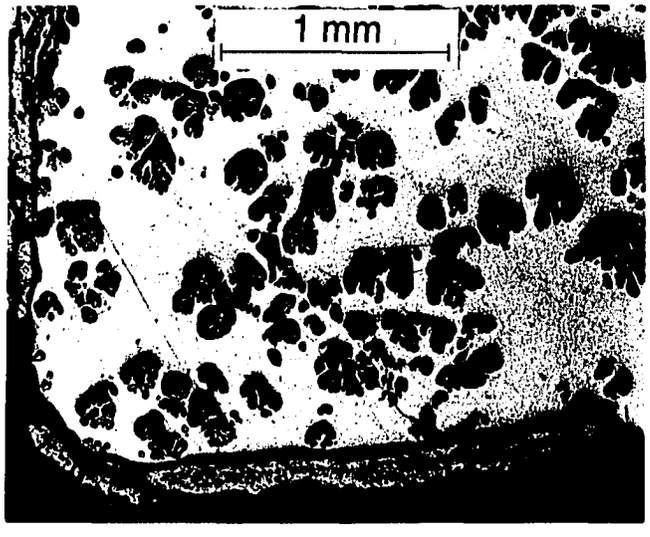

3b. Uncoated Graphite: Cu-15v/o Nb

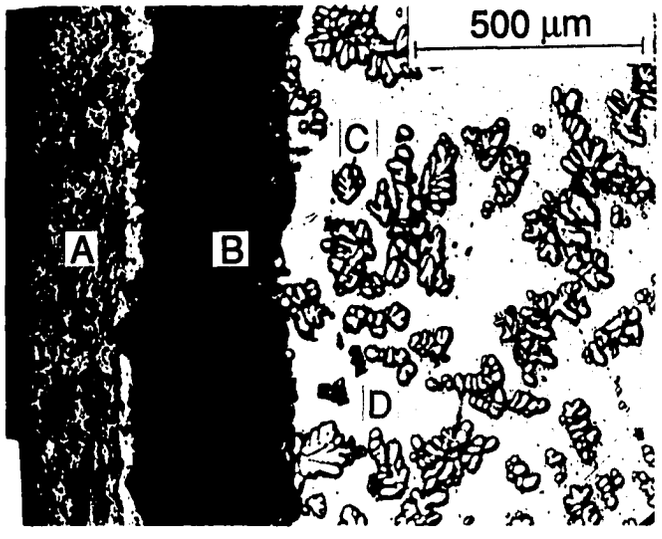

4b. W/ZrO_2•8w/oY_2O_3: Cu-15v/o Nb

Fig. 3 - Optical micrographs of uncoated graphite/Cu-alloys.

Fig. 4 - Optical micrographs of W/ZrO_2•8w/oY_2O_3/Cu-alloys.

Ta-coated crucibles. The tantalum coatings were chemically reactive with both the Cu-15v/o Cr and Cu-15v/o Nb alloys. Specifically, tantalum was detected in Cr-rich and Nb-rich precipitates within the copper matrix. Furthermore, chrome and niobium were found within the bulk of the tantalum coating. Figure 5 displays the microstructures of the two copper alloys in contact with the tantalum coating. EDS results from the spots labeled in these samples are summarized in Table I. In addition to the apparent elemental transport of the chrome, niobium and tantalum, large scale migration of copper was observed. Spot B in Figure 5b shows a large pocket of copper-rich metal which resided within the coating after solidification. The transport mechanism for the large scale migration is not known, but it may have been facilitated by the porous coating structure which could attract the copper-rich molten metal via capillary forces.

TaC-coated crucibles. The TaC-coated crucibles resulted in chemical incompatibility with the Cu-15v/o Cr and Cu-15v/o Nb alloys similar to the pure tantalum coating. The Cu-15v/o Cr alloy interaction with the TaC coating was chemically unsuitable; nevertheless, it was very interesting. Figure 6a highlights a region with residual alloy at the graphite crucible wall. The bulk of the metal climbed out of the crucible during melt processing. The majority of the metal analyzed consisted of tantalum-rich spheriodal precipitates within a chrome-rich matrix. Again, the morphology of the tantalum phase suggests a liquid immiscibility during processing, as was seen in the Cu-15v/o Cr alloy tested in the uncoated graphite crucible. Localized copper-rich regions were found both in areas adjacent to and over 100 μm away from the tantalum-chrome clusters.

Table 1. EDS Results From Selected Spots in Referenced Figures

Coating Material	Alloy Material		EDS Spot Analysis Label				Figure to be Referenced
	Cu 15v/oCr	Cu 15v/oNb	A	B	C	D	
ZrO_2 8w/oY_2O_3	X		W	Zr/Y	Cr	Cu	4a
ZrO_2 8w/oY_2O_3		X	W	Zr/Y	Nb	Cu	4b
Ta	X		Ta/Cr	Cu	Cr	Ta/Cr	5a
Ta		X	Ta/Nb	Cu	Cu	Ta/Nb	5b
TaC	X		Ta	Cr			6a
TaC		X	Ta/Nb	Cu	Ta/Nb	Ta/Nb	6b

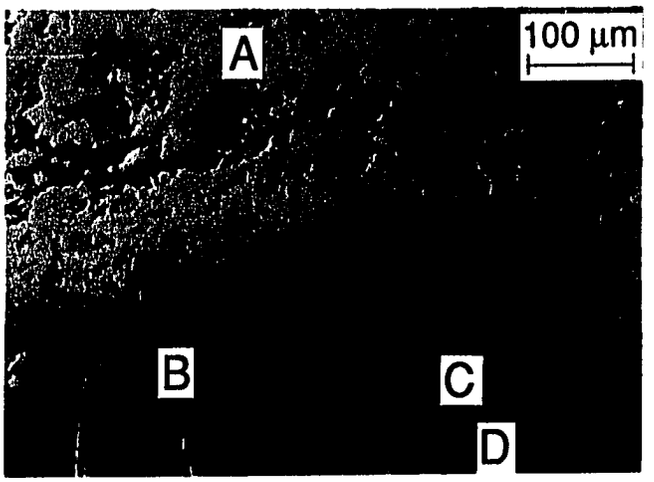

5a. Ta: Cu-15v/o Cr

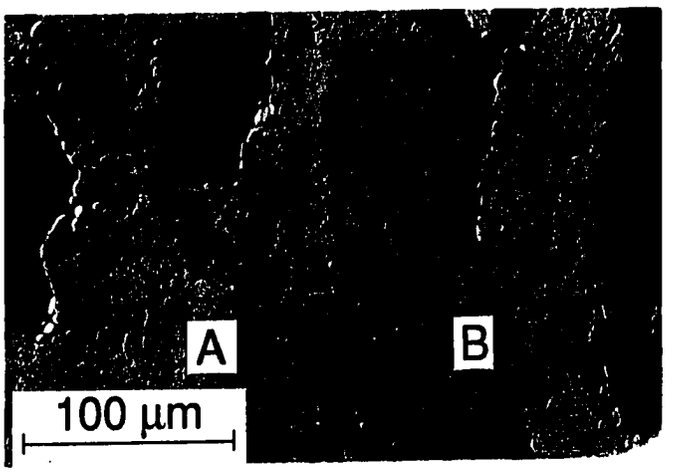

6a. TaC: Cu-15v/o Cr

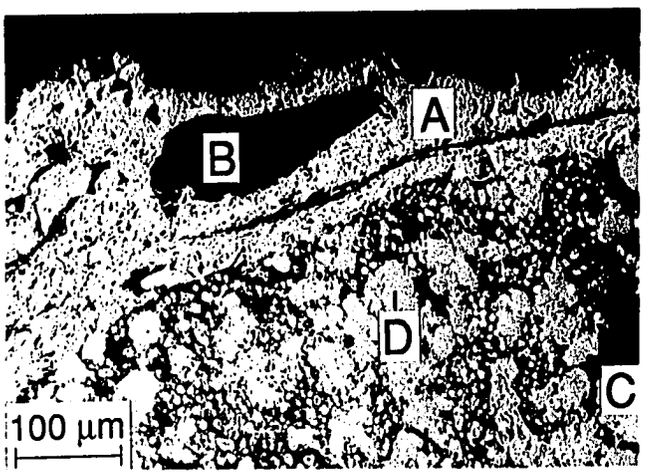

5b. Ta: Cu-15v/o Nb

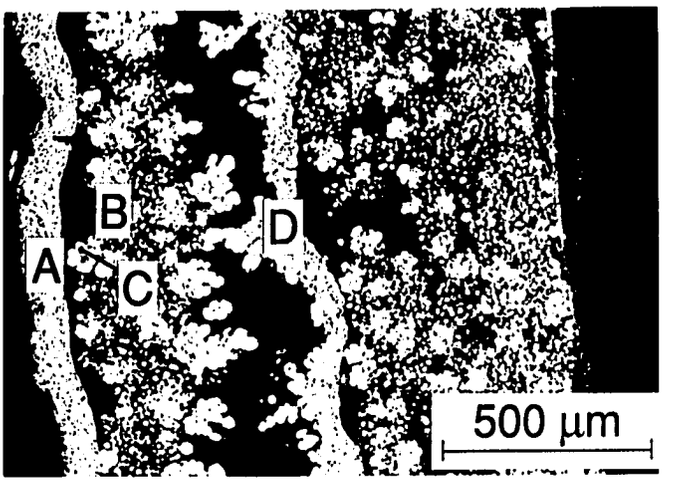

6b. TaC: Cu-15v/o Nb

Fig. 5 - SEM micrographs of Ta/Cu-alloys.

Fig. 6. SEM micrographs of TaC/Cu-alloys.

Figure 6b shows the macrostructure of the Cu-15v/o Nb processed in the TaC-coated crucible. The spots labeled in the figure correspond to the EDS results summarized in Table I. Again, contamination of the melt by tantalum was observed, as indicated by spots A, C, and D.

TaB_2-coated crucibles. A cursory analysis of the TaB_2 coating system was made. Tantalum again was found in niobium-rich dendrites and also in chrome-rich areas.

CONCLUSION

A series of uncoated and plasma sprayed graphite crucibles were tested under conditions emulating HPGA processing as containment crucibles for Cu-15v/o Cr and Cu-15v/o Cr alloys. The uncoated graphite crucibles physically contained the molten alloys, i.e. no substantial wetting occurred; however, carbon contamination of the melt was observed. Tantalum based coatings were severely wet by both copper alloys and chemically reacted with the melts. Tantalum was detected in the melt and, where analyzed, chromium and niobium were found within the bulk of the coating. The ZrO_2•8w/o Y_2O_3 coatings which were applied over a tungsten bond coat, were not wet by the molten alloys and were chemically stable to the levels discernable by the analytical techniques used in the current study. Future work at the Ames Laboratory Plasma Spray Facility will include the use of advanced analytical methods like inductively coupled plasma-atomic emission spectroscopy (ICP-AES) and scanning ion laser mass spectroscopy (SLIMS) to more precisely characterize the diffusion phenomena at plasma spray-molten alloy interfaces. Additionally, ongoing evaluation of other crucible coatings and alloy systems is being aggressively pursued.

ACKNOWLEDGEMENTS

Work was performed in the Materials Preparation Center at the Ames Laboratory which is operated for the U.S. Department of Energy by Iowa State University under contract No. W-7405-Eng-82. Support was provided in part by the office of Basic Energy Sciences through the Center of Excellence for Materials Synthesis and Processing.

The authors gratefully acknowledge the technical assistance of Iver E. Anderson, Frederick A. Schmidt and John D. Verhoeven.

REFERENCES

1. J.D. Verhoeven, W. A. Spitzig, F. A. Schmidt, and C. L. Trybus, *Mats. and Man. Processes, 4* (2), 197-209 (1989).

2. J. D. Verhoeven, W. A. Spitzig, F. A. Schmidt, P. D. Krotz, and E. D. Gibson, *J. Mat. Sci., 24.* 1015-20 (1989).

3. J. F. Smith, O. N. Carlson, and R. R. deAvillez, *Binary Phase Diagrams*, 2nd Edition, Vol. 1, p. 863, ed. by T. B. Massalski, ASM International, Materials Park, Oh (1990).

4. M. Venkatroman, and J. P. Neumann, *Binary Phase Diagrams*, 2nd Edition, Vol. 1, p. 837, ed. by T. B. Massalski, ASM International, Materials Park, Oh (1990).

PAPER 3. DEFORMATION PROCESSED WIRE PREPARED FROM GAS ATOMIZED Cu-Nb ALLOY POWDERS

T. W. Ellis, I. E. Anderson, H.L.Downing*, and J. D. Verhoeven
Department of Materials Science and Engineering and Ames Laboratory
Iowa State University, Ames, IA 50011
* Dept. Physics, Drake University, Des Moines, IA 50311

ABSTRACT

Wires have been fabricated by deformation processing of precursor billets that were prepared from alloy powders made by high pressure gas atomization (HPGA) of a copper-20vol.% niobium melt. The powders were classified and a larger size fraction, whose microstructure consisted mainly of 0.4 mm diameter Nb dendrites, was fabricated into the precursor billet by powder metallurgical techniques. The deformation processed wire prepared from the powder alloy billet gave significantly increased strengths at a given level of deformation strain over similar material produced by consumable arc casting. This may be attributed to the smaller initial Nb dendrite size of the alloy powder used for the precursor billet. However, the electrical conductivity of the powder material at a given strength level was significantly lower than the arc cast material. The cause of the reduction of the conductivity is uncertain and possible reasons are discussed.

INTRODUCTION

Deformation processed Cu-refractory metal materials have been under development for some time, originally as a precursor material for the fabrication of superconducting wire by the so-called *in situ* bronze process. Currently these materials are of interest for their combination of high electrical conductivity and high mechanical strength [1,2]. They are produced by large mechanical deformation of Cu-X alloy billets, where X is a refractory metal, e.g., niobium or tantalum. The precursor billets are usually produced by consumable arc melting and chill casting. It was demonstrated [3,4] that a reduction in scale of the original cast microstructure would produce increased strength at a given level of deformation strain. A new route for the production of Cu-Nb alloy powder with a very fine microstructure has become available to the authors with the installation of high pressure gas atomization (HPGA) facilities at the Ames Laboratory. Powders of Cu-Nb have been prepared by HPGA, consolidated by conventional powder processing techniques to prepare precursor billets, and reduced to wire by deformation processing. In this work the electrical and mechanical properties of deformation processed wires made from gas atomized copper-niobium alloy powders have been measured and are related to microstructural characteristics.

EXPERIMENTAL PROCEDURE

A Cu-Nb alloy powder was produced by HPGA from a melt of Cu-20 v/o Nb using argon for the atomization gas. The starting elemental charge was C10100 Cu and 99.9% Nb prealloyed by consumable arc melting followed by chill casting. The alloy charge was melted with an induction furnace at 3000 Hz in a fully dense cer-met crucible composed of 40 v/o ZrO_2 in a Mo matrix. The melt temperature at the start of the gas atomization pour was 2000°C. The 1 kg powder yield that resulted was collected, stored, and sieved under an argon atmosphere. A 38-63 μm sample was obtained and consolidated by cold isostatically pressing at 310 MPa to produce a material approximately 85% dense with open porosity. The cylindrical compact was placed in a copper can and hot vacuum out-gassed at 800°C for 4 hours, sealed by electron beam welding, and, then, hot isostatically pressed at 310 MPa for 4 hours at 800°C.

After consolidation the material was cold swaged from 25.4 mm to 2.9 mm , then drawn to 1.3 mm where fracture by "center bursting" became a problem. At this point the as-drawn material was swaged to 0.79 mm and drawn to a final diameter of 0.36 mm. This procedure was done using only material deformed to one die before center-bursting was noted. Further mechanical reduction was discontinued due to the reoccurrence of center bursting of the wire.

Mechanical testing was done at a strain rate of 0.25 mm/min. after a gauge section was produced by abrasive polishing. All testing was at ambient temperature. Electrical resistivity measurements were done by the standard four probe method as previously described [2]. Heating rates during the resistivity cycle were 1°C per minute from ambient temperature to 800°C with a 2 hour hold at 800°C followed by furnace cooling to room temperature at 1°C per minute.

RESULTS AND DISCUSSION

The microstructure of these spherically shaped alloy particles produced by HPGA, has been found to be dependent on the particle size [5]. A mixed dendritic/spheroidal niobium morphology has been noted, with the volume fraction of spheroids increasing as the particle size decreases. For the size cut used in the present experiments, the spheroids have a diameter in the range of 1 to 3 μm and the diameter of the secondary dendrite arms has been found to fall between 0.3 to 0.5 μm [5]. A more complete presentation of the microstructure as a function of particle size can be found in the work by Zeik et al.[5].

The presence of the spheroids in the gas atomized particles is believed to result from a metastable monotectic reaction. Previous research [6] has demonstrated that this reaction is induced by the large undercoolings which accompany rapid solidification. The fraction of the microstructure consisting of spheroids increases as the solidification rate increases, and therefore, as expected, larger fractions of spheroids were found in the smaller sized particles. In the larger powder sizes used here, the monotectic spheroids are not as prevalent and, as shown in Fig. 1, the niobium morphology is mostly dendritic, with the spheroids found mainly near the outer surface of powder particles. For comparison purposes Fig. 2 presents a micrograph of Cu-20 v/o Nb material produced by consumable arc melting. The average secondary dendrite arm diameter for the arc cast material was reported [3,4] to be 3.8 μm, compared to an average secondary arm diameter of a dendrite ≈ 0.4 μm for HPGA material.

Figure 1. The edge, lower border of micrograph, of a powder particle showing fine Nb dendrites in the interior and spheroids near the surface. Backscatter SEM micrograph at original magnification of 2510X

The data collected on ultimate tensile strength versus deformation strain, h, are given in Table I, where h is defined as the natural log of the ratio of the cross-sectional areas of the original as-HIPped cylinder to the final wire. A plot of ultimate tensile strength versus deformation strain is given in Fig. 3 and compared to the results on the arc cast material [3]. As can be seen the UTS of the HPGA produced powder in the HIPped condition ($\eta = 0$) is considerably higher than in the arc cast material. This would be expected because, as illustrated above, the microstructure in the powder processed material is much finer than in the arc-cast specimen. TEM micrographs in Fig. 4 of both the HPGA produced powder wire and arc cast wire drawn to the same strain ($\eta = 7.9$) clearly show that the spacing between the niobium

filaments is much smaller in the powder case as compared to the arc cast material. This result confirms the previous findings [3] that a finer starting dendritic microstructure will develop a finer filament spacing and higher mechanical strength for a given deformation strain. This demonstrates that utilizing alloy powders in the precursor billets of deformation processed materials provides a method of achieving increased strength at a give level of deformation.

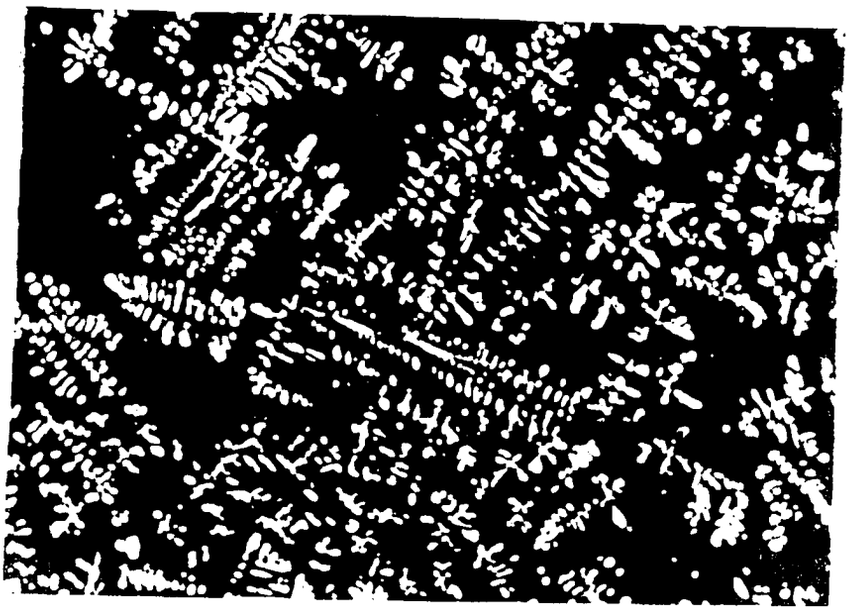

Figure 2. Optical micrograph of arc cast Cu-20v/o Nb ingot. Original magnification is 107X

Table 1. Summary of mechanical deformation procedure and measured ultimate tensile strengths

η	Mechanical Deformation	UTS (MPa)
0	None, as Hipped	665
4.84	Drawn only	884
5.52	"	1060
6.77	"	1220
7.70	"	1560
4.84	Swaged only	884
7.30	Drawn to 1.25mm, Swage to 0.78 mm, Drawn to 0.64 mm.	1320
8.72	Drawn to 1.25mm, Swage to 0.78 mm, Drawn to 0.36 mm.	1640

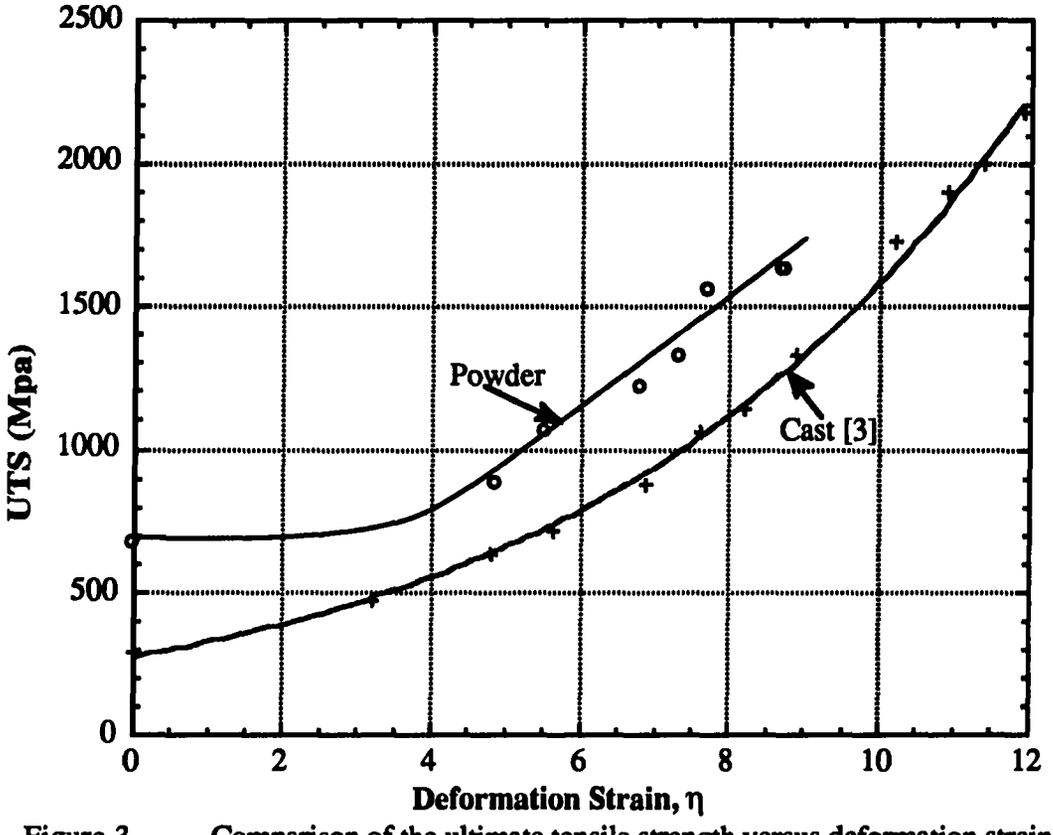

Figure 3. Comparison of the ultimate tensile strength versus deformation strain for Cu-20 ^{v}/o Nb wires prepared from arc cast and powder processed material

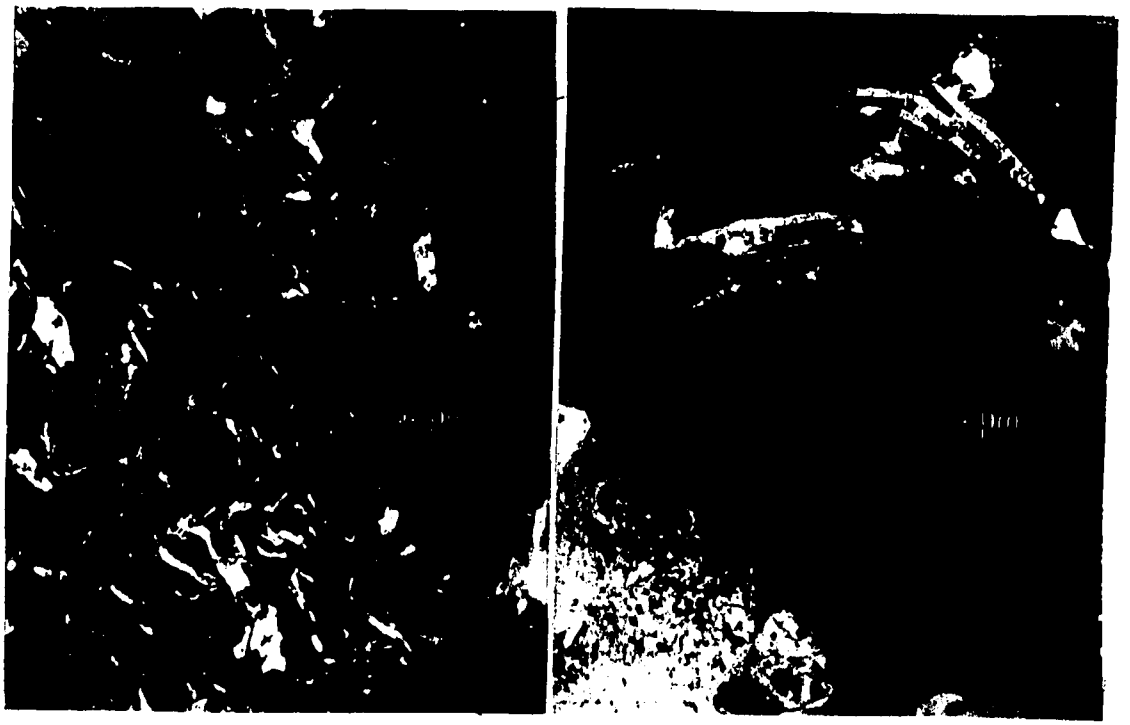

(a) (b)

Figure 4. TEM conical scanning dark field image of transverse section of wire made from Cu-20^{v}/o Nb both drawn to $\eta = 7.9$. (a) Powder processed material. (b) Arc cast material. Original mag. = 85, 000X

There were some unexpected differences found between the alloy powder material and the arc cast material. The maximum deformation strain possible without breakage for the powder processed material was $\eta = 8.5$. With the arc cast material deformation strains of $\eta >$ 12 were obtained without breakage. TEM micrographs of transverse sections of the two materials at the same level of strength (UTS = 1570 MPa) are shown in Figs. 4a and 5. It is seen that, at the same level of strength, the Nb filament thickness of the powder material is slightly smaller than for the arc cast material and the aspect ratio (thickness/width) of the Nb ribbons is significantly smaller for the powder material. In order to evaluate the impurity level of the samples, several chemical analyses were carried out and the results are presented in Table 2. The first column lists the results obtained by scanning laser ion mass spectrometry (SLIMS) analysis, given in ppm by weight, on the as- HIPped material. All remaining elements in the periodic table were found to be present below the detectability limit of the instrument, which was less than 0.2 to 4 ppm atomic. The second column lists the impurity results for the as-prepared powders, where C, N, and O were measured by vacuum fusion

analysis and Mo was measured by wet chemistry. The SLIMS method should be regarded as only approximate for the three gaseous elements and, also, for the Mo because of its high value, indicated by parenthesis around their respective values. The results show a significant amount of Zr, Mo, and Be contamination in the melt. The Zr and Be are almost certainly present as oxides. The probable source of the Zr is the ZrO_2 content of the cer-met crucible brought about by the slow dissolution of the molybdenum cer-met matrix phase, freeing ZrO_2 particulates from the crucible wall (5). It is most likely that the residual Mo is present as a dissolved element in the Nb phase, as its solubility in Cu is negligible and its oxide is volatile at the melt temperatures. Consistent with this explanation, discrete inclusions of Mo were not found in the SEM analysis. The presence of molybdenum in the niobium reinforcing phase does not significantly alter the either the phase equilibria nor the bulk composition of the alloy. However, the mechanical properties of the niobium will be altered to some extent. The clear source of residual Be (as BeO) was a mild erosion of the BeO stopper rod used in the bottom-pour crucible design of the HPGA promoted by induction field-driven melt stirring.

Table 2. Chemical Analysis by Mass Spectrometry, Vacuum Fusion and Wet Chemistry

Element	ppmw(MS)	ppmw(other)
Be	76	
C	(13)	120
N	(4)	43
O	(260)	290
Al	2	
Si	8	
Ca	8	
Cr	153	
Fe	49	
Ni	43	
Zr	350	
Mo	(46000)	18000 (1.8 $^{w}/_{o}$)
Ta	160	
W	11	

The difficulty of drawing wire beyond $\eta = 8.5$ may be due to the presence of small inclusions in the microstructure. There are two possible reasons why small inclusions might be present in the powder material. First, inclusions of ZrO_2 and BeO were probably acquired during melting, as described above. The examination of fracture surfaces by SEM has revealed ZrO_2 particles at the apparent fracture nucleation sites (7). Detection of BeO particulate inclusions was not possible using EDS x-ray analysis within the SEM. The second possible reason relates to the fact that when the powder was observed after gas atomization it was found to have the Nb (dull gray) color. It is known that solidified Cu-

Figure 5. TEM conical scanning dark field image of transverse section of wire made from arc cast Cu-20v/o Nb alloy and drawn to $\eta = 9.1$. This material has a comparable strength, 1570Mpa, to the powder processed material h =7.9. Original mag. = 85, 000X

Nb alloys often have a very thin metallic colored Nb rich layer on their surfaces and such was the case with the powders. It is likely that during the HIP operation the particles became coated with an increased Nb oxide layer because of the high chemical affinity of Nb for O_2. Remnants of this oxide could therefore be present as inclusions in the drawn wire. However, if it is assumed that the Zr and Be are present as oxides, then the data of Table II indicates that the amount of Nb oxide present in the final material must be very small. The presence of inclusions, especially ZrO_2 and BeO, could account for some of the differences between the powder and arc cast materials noted above. They could act as crack nucleation sites and could account for the reduced drawability of the powder processed material. If the inclusions had a negative effect upon the strength, then the Nb filaments would need to be finer in the powder material to give the same strength, as appears to be the case in Figs. 4 and 5.

Resistivity experiments revealed a significant difference between the powder processed wire and chill cast materials. Figure 6 presents resistivity versus temperature data for the powder and the cast wires of Figs. 4a and 5. The upper branch of each data set gives the resistivity upon heating up to 810 °C, and the lower branch gives the resistivity upon cooling after a 2 h hold at 800 °C It is seen that after the 2 h annealing treatment at 800 °C, the room temperature resistivities of both materials are essentially the same. However, the initial resistivity of the wires prepared from powder material is significantly higher than for wires prepared from cast material. The data illustrate that, at the same level of strength the resistivity of the as-drawn powder material is higher than the cast material. This result is illustrated more generally by Fig. 7, which plots the ultimate tensile strength versus the as-drawn electrical conductivity. The conductivity is given in terms of the percent of the international annealed Cu standard, %IACS, where the standard pure Cu resistivity is taken at 20 °C as 1.724 μΩ-cm.

The total electrical resistivity of these materials can be expressed as the sum of individual contributions from electron scattering with interfaces, impurities, dislocations, and phonons. Previous resistivity studies on the arc cast material [2] have shown that at h values greater than around 6 a significant fraction of the resistivity is due to electron scattering at Cu-Nb interfaces. An annealing treatment of the arc cast material at 750 °C was shown to reduce electron scattering from Nb dissolved in the Cu matrix to a negligible level by promoting Nb precipitation. It is therefore expected that the thermal treatments associated with the HIP consolidation of the powders would have reduced the level of Nb dissolved in the Cu phase to the point where it would make a negligible contribution to resistivity. The dislocation scattering contribution to resistivity was shown to be small (0.1 μΩ-cm) and the dislocation density essentially constant with strain above η values of ≈ 4 [2]. Therefore, it seems likely that the

increased resistivity (reduced conductivity) of the powder processed material at a given strength must arise either from impurities dissolved in the Cu phase or from increased interface scattering. To assess the possible contribution of impurity scattering effects, consideration was given to the dissolved elements most detrimental to the resistivity of Cu, i.e., Ti, P, Si, Fe and Be (8). Of these five elements, only Si, Fe, and Be were detected in the consolidated samples. Upon calculating the dissolved contribution to the resistivity from Si, Fe, and Be (with Be here assumed as an elemental metal in solution with Cu, not as BeO), the contribution to the total reduction of conductivity from the levels listed in Table II, is found to be less than 0.05 % IACS. The measured reduction in conductivity of the powder processed wires, as Fig. 7 gives, is at least 40 % IACS. Hence, it seems fairly certain that the reduction in conductivity of the powder material is not due to dissolved impurities in the Cu matrix.

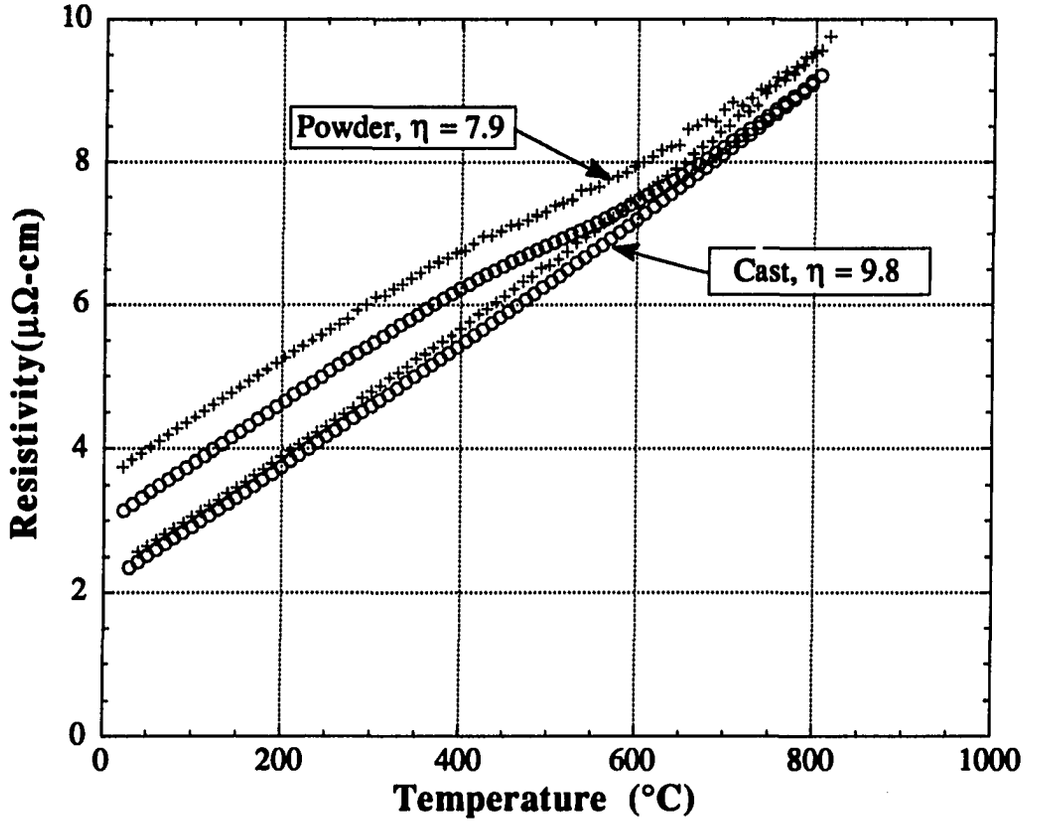

Figure 6. Electrical resistivity versus temperature for powder and cast Cu-20 v/o Nb wire deformed to η values producing a strength level of 1570 MPa

From the preceding considerations the cause of the increased resistivity of the powder materials at a given level of strength (found to be ≈ 0.6 μΩ-cm at 1570 MPa, as shown in Fig. 6) appears to be increased scattering at Cu interfaces. Two types of Cu interfaces are present in the wires: Cu / inclusion and Cu / Nb filament interfaces. The Cu/inclusion interfaces may be further subdivided into two types: 1) those associated with ZrO_2 and BeO particles produced in the melt processing, and 2) the Nb oxide skins removed from the powder surfaces during the very large deformation. TEM evidence did not reveal a significant volume fraction of such inclusions. But, because some of the inclusions may have sizes in the low nanometer range, particularly the Nb oxide skin remnants, and because high resolution TEM was not employed, it is not possible to eliminate experimentally Cu / inclusion interfaces as a significant contribution to increased resistivity in the samples.

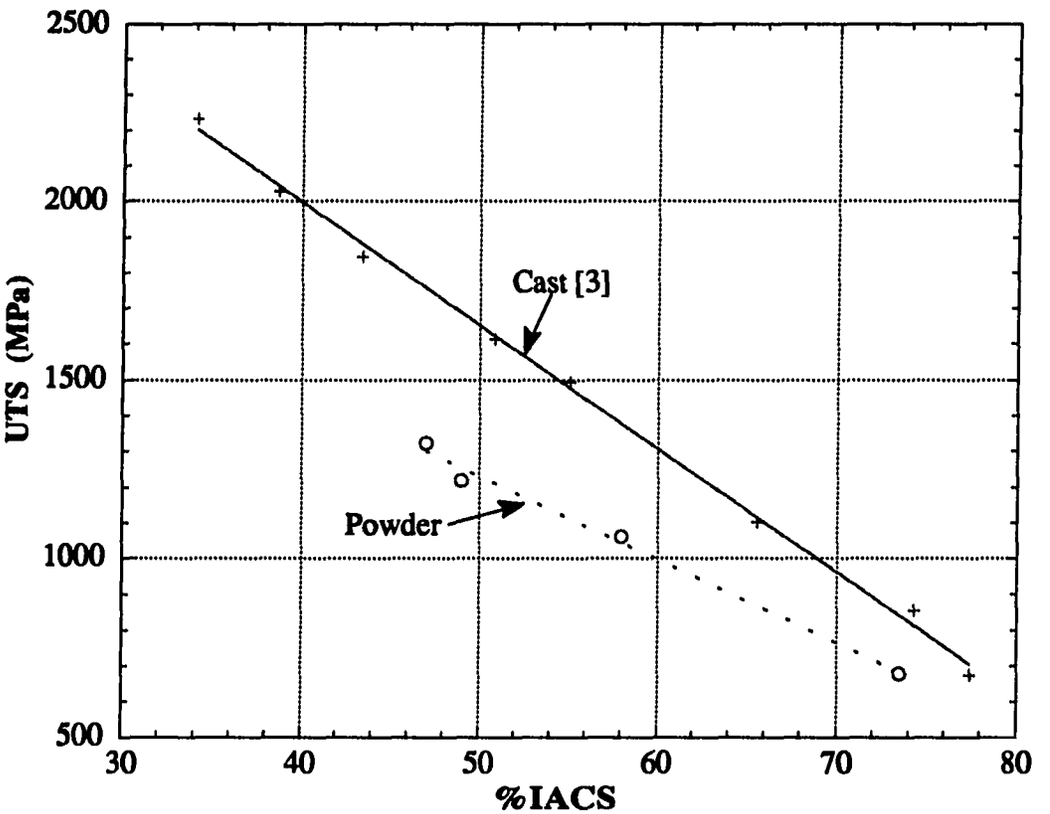

Figure 7. Comparison of the ultimate tensile strength versus conductivity for Cu-20 v/o Nb wires prepared from arc cast and powder material

Previous research [1] on chill cast Cu-Nb alloys, as well as Cu-Ta and Cu-Cr alloys has found that at a given volume fraction refractory phase there is a unique relationship between ultimate tensile strength and electrical conductivity in these deformation processed alloys. The finer refractory metal filaments formed at higher deformations produce increased strength along with decreased conductivity; and the data fits the same strength/conductivity function for the different alloys, and for the same alloys with different initial dendrite sizes, as long as the volume fraction of the refractory phase is constant. The data of Fig. 7 for the powder processed material do not conform with these previous results for chill cast materials. If additional Cu / Nb filament interfaces, rather than Cu/inclusion interfaces, cause the increased resistivity of the powder processed wires for the same volume fraction of Nb, then the Nb ribbons must be thinner and more numerous at the same level of strength compared to the chill cast material. There are clear morphological differences in the Nb filaments between Figs 4a and 5. It is possible that due to the inclusion content of the powder material the Nb filament morphology is sufficientiy changed that, to achieve a given level of strength, a finer filament size is required which leads to a reduced conductivity. This type of result has been found with sheet material, where the strength/conductivity function lies well below that of wire material [1]. Further investigation is required to understand the cause of the reduced strength/conductivity data for the powder processed material. New efforts will be initiated to generate improved powder processed Cu-Nb materials using prc visions to significantiy reduce the possibility of inclusion contamination.

CONCLUSION

It has been shown that by preparing deformation processed Cu-20 v/o Nb alloys starting with precursor billets made from HPGA alloy powders much smaller drawing strains are required to obtain a given strength level than is possible with precursor billets of arc cast Cu-20 v/o Nb alloys. The higher strengths result from the finer Nb filaments produced from the smaller Nb dendrites in the powder processed precursor billets. Significant differences were found between the powder and arc cast materials. At a given level of strength the powder material had Nb ribbon filaments with a significantly smaller aspect ratio and slightly smaller thickness and it had a significantly higher resistivity. Also, the powder material could not be drawn nearly as far without breakage as the cast material. The increased oxide inclusion level present in the powder material may be the cause of these differences, but this conclusion is uncertain and additional studies are needed. This tentative conclusion also emphasizes the fact that additional powder processing research is necessary to produce a clean Cu-Nb microstructure by this new route to fully test the potential benefit of an ultrafine rapidly solidified morphology on strength and conductivity.

ACKNOWLEDGEMENTS

The authors would like to thank the following Ames Lab personnel for their assistance, F.C. Laabs whose knowledge of TEM and the use of scanning conical dark field imaging was invaluable in performance of this work, R. L. Terpstra for his work in preparing the atomizer, and L.K. Reed for his aid in mechanical testing. In addition, discussions with W.A. Spitzig, L.S. Chumbley, and E.D. Gibson have been helpful. This work was performed at the Ames Laboratory operated for the U.S. Department of Energy by Iowa State University under contract number W-7405-ENG-82.

REFERENCES

1. J.D. Verhoeven, W.A. Spitzig, F.A. Schmidt, and C.L. Trybus, Materials & Manufacturing Processes, 1989, Vol. 4, pp 197-209.

2. J.D. Verhoeven, H.L. Downing, L.S. Chumbley, and E.D. Gibson, J. Appl. Phys, 1989, Vol. 3, pp 1293-1301.

3. W. A. Spitzig and P. D. Krotz, Scripta Met, 1987. Vol. 21, pp 1143-1146.

4. J.D. Verhoeven, W.A. Spitzig, F.A. Schmidt, P.D. Krotz, and E.D. Gibson, J. Mat Sci, 1989, Vol. 24, pp 1015-1020.

5. K.L. Zeik, I.E. Anderson, P.R. Howell, and D.A. Koss, Met. Trans. A, (in press).

6. J.D. Verhoeven and E.D. Gibson, J. Mat. Sci., 1978 Vol. 13, pp 1576-1582.

7. K.L. Zeik, PhD Dissertation, Pennsylvania State Univ., March 1991.

8. P.W. Taubenblat, W.E. Smith, and A.R. Gravino, High Conductivity Copper and Aluminum Alloys, AIME Proc, 1984, pp 19-31.

PAPER 4. NEW APPLICATIONS OF DEFORMATION PROCESSING FOR THE FORMATION OF METAL METAL MATRIX COMPOSITES

Timothy W. Ellis, Ames Laboratory, U.S. D.O.E.,
Iowa State Univ., Ames, IA 50011

ABSTRACT

This paper surveys new extensions in the development of deformation processed metal metal matrix composites. These studies have explored new alloys systems, methods of production, and the engineering applications of these materials.

INTRODUCTION

Deformation processed copper-refractory metal alloys have been under extensive development for quite some time at the Ames Laboratory (1). Interest in these alloys is sparked by their unique combination of high mechanical strength with excellent electrical conductivity. The knowledge and experience gained in the development of these alloys is being used to develop other deformation processed composite materials.

The particular microstructure which defines a deformation processed metal-metal matrix composite, DMMCs, is unique in terms of structure and processing. Common polymer matrix composite materials have a continuous polymer matrix reinforced by the presence of fibers of inorganic or organic material. In DMMCs a continuous metallic matrix phase is reinforced by a high aspect ratio non-continuous metallic reinforcing phase. The fibrous morphology of the reinforcing phase is produced by the codeformation of the matrix and reinforcing phases. Therefore, the fibrous morphology of the reinforcing phase is formed in-situ during deformation of the material; a distinction that separates these materials from the wide range of non-metallic reinforced metal matrix materials, e.g. SiC fibers in aluminum.

THEORY

Copper-Niobium alloys show that the high aspect ratio fibrous morphology can be produced by simultaneous deformation processing of a copper matrix and niobium reinforcing phase Further investigation showed mechanical strengths far in excess of those predicted by a simple rule of mixtures calculation (2). Some of the fundamentals of this type of composite have been previously presented by several authors (3, 4).

Deformation processing of a two phase immiscible alloy, for example the copper-niobium alloy, (see phase diagram presented in Figure 1), produces a microstructure consisting of a continuous matrix phase and a high aspect ratio fibrous phase. Prototypical microstructures, of a copper-20 vol. % niobium alloy, formed upon deformation processing, rolling and drawing respectively, are shown in Figure 2. The precursor material was produced by consumable arc melting for which the original starting microstructure is shown in Figure 3. The as cast microstructure consists of primary niobium dendrites within a continuous copper matrix.

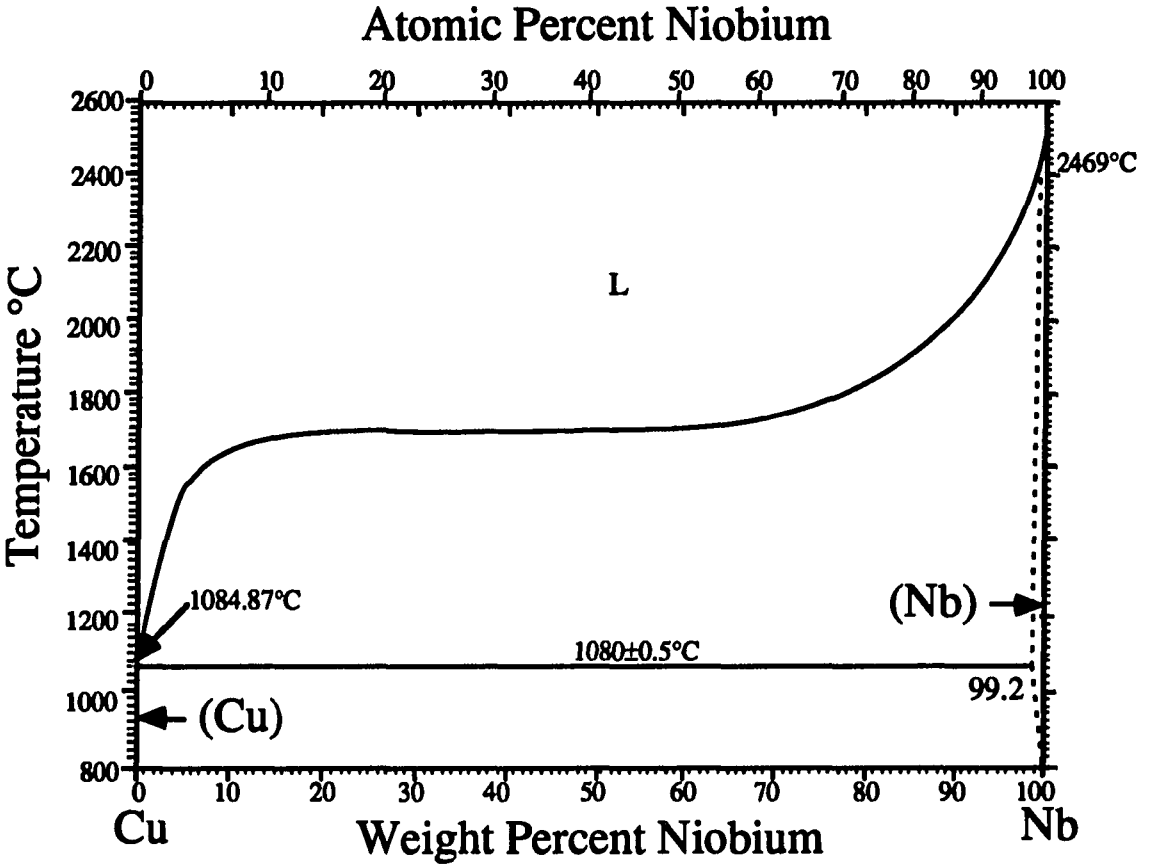

Figure 1. Equilibrium Phase Diagram for the Copper-Niobium System (7)

Niobium fibers form from the primary dendrites during deformation processing. They have been shown to deform in plane strain conditions which is a result of the texture formed upon deformation (2). During deformation both the reinforcing phase and matrix phase become highly textured; in niobium a BCC metal the texture is <1 1 0>. Texture development limits the number of available slip systems to two which produces the plane strain condition giving ribbon shape cross section. Other copper-X alloys investigated have shown identical behavior, X= (Cr, Fe, Mo, Ta, V, Re). Research done on deformation processed composites with other crystallography's has shown similar results. The microstructures formed by deformation processing of yttrium-titanium (HCP-HCP) and yttrium-niobium (HCP-BCC) are shown in Figures 4 and 5. The ribbon like morphology of the reinforcing phase indicates that the plane strain condition can be obtained in other crystallographic besides that of the Cu-X, alloys a FCC-BCC system. This is an interesting result as the actual crystallographic textures developed are different for each crystal structure. Since similar morphologies are produced in materials with different crystal structures this processing method has a much wider application.

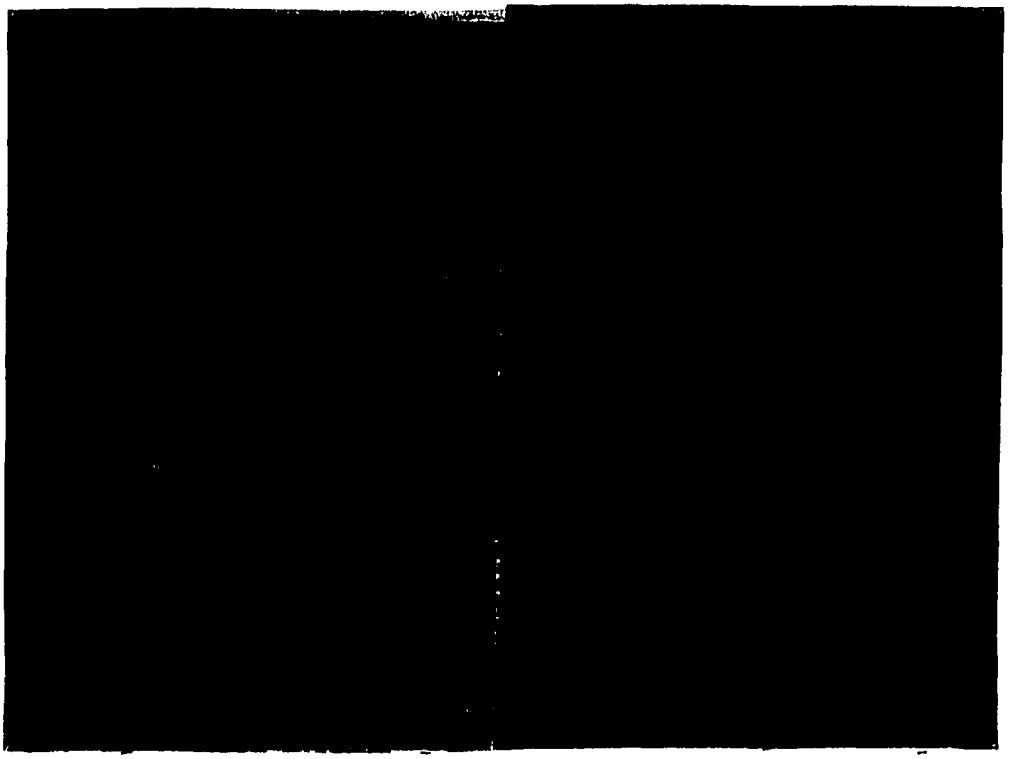

Figure 2. Microstructure of Deformation Processed Sheet and Wire Material, Section is Perpendicular to Rolling or Drawing Direction. of a Cu-20 v/o Nb alloy

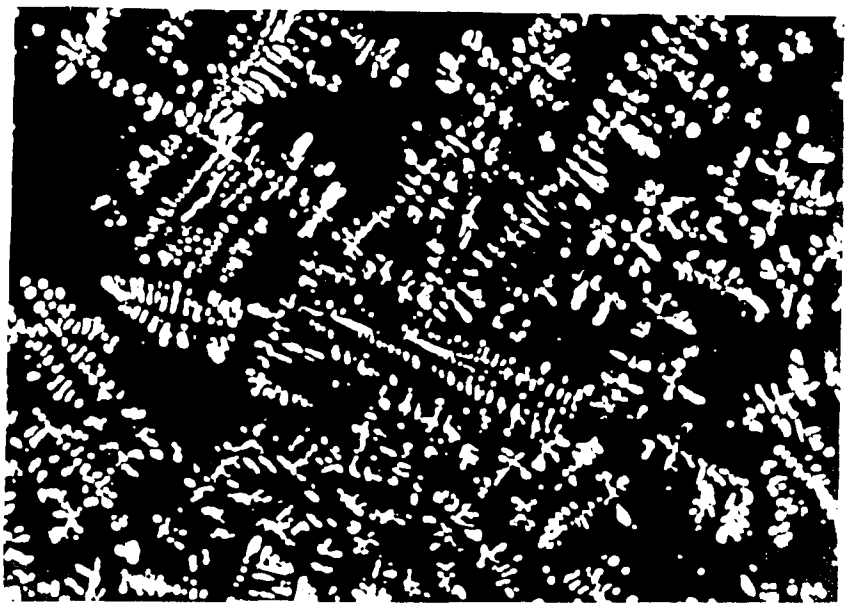

Figure 3. Microstructure of Consumably Arc-Cast Copper-20 vol. % Niobium

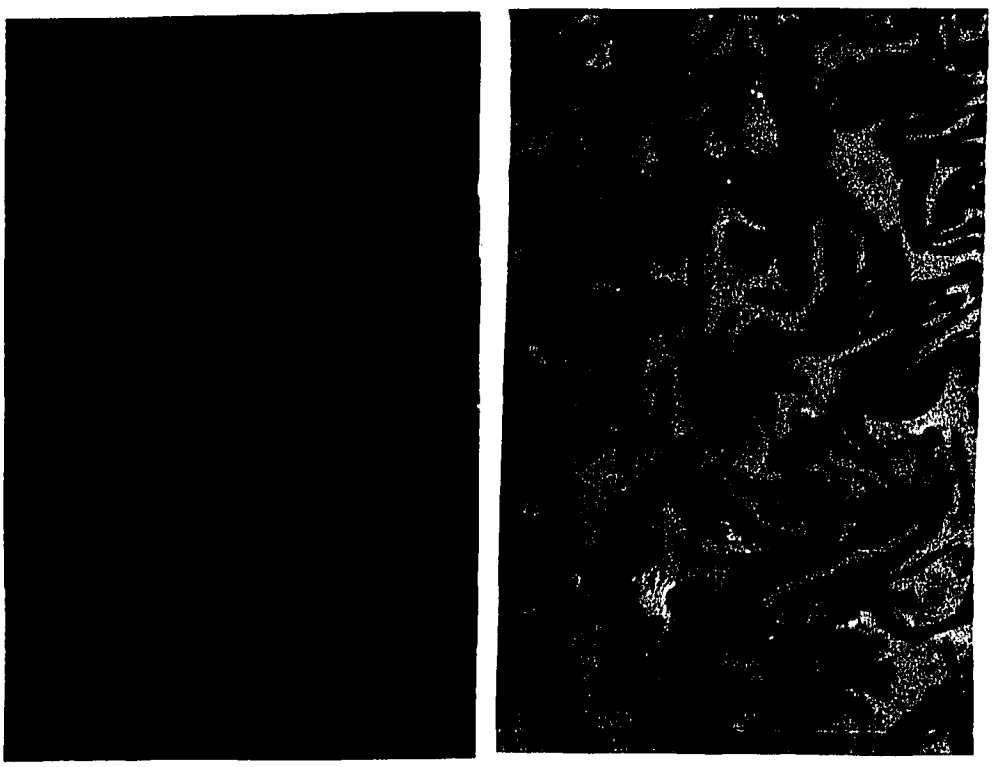

Axial Transverse

Figure 4. Microstructure of Deformation Processed Titanium-50 vol. % Yttrium alloy in Axial and Transverse Section

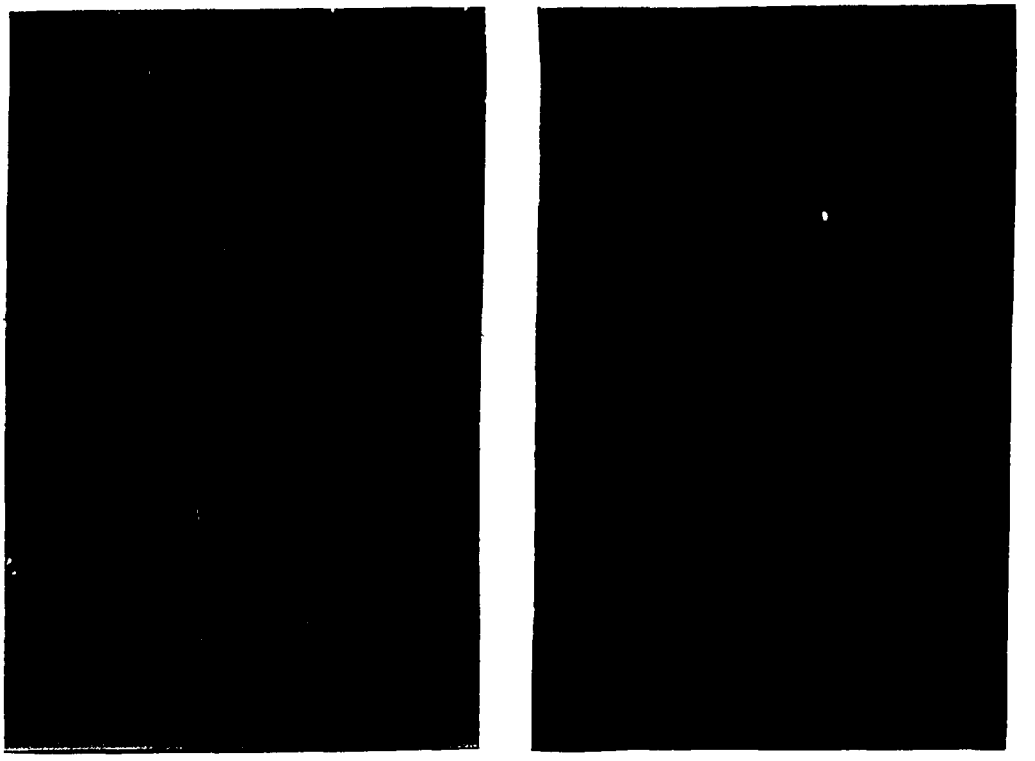

Axial Transverse

Figure 5. Microstructure of Deformation Processed Yttrium-20 vol. % Niobium alloy in Axial and Transverse Section

PHASE EQUILIBRIA

Two general methods are available for the production of precursor material. Precursor billets to be deformation processed can be produced using solidification and powder processing. Both approaches may be viable means for precursor alloy production for any particular alloy system. Consideration of phase equilibria is necessary in the design of these materials. A prototype for metallurgical systems amenable to deformation processing for the development of a composite has been presented, that is copper-niobium, as shown in Figure 1. Low mutual solubility in each of the metals within this alloy would indicate that the physical properties of each component are similar to those of the pure elements. In the Cu-X systems this factor allows the Cu matrix to maintain its high electrical conductivity. The high strength developed in DMMCs results from the codeformation of the matrix and minor phase producing a very fine spacing of the minor phase. Experience has shown that the flow stress of the matrix and minor phase must be roughly equal to allow codeformation.

Table 1. Possible Equilibrium Systems for Deformation Processed Composites (7)

Matrix Material	Reinforcing Phase
Aluminum	Be, Sn, Zn
Copper	Ag, Cr, Co, Fe, Ir, Mn, Nb, Os, Ta, Re, Rh, Ru,, V, W
Iron	Ag, Cu, In, La, Mn, Os, Ru
Magnesium	Cr, Fe, Hf, Li, Mo, Re, Sc, Ta, Ti, V, W, Zr
Molybdenum	Pd, Pu, Sc, Ti, Th, Y
Niobium	Sc, Ti, Th, U, Y, Zr
Nickel	Cr, Os, Re, Ru, W
Titanium	Mg, Mo, Th, V, Y, W
Yttrium	Cr, Hf, Mo, Mn, Nb, Pu, Sc, Ta, Ti, Th, V, W, Zr

Note: Other metals within the same group have similar equilibria.

Therefore, the ductility or plastic deformation behavior of the material needs to be considered. Table 1 gives a listing of systems which would appear to display the proper equilibrium phase diagrams for the production of DMMCs by deformation processing. What can be seen in the above list is the great variety of systems possessing the proper phase equilibria to produce these materials. However, this does not imply that other systems in which intermetallic compounds exist may not be used to form deformation processed composite materials. Difficulties may result because the formation of brittle intermetallics would limit the ductility of either the matrix or reinforcing phase. However, it is often possible to first form a filamentary composite by deforming two ductile phases, and then form a brittle intermetallic phase have useful electrical or magnetic properties by a diffusion anneal. This method has been used to produce Nb_3Sn fibers within a copper matrix by the so called bronze process for the production of superconducting wire (8)

PRECURSOR ALLOY PRODUCTION

Solidification processing of precursor alloys for further deformation processing to produce composite materials has been studied extensively. Precursor alloys have been produced by several solidification processing methods here at the Ames Laboratory as listed in Table 2. Consumable arc casting and high pressure gas atomization, HPGA, followed by powder copmpaction are the methods of choice for the production of precursor billets as the alloys produced have a very refined initial starting microstructure. This reduces the total amount of deformation necessary to obtain any particular microstuctural refinement (9, 10, 11). In alloy preparation chemical contamination of precursor material should be kept to a minimum. Many refractory metals, which have desirable properties, are very susceptible to embrittlement by carbon, oxygen, and nitrogen. Homogeneity of the microstructure is also important as large unalloyed globules or large variations in dendrite size across a precursor billet can lead to non-uniform deformation and over working of limited areas leading to fracture or breakage of the billet during deformation processing. Tables 2 and 3 list the methods employed to produce the various precursor alloy billets investigated here. Powder metallurgical techniques have been used with great success to produce precursor billets. Billets can be formed from prealloyed powders produced by HPGA, mechanical alloying, or mixed elemental powders (10, 11). The use of HPGA and mechanically alloyed precursor powders allows refinement of the microstructure prior tc formation of billets to be deformation processed. Consolidation of the billet is done by several methods, including hot or cold isostatic pressing and/or extrusion. One must be careful in heating mechanically alloyed or deformation processed composites as the thermal stability of DMC microstructures has been found experimentally to be quite poor. An explanation of this phenomena was put forth by Kampe et al based on analysis of the Rayleigh stability of a fibrous shape at elevated temperatures (13, 14).

Table 2. Solidification Methods for the Production of Precursor Materials for Deformation Processing

Method	Alloy Systems
Bottom Pour chill Casting	Cu-Cr, Cu-Co, Cu-Fe, Cu-Nb, Cu-V
Consumable Arc Melting	Cu-Cr, Cu-Nb, Cu-Re, Cu-Ta, Y-Ti
Non-Consumable Arc-Melting	Y-Cr, Y-Mo, Y-Nb, Y-Ti, Y-V, Y-Zr

Table 3. Powder processed Deformation Processed Alloys

Method of Powder Production	Alloy System
High Pressure Gas Atomization (HPGA)	Ag-Cu, Cu-Cr, Cu-Nb
Mechanically Alloyed	Cu-X (X= Cr, Mo, Nb, Ta, V,W) Al-Fe, Al-Nb Mg-R (R= Cr, Fe, Mo, Nb, Ti, V)
Mixed Elemental Powders	Cu-X (X= Mo, Nb, W) Al-Z (Z= Fe, Nb, Ta)

These processing methods are normally used in conjunction with one another to assure a fully dense material prior to cold deformation processing. After full consolidation has been achieved conventional mechanical processing is undertaken. Powder processing is most amenable to the production of alloys which cannot be sucessfully melt processed because of the physical chemistry of the constituent elements.

NEW HORIZONS

Development of DMMCs has recently taken some new twists. This can be best illustrated by several systems investigated here at the Ames Laboratory. Gibson and Verhoeven have deformation processed aluminum-niobium and aluminum-tantalum alloys (12). Deformation processing the material is used to produce a fine filamentary structure. The alloy was then used for the preparation of electrical capacitors. Deformation processing produces the very fine microstructure necessary to give a large niobium or tantalum surface area. These surfaces were then selectively oxidized to produce a dielectric layer. High surface area is imperative as the capacitance of the device is dependent upon the amount of oxide surface. This process was investigated as a replacement for the conventional powder processed capacitors presently available commercially. Capacitors were manufactured from precursor billets produced from mixed elemental powders which were cold isostatically pressed and deformed, at room temperature, within a steel can. Binary elemental alloys would be unavailable through solidification metallurgy due to intermetallic compound formation. Cold deformation was chosen to also limit the possibility of intermetallic compound formation.

Recently work has been done on the production of several new deformation processed structural alloys. Yttrium based systems are of great interest due to its relatively high melting point, 1522°C, and low density, 4.54 grams/cm^3 (15). Yttrium has a very low solubility for the group IV, V and VI metals in its low temperature alpha phase (HCP). Additionally, the group IV, V and VI metals does not significantly enhance the stability of the high temperature Beta phase (BCC). The a-b transus in Yttrium-refractory metal alloys is in the range of 1000-1200°C, which is much high than the 600-800°C range for comparable titanium alloys. Therefore, it may be possible to form DMMC's which would have suitable physical properties for use in the 600-900°C range. An area of particular development is the production of Yttrium-Titanium alloys with superior properties and lower densities than available in common titanium alloys.

As shown in Figure 6 for a copper-20 vol. % niobium alloy and two titanium-yttrium alloys, 20 and 50 vol. %, the ultimate tensile strength (UTS) increases as a function of eta (η) (6). Eta is define as the natural log of the ratio of the reduction in area, $\eta = \log A_f/A_i$, where A_f is the final cross sectional area and A_i is the initial cross sectional area.

A similar processing program is utilized for the development of magnesium based systems. Refractory metals have a very low solubility in magnesium. Composites materials, in these systems, are produced by powder methods due to the low boiling point of

magnesium (1107°C). These materials were produced by mechanical alloying, followed by cold consolidation similar to that used in the aluminum based systems. In Figure 2, Vickers hardness for several mechanically alloyed magnesium based systems are compared to pure magnesium and an average value for precipitation hardened magnesium alloys. The target application here is an alternative to high strength aluminum alloys at temperatures greater than 300°C. Since most high strength aluminum alloys are precipitation hardened the long term mechanical stability at elevated temperatures is quite poor. Precipitates formed by aging coarsen at these temperatures bringing a subsequent reduction in strength. Since the homologous temperature of the refractory metal reinforcing phase is so low coarsening is not expected possibly in the 300-400°C range. It is also known that magnesium wets other metals quite well. Therefore, one would expect that matrix/particle bonding would be superior to that where an inorganic solid e.g., SiC, is used to reinforce the matrix material.

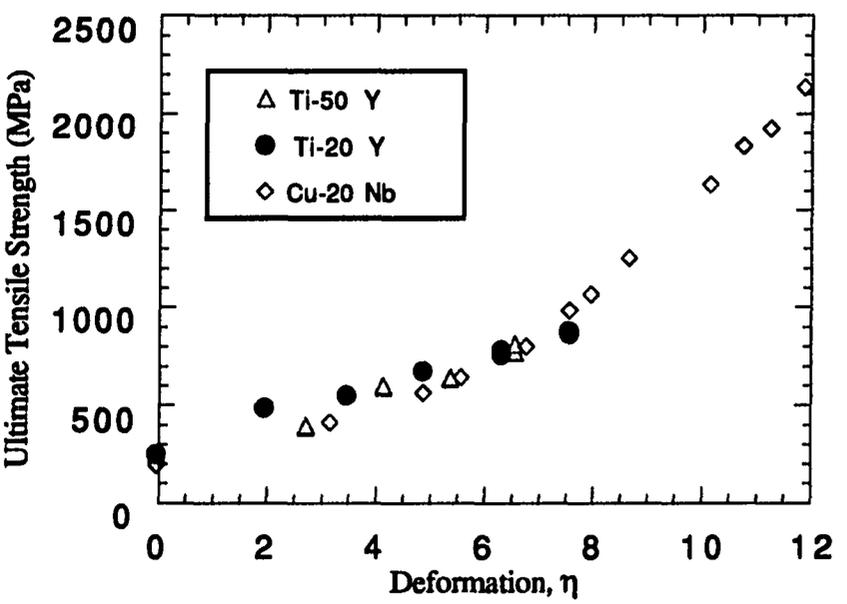

Figure 1. Ultimate Tensile Strength of a Copper-20 Vol. % Niobium alloy, Titanium-20 Vol. % Yttrium and Yttrium-50 Vol. % Titanium versus Eta

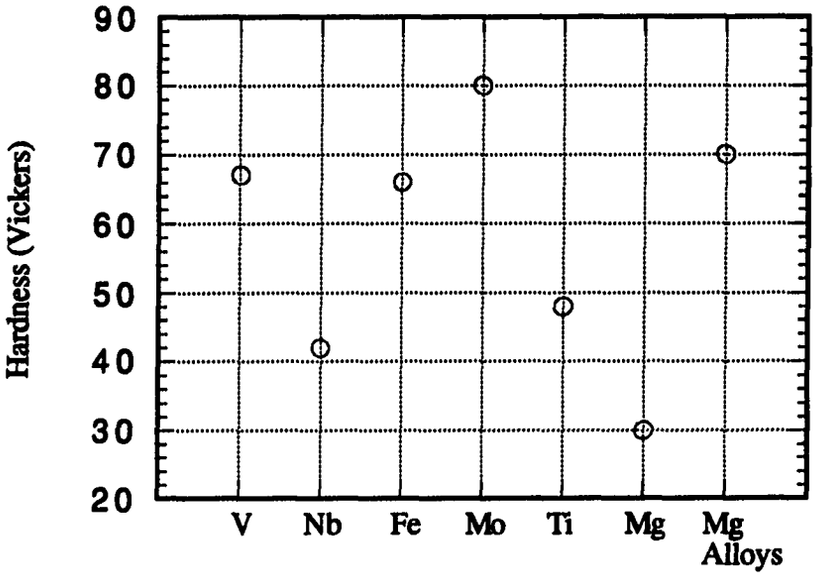

Figure 2. Vickers Hardness for Several Magnesium- 20 Vol.% Refractory Metal Systems

CONCLUSION

Deformation processed metal-metal matrix composites offer a unique solution to microstructural design. As demonstrated this process can produce very fine microstructure in a multitude of alloy systems. These materials can develop very high mechanical strengths without affecting the basic physical properties of the matrix phase. Additionally, the production of a DMMC can have other non-structural use as shown by the development of electrical capacitors from these materials. Future developments in this area will focus on using this method to produce very fine microstructures for a variety of structural and other applications

ACKNOWLEDGMENTS

The author would like to thank the following Ames Laboratory personnel with out whom the study would not have been possible. The copper-refractory metal deformation processed composite work done by Dr. John Verhoeven and Dr. William Spitzig has provided the basis for all extension work into other alloy systems. The processing knowledge and skill of Mr. Ed Gibson, Mr. Alan Russell, Mr. Frederick Schmidt, Mr. Larry Jones and Mr. Lester Reed was invaluable in producing these alloys. This work was sponsored by the Office of Basic Energy Sciences, Division of Material Science U. S. Dept. of Energy and performed at the Ames Laboratory operated by Iowa State University for the U. S. Dept. of Energy under contact no. W-7405-ENG-82.

REFERENCES

1. J.D. Verhoeven et al., *Journal of Metals*, Sept (1986)

2. J. Bevk, J.P. Harrbison and J.L. Bell, *J Appl. Phys*, 1978, Vol 49, pp 1143

3. W.A. Spitzig, C.L. Trybus and J.D. Verhoeven, "**Metal Matrix Composites: Processing and Interfaces,**" R.K. Everett and R.J. Arsenault eds. Academic Press, San Diego, Ca pp. 151 (1991)

4. J.D. Verhoeven, L.S. Chumbley, F.C. Laabs and W.A. Spitzig, *Acta. Metall. Mater*, 1991, Vol. 39, No. 11, pp 2825.

5. D. Dew-Hughes, P.G. Quincey and P.L. Upadhyay, *Mat. Sci. and Tech*, 1987, Vol. 3, pp 936

7. J.B. Massalski, in "**Binary Alloy Phase Diagrams,**" American Society for Metals, Volumes 1,2, and 3, Metals Park, Ohio, 1990.

6. A.M. Russell, J.A. Jensen, L.S. Chumbley, D.G. Konitzer and T.W. Ellis, **Proceedings of the Seventh World Conf. on Titanium**, in print

8. For review see M Suenaga, **Superconductor Material Science, Metallurgy, Fabrication and Application**, edited by S Foner and B.B. Schwartz, Plenum Press, New York, 1981, pp 201

9. W.A. Spitzig and P.D. Krotz, *Scripta Met*, 1987, Vol 21, pp 1143.

10. J.D. Verhoeven, W.A. Spitzig, F.A. Schmidt, P.D. Krotz, and E.D. Gibson, *J Mat Sci*, 1989, Vol 24, pp 1015.

11. T.W. Ellis, I.E. Anderson, H.L. Downing, J.D. Verhoeven, *Met. Trans. A.*, vol. 24A, 1993 pp 21

12. Alloys, E.D. Gibson and J.D. Verhoeven, *J. Mat. Sci: Mat. in Elec.*, 2 (1991) pp 236

13. J.C. Kampe, T.H. Courtney and Y Leng, *Acta Metall*, 1989, Vol 37, No 7, pp 1735

14. T.H. Courtney and J.C. Kampe, *Acta Metal*, 1989, Vol 37, No 7 pp 1747

15. K.A. Gschneidner, **Bul. Alloy Phase Diagrams**, Vol. 11 No. 3 1990

PAPER 5. METAL MATRIX COMPOSITES PRODUCTION FROM YTTRIUM BASED OR HIGH YTTRIUM CONTENT ALLOYS

Timothy W. Ellis, Ames Laboratory, U.S.D.O.E.,
Iowa State Univ., Ames, IA 50011-3200 USA

ABSTRACT

Recently the production of metal matrix composite from yttrium or high yttrium content alloys has been surveyed. Composite materials have been produced by directional solidification and/or cooling in the yttrium-oxygen system. Additionally, metal-metal matrix composites were produced by deformation processing. These materials are analogous to those formed in copper-niobium alloys and have been produced in the yttrium-titanium system and in the yttrium-niobium system. Here a precursor alloy is cold worked such that both phases co-deform. This produces a fine filamentary reinforcing phase within a continuous matrix phase. Both methods produce materials with interesting microstructures and possible new methods for the production of structural materials from yttrium, scandium or the other rare earth metals.

INTRODUCTION

Rare earth metallurgy is noted for many contributions to modern technology, however, rare earth based structural alloys are noticeably absent. The high cost of the rare earth metals in addition to their limited availability has stymied the development of structural alloys of these materials. This is particularly unfortunate in the case of yttrium and scandium which have very attractive physical properties. Although metal cost is still a problem, the technological maturity of other low-density high-tech structural alloy material, e.g. beryllium, titanium, warrants this new investigation. The rare earths are essentially unexplored territory for the development of new structural materials.

The focus of research into new structural rare earth alloys has followed two paths concurrently: 1) rare earth metal matrix composites produced by directional solidification or heat treatment with compound forming non-metals, as modeled by the yttrium-oxygen system, and 2) rare earth-refractory metal alloys which are deformation processed to produce in-situ metal-metal matrix composites. In both processes it is desired to produce a rare earth metal matrix which is reinforced by the presence of a large volume fraction of fibers or particles of a second phase. (1)

DIRECTIONALLY THERMALLY PROCESSED COMPOSITES

Our preliminary work has been done on the yttrium-oxygen system, phase diagram shown in Figure 1. (2) Two approaches have been made to the formation of metal matrix composites. The first approach used to produce a composite was through directional solidification of alloys of eutectic composition, 37.4 at. % oxygen. To produce these composites yttrium, and yttria, Y_2O_3, were combined in a tantalum crucible and directionally

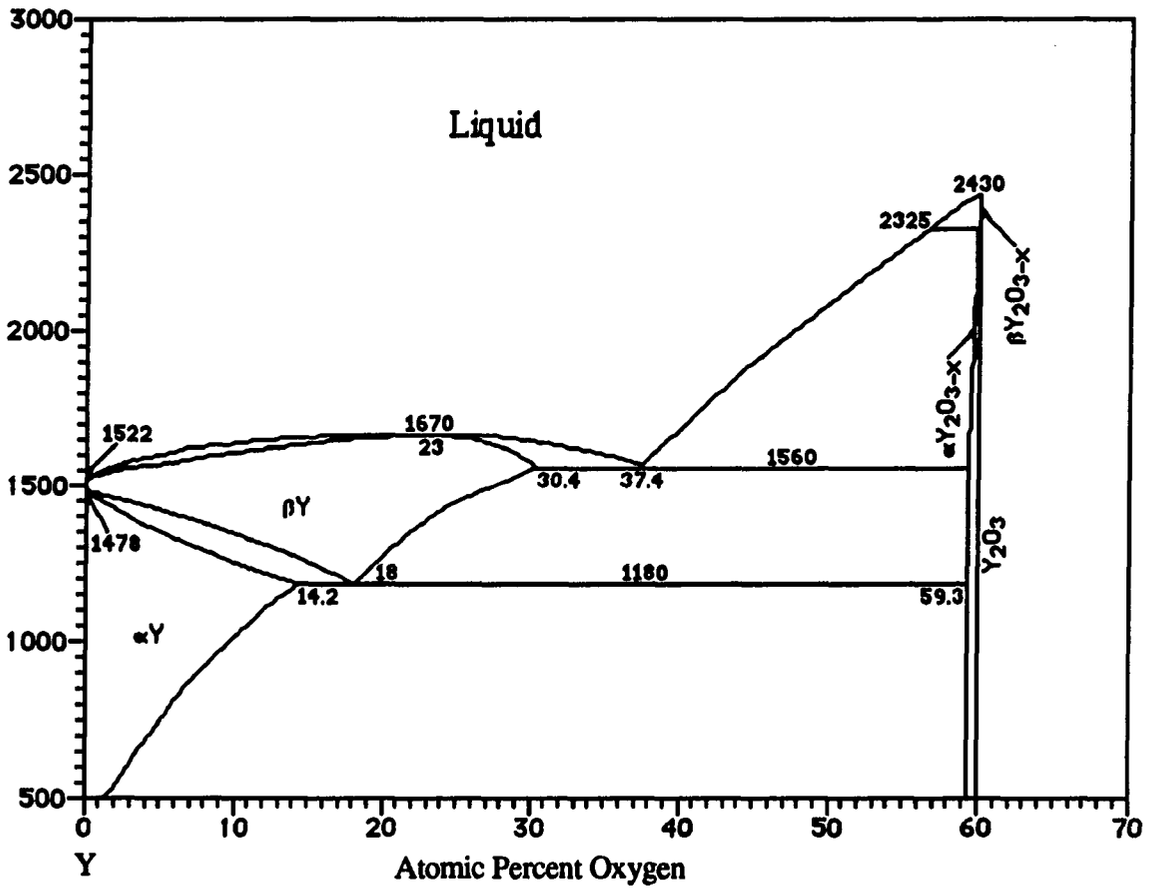

Figure 1. Equilibrium Phase Diagram for the Yttrium-Oxygen System

solidified by the Bridgeman technique. This was done at withdrawal velocities of 1, 10, 100 and 500 mm/sec. The microstructures were all similar to that shown in Figure 2 for a withdrawal velocity of 100 mm/sec. Eutectic yttria appears to grow with a very faceted morphology which is to be expected. Eutectic spacings were found to vary from 350 mm to 100 mm over the velocity range explored. This spacing was felt too be to large to provide significant strengthening. Therefore, attention was refocused on the eutectoid reaction present at a composition of 18.0 at. % oxygen. The feasibility of strengthening by controlled eutectoid growth in this system was accomplished by performing a jominy test on a bar of eutectoid composition, i.e. 18.0 at. % oxygen. (2) Jominy tests are very commonly used to evaluate the hardenability of steel alloys. (3) To perform a jominy test, a bar of 2.5 cm diameter and 10.5 cm length is solutionized to assure uniform composition in our experimental work (1400°C for 2 hours), which is then quenched by the impingement of a water stream at one end. This provides for essentially uni-directional heat flow with the cooling rate varying from a very fast quench at the jet end to a very slow cool on the opposing end. To evaluate the hardenability, hardness measurements are made along the length of the bar. This was done in our experimental work using a Vickers indentor and a 50 Kg load. In Figure 3 the measured Vickers hardness is plotted versus distance.

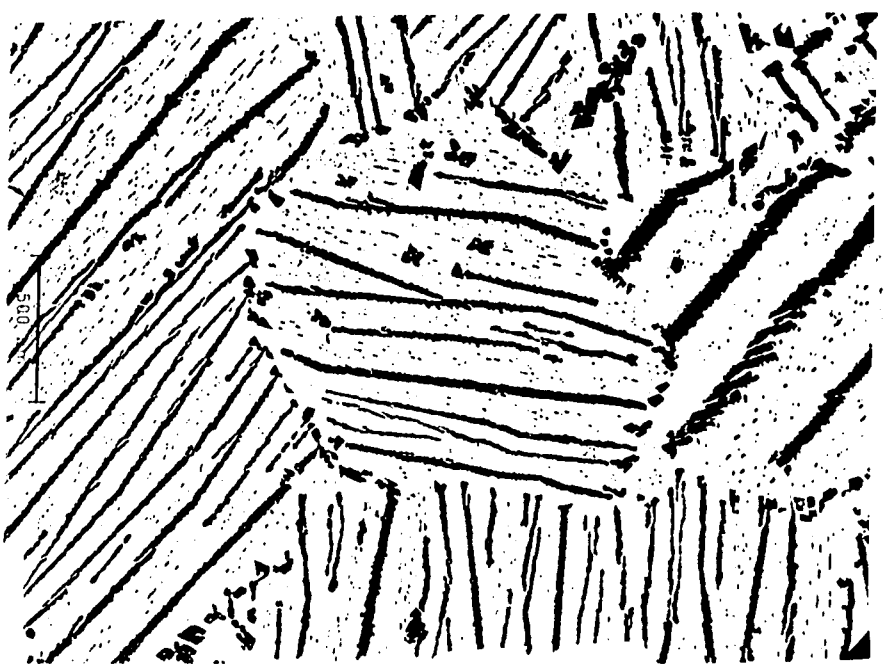

Figure 2. Microstructure Yttrium-Yttria Eutectic Directionally Solidified at 100 Microns per Second

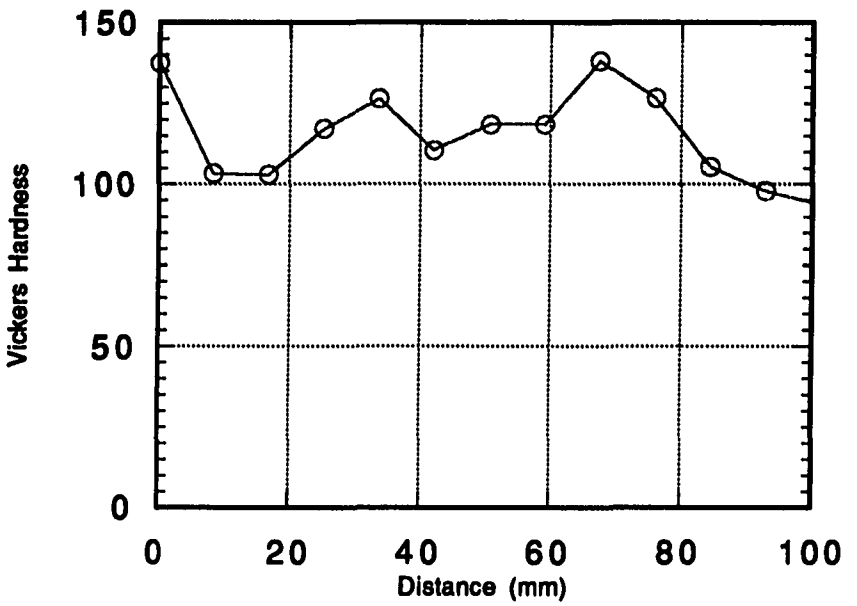

Figure 3. Vickers Hardness versus Distance from the Quenched End for a Yttrium-18.0 At. % Oxygen Jominy Test Bar

By observation one finds that the results are rather random until approximately 7.0 cm from the quenched end where a regular reduction of hardness with distance is found. This type of two region curve is not uncommon in some steels.

Although the actual processes which produce this variability in the hardness at high cooling rates need further investigation it is apparent that solutionizing and controlled cooling can lead to hardening in this system to a depth of at least 7.0 cm. The microstructure of this material, as done by optical microscopy, is shown in Figure 4.

Generally the microstructure consists of a yttrium matrix phase with yttria precipitating out either as a eutectoid product or as large flakes. Large flakes of yttria as the continuous phase could lead to very poor tensile properties. However, additions of other elements may change the morphology of the yttria and the subsequent problems.

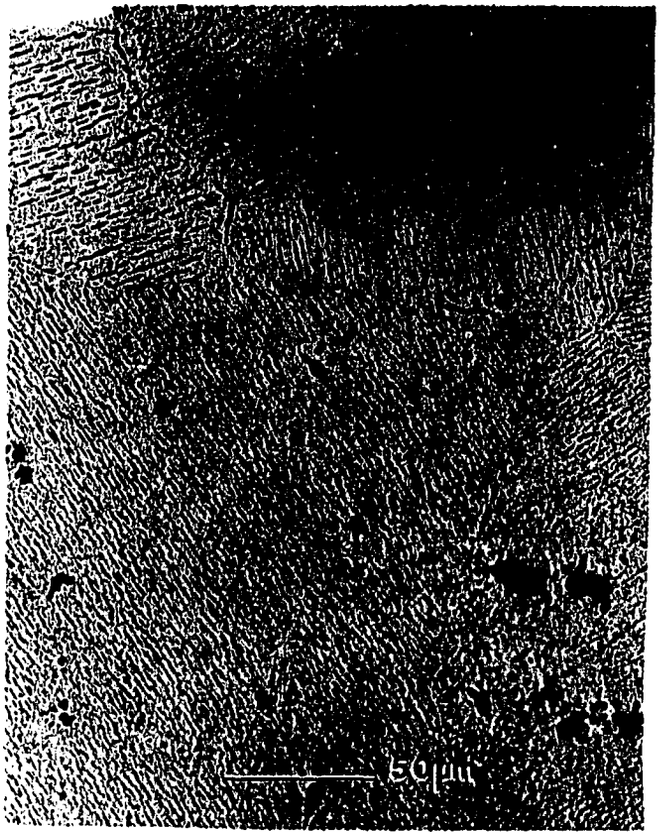

Figure 4. Microsturcture of a Yttrium-18.0 At. % Oxygen 1/4 Inch from the Quenched End

DEFORMATION PROCESSED COMPOSITES

Deformation processing of immiscible yttrium-refractory metal alloys, e.g. titanium, niobium, vanadium, chromium, molybdenum, has proven a new method for the production of rare earth based structural alloys. Some of the fundamentals of this type of composite have been previously presented by several authors. (4, 5, 6) Deformation processing of a two-phase immiscible alloy, as an example the yttrium-titanium phase diagram presented in Figure 5, produces a microstructure consisting of a continuous matrix phase and a high aspect ratio fibrous phase.

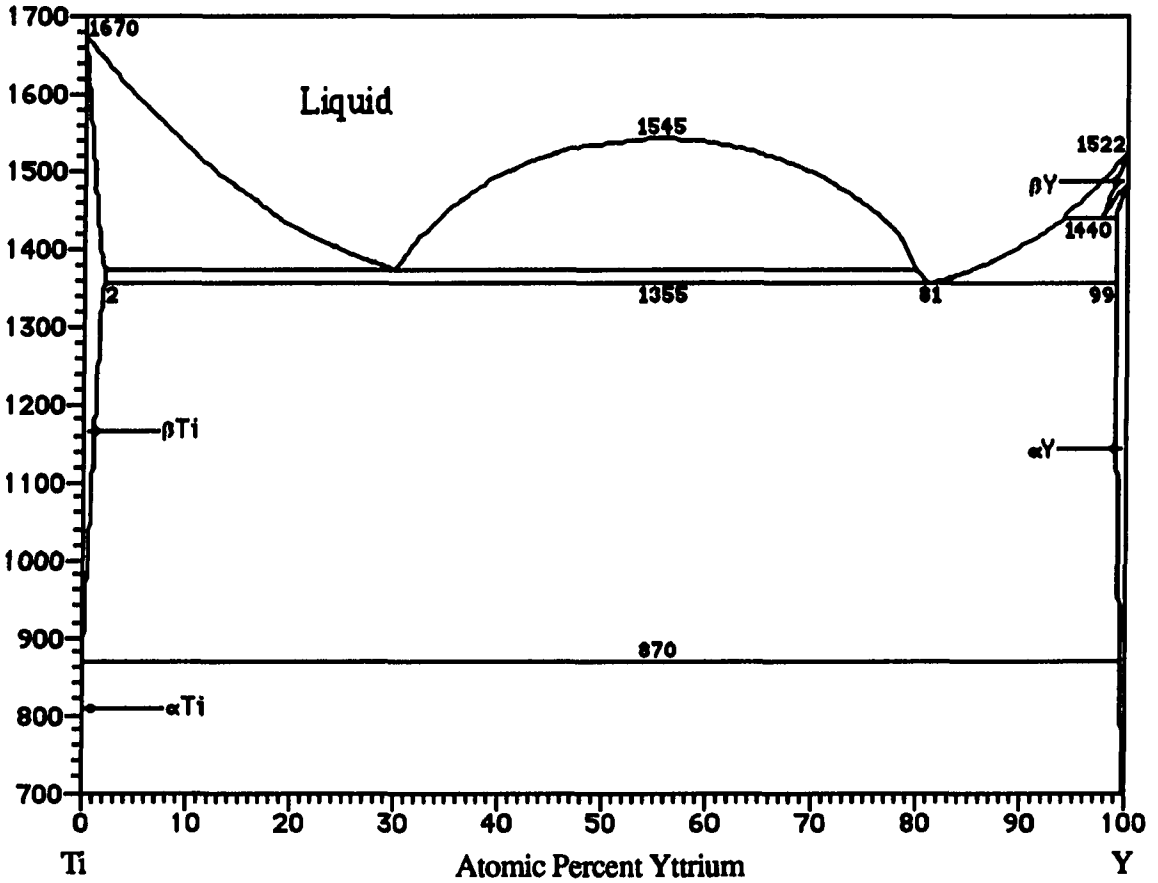

Figure 5. Equilibrium Phase Diagram Yttrium-Titanium System

The particular microstructure which defines a deformation processed metal-metal matrix composite, DMMCs, is unique in terms of structure and processing. Common polymer matrix composite materials have a continuous polymer matrix which is reinforced by the presence of fibers of inorganic or organic material. In DMMCs a continuous metallic matrix phase is reinforced by a high aspect ratio non-continuous metallic reinforcing phase; the fibrous morphology of the reinforcing phase being produced by the co-deformation of the matrix and reinforcing phases. Therefore, the fibrous morphology of the reinforcing phase is formed in-situ during deformation of the material, a distinction that separates these materials from the wide range of non-metallic reinforced metal matrix materials, e.g. SiC fibers in aluminum. Prototypical microstructures for these materials formed upon deformation processing is shown in Figure 6 for a yttrium-titanium alloy.

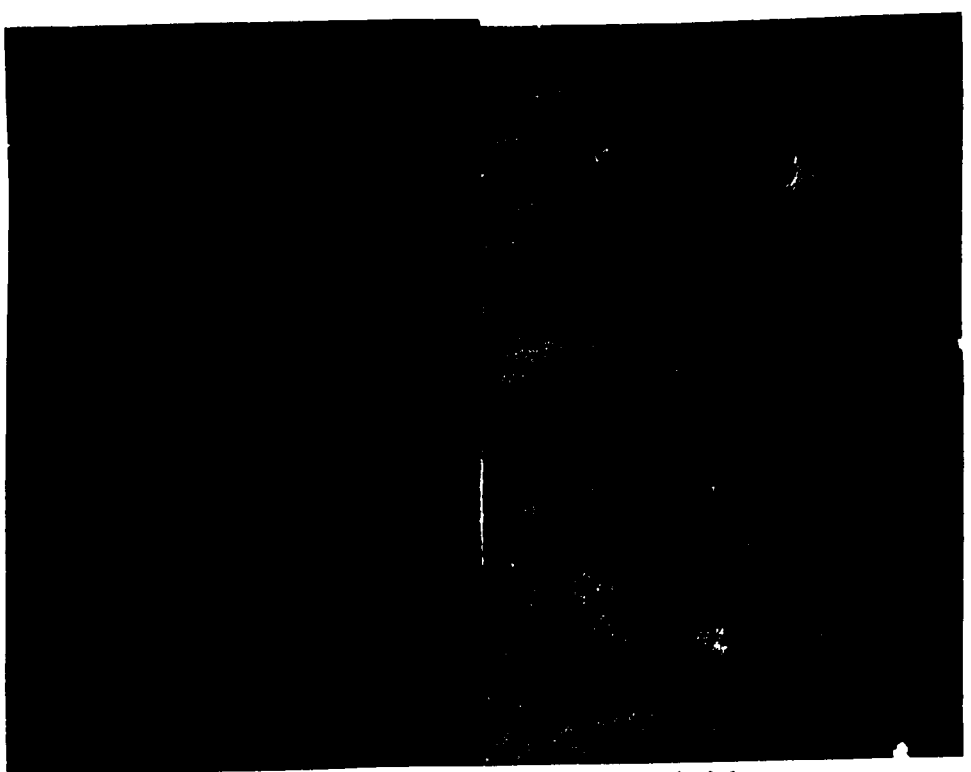

Transverse Axial

Figure 6. Microstructure of Deformation Processed Titanium- 50 vol. % Yttrium

During deformation both the reinforcing phase and matrix phase become highly textured. Texture development limits the number of available slip systems which produces the ribbon-shaped cross section to the filaments as seen in Figure 5.

As shown in Figure 7 for two titanium-yttrium alloys, 20 and 50 vol. %, the ultimate tensile strength (UTS) increases as a function of eta (η). A copper-20 vol. % niobium alloy is shown for comparison. (6) Eta is defined as the natural log of the ratio of the reduction in area, $\eta = \log A_f/A_i$, where A_f is the final cross sectional area and A_i is the initial cross sectional area. The ultimate tensile strength of these alloys is increased from approximately 250 Mpa at an $\eta = 0$, to 950 Mpa at an $\eta = 8$. Following the copper-niobium example, increasing the value of h should lead to much larger increases in UTS of these alloys. These experiments, however, have proved the validity of this approach for producing high strength alloys based on yttrium.

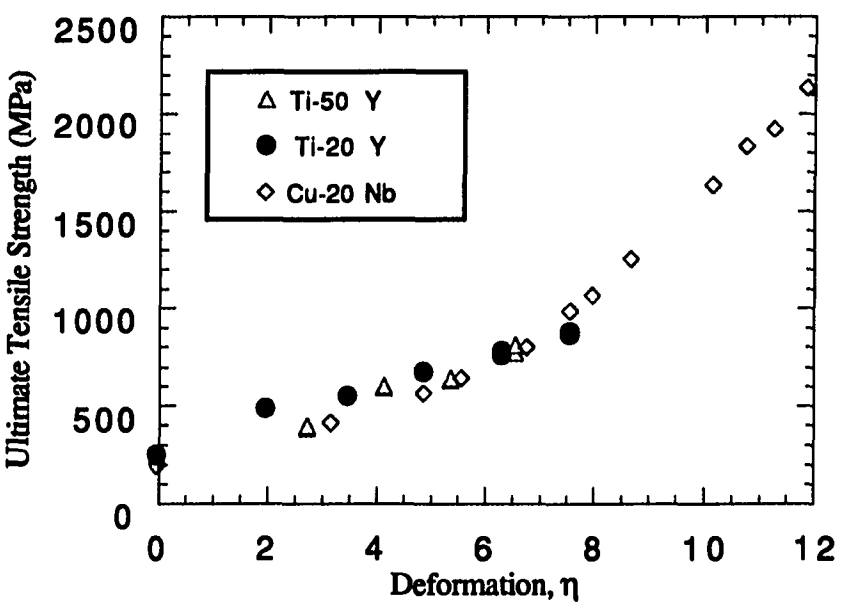

Figure 7. Ultimate Tensile Strength alloy, Titanium-20 Vol. % Yttrium, Yttrium-50 Vol. % Titanium and of a Copper-20 Vol. % Niobium versus Eta

CONCLUSION

The desire of this survey was to investigate the feasibility of yttrium, and by analogy the other rare earth elements, as the primary phase of metal matrix composite materials. This has been done by two different methods: First, the growth of yttria fibers within a yttrium matrix by manipulation of the eutectic and eutectoid reaction; secondly by deformation processing of yttrium-refractory metal alloys in a manner analogous to that undertaken in copper-refractory metal alloys.

ACKNOWLEDGEMENTS

The author would like to thank the following Ames Laboratory personnel Dr. John Verhoeven and Dr. William Spitzig, as the copper-refractory metal deformation processed composite work done by them has provided the practical and theoretical basis for this work. Also the expertise of Mr. Frederick Schmidt of the Materials Preparation Center, Ames Laboratory, was invaluable in understanding the processing limits of yttrium alloys. This work was sponsored by the Office of Basic Energy Sciences, Division of Material Science, U. S. Dept. of Energy and performed at the Ames Laboratory operated by Iowa State University for the U. S. Dept. of Energy under contract no. W-7405-ENG-82.

REFERENCES

1) J.D. Verhoeven et al., *Journal of Metals*, Sept (1986)

2) J. L. Murray, J.B. Massalski in *"Binary Alloy Phase Diagrams,"* American Society for Metals, Volumes 1, 2, and 3, Metals Park, Ohio, (1990).

3) W. F. Smith, *Structure and Properties of Engineering Alloys*, McGraw-Hill, New York, p. 127 (1981).

4) W.A. Spitzig, C.L. Trybus and J.D. Verhoeven, R.K. Everett and R.J. Arsenault eds*Metal Matrix Composites: Processing and Interfaces*, . Academic Press, San Diego, CA p. 151 (1991).

5) J.D. Verhoeven, T.W. Ellis, L.D. Jones, and A.M. Russell, U.S. Patent #5200004 granted April 9, 1993.

6) J.D. Verhoeven, W.A. Spitzig, F.A. Schmidt, P.D. Krotz, and E.D. Gibson: *J.Mat Sci*, 1989, Vol 24, pp 1015.

GENERAL SUMMARY

The thrust of this research effort was to improve and extend the range of deformation processed metal metal matrix composites, DMMCs. First, extending the range of physical properties available. Second, improve the methodology for production of these materials. Finally, extending the concept of deformation processed metal matrix composites into other alloy systems.

The desire to improve and extend the range of properties available in DMMCs has motivated a study on the possibility of carrying out precipitation hardening of the matrix phase. The use of precipitation hardening was studied in hyper-eutectic copper-chromium alloys. Though hypo-eutectic copper-chromium had been extensively studied by other authors as presented in the review in paper 1, a literature survey has revealed very little work on hyper-eutectic copper chromium alloys. The combination of precipitation hardening in conjunction with the production of a DMMC had not undergone either an extensive experimental or theoretical treatment. In this study the primary task was to develop an understanding of the precipitation phenomena and whether this would provide a road to improvement in the properties available in these materials. Isothermal electrical resistivity measurements were used to evaluate the kinetics of precipitation in these alloys and using this information a study was made of the mechanical properties produced. Microstructural evaluation was accomplished by TEM. The physical properties, mechanical strength, and electrical resistivity were correlated with microstructural developments brought about by thermomechanical treatment. This information was then used to optimize both the physical and electrical properties of the alloy. The optimum properties were developed in this alloy by multi-step processing using sulutionizing/quenching, followed by cold deformation, aging and further cold deformation. This produced a material with a figure of merit = 3.25 which is comparable to copper-niobium alloys and superior to commercial copper-beryllium. Microstuctural evaluation has shown that the optimum properties are developed when there a no precipitates in the matrix material. Maximum properties are developed when the material most closely models the copper-niobium case. Therefore, precipitation hardening of the matrix does not lead to the best combination of properties, however, management of the precipitation reaction is crucial to removing the precipitates from the matrix in order to develop the best combination of electrical conductivity and mechanical strength.

Improvement in material production is basic to refinement of the microstructure to obtain an inter-particulate or inter-fiber spacing in the sub-micron range, which is key to

development of high mechanical strength in DMMCs. Homogeneity of the microstructure is also important as large unalloyed globules or large variations in dendrite size across a precursor billet can lead to non-uniform deformation and over working of limited areas leading to fracture or breakage of the billet during deformation processing. Additionally, chemical contamination of precursor material should be kept to a minimum. Many refractory metals, which have desirable properties as reinforcement, are very susceptible to embrittlement by carbon, oxygen, and nitrogen.

Solidification processing by crucible based rapid solidification techniques can produce very refined starting microstructures. In paper 2 new materials for crucible melting were investigated. Since crucible melting is a widely accepted industrial practice, some time was expended during this investigation on possible containment systems for the copper-refractory metal alloys. This screening study proved to be very successful in producing new methodologies for crucible melting. A new crucible refractory systems was developed that allowed melting of these alloys to 2100°C and to maintain low contamination. The containment system develop is a graphite crucible plasma sprayed with 1 mm of tungsten and overcoated with 2 mm of yttria stabilized zirconia. The graphite crucibles provide good coupling to the induction field and excellent high temperature stability. The yttria stabilized zirconia is not wetted by the melt nor does it chemically react with the copper or refractory metal. The tungsten layer acts as a carbon migration barrier preventing a carbothermic reduction between the crucible and the oxide coating.

The use of High Pressure Gas Atomization (HPGA) and mechanically alloying (MA) to produce precursor powder for billets to be deformation processed was presented in papers 3 and 4. HPGA was used in this experimental work (Cu-18.0 vol. % Nb) to investigate the use of rapid solidification to reduce the microstuctural scale prior to deformation processing while MA magnesium-refractory metal based systems have been deformation processed as a part of this study. Both processing techniques have proved very successful in meeting the goals for precursor material. The copper-niobium alloys produced by HPGA obtained higher strength at a lower η value than material produced by any other method. However, the combination of electrical conductivity and mechanical strength was inferior to other processing techniques. Magnesium alloys produced by MA have hardness properties comparable to those of the best commercially available precipitation hardened materials. This program demonstrated that MA can be a viable means to produce materials unavailable by melt processing.

Extension into other alloy systems was investigated in paper 4 and 5. The first consideration in the investigation of deformation processed metal-metal matrix composites is the development of the desired microstructure of a continuous matrix phase and a high aspect ratio fibrous reinforcing phase. During deformation both the reinforcing phase and matrix phase become highly textured. The <110> texture development in the niobium limits the number of available slip systems to two, which produces a ribbon shape cross section of the niobium, a BCC metal. Other copper-X alloys investigated have shown identical behavior, X= (Cr, Fe, Mo, Ta, V). The kinked morphology of the fibers produced by wire drawing are brought about by the axisymmetric nature of this deformation process. In the work presented here fiber morphology of wire drawn material is not, however, limited to composites FCC-BCC crystallography, as is the case in the Cu-X examples. The research done on deformation processed composites with other crystallographies has shown that the kinked ribbon fibers which produce the high strength in the Cu-X alloys can be achieved fairly widely Deformation processing to form composites with other crystallographies has shown similar results to the FCC-BCC case. The following systems have been deformation processed: HCP-HCP (yttrium-titanium), an HCP-BCC (magnesium-refractory metal), and FCC-HCP (copper-rhenium). The ribbon morphology probably results because of the limited number of slip systems in the HCP. This discovery expands the vista available to DMMC materials to systems with a limited number of slip systems.

LITERATURE CITED

1. J.D. Verhoeven et al., Copper-Refractory Metal Alloys, J. of Metals, 1015, Sept (1986).

2. J. Bevk, J.P. Harrbison and J.L. Bell, J. Appl. Phys., Vol. 49, 1143 (1978).

3. W.A. Spitzig, C.L. Trybus and J.D. Verhoeven, "Metal Matrix Composites: Processing and Interfaces", R.K. Everett and R.J. Arsenault, Eds. Academic Press, San Diego, Ca. 151 (1991).

4. W.A. Spitzig Acta Metall. Mater., Vol. 39, No. 6, 1085 (1991).

5. J.D. Verhoeven, W.A. Spitzig, F.A. Schmidt, P.D. Krotz, and E.D. Gibson, J. Mat. Sci,. 1989, Vol. 24, 1015 (1989).

6. T.W. Ellis, I.E. Anderson, H.L. Downing and J.D. Verhoeven: Met. Trans. A, Vol. 24, 21 (1993).

7. D. Dew-Hughes, P.G. Quincey and P.L. Upadhyay, Mat. Sci. and Tech., Vol. 3, 936-944 (1987).

8. J.D. Verhoeven, L.S. Chumbley, F.C. Laabs and W.A. Spitzig, Acta. Metall. Mater, Vol. 39, No. 11, 2825 (1991).

9. P.D. Funkenbush, T.H. Courtney and D.G. Kuibsh, Scripta Metall. Vol. 18, 1099 (1984).

10. Y. Leng, T.H. Courtney and J.C. Malzahn Kampe, Mat. Sci. Eng. Vol. 94, 204 (1987).

11. J.D. Verhoeven, H.L. Downing, L.S. Chumbley and E.D. Gibson, J. Appl. Phys., Vol. 65, No. 3, 1293 (1991).

12. J.G. Sevillano, Strength of Metals and Alloys, Proc. ICSMA 5, P. Haasen, V. Gerold and G. Kowtorz, Ed., Pergamon Press, Oxford, England, 819 (1980).

13. J.S. Koehler, Phys. Rev., Vol. 2, 547 (1970).

14. A. Kelly, Phil. Trans. R. Soc. Lond. A, Vol. 322, 409.(1987).

15. D.J. Chakrabarti and D.E. Laughlin, Copper-Chromium Phase Diagram, Phase Diagrams, T.B. Massalski, Ed, ASM International, Metals Park, Oh (1984).

16. H. Dyiec, Z., Rdzawski and M. Richert, Mater. Sci. Eng., A, A108, 97 (1989).

17. Z. Rdzawski, H. Dydiec and M. Richert, Z Metallkd., 79 (11), 746 (1988).

18. N. Rashkov and Z. Martinova, Z Metallkd, 79 (11), 752, (1988).

19. M.E. Drits, N.R. Bochvar, E.V. Lysova and N.P. Leonova, Soviet Journal of Non-ferrous Metallurgy, Vol. 2, 312 (Eng. trans), (1976).